PART I. APPLICATION OF THE FABRY-PEROT INTERFEROMETER FOR HIGH RESOLUTION STUDIES

PART II. HYPERFINE STRUCTURE IN BROMINE

being the

Thesis submitted to the University of London

for the

DEGREE OF DOCTOR OF PHILOSOPHY

in

PHYSICS

by

JAGANNATH D. RANADE

Physics Laboratory,
Royal Holloway College,
(University of London)
Englefield Green,
Surrey.

MAY 1950.

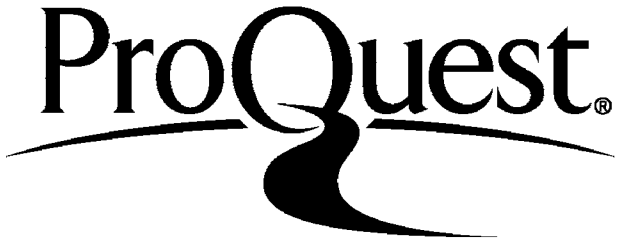

PART I. Application of the Fabry-Perot Interferometer for High Resolution Studies.

Part II. Hyperfine Structure in Bromine.

A B S T R A C T

PART I

The Fabry-Perot interferometer is generally used in transmission. It is described how it can be modified so that the fringes can be used in reflection. The general theory of the reflection fringes is considered. It is shown that the interferometer used in reflection is about 30 times faster in light speed than one used in transmission. It is shown how the technique can be adopted to the measurement of wavelengths and to the evaluation of the line-widths of lines from weak sources.

PART II

Hyperfine structure examinations are carried out over the range λ 6000 to λ 3700 in the arc spectrum of bromine and over the range λ 5500 to λ 3900 in the spark spectrum of bromine. Twenty-one lines in the arc spectrum of bromine are examined. Eighteen classified and twenty unclassified lines in Br II spectrum are measured for the first time and hyperfine structure term interval factors are derived for fourteen terms in the

spark spectrum of bromine.

The theory of the hyperfine structure analysis is considered in brief. Both the arc and the spark spectra are obtained by employing a circulating system and a high frequency oscillator. The analysis of the lines fits well the term scheme. A few anomalies have been noted and have been accounted for, some of them being due to faulty interpretations of the lines by previous workers. Deviations from the interval rule occur in the arc spectrum of bromine and these are completely explained by the existence of an electrical quadrupole moment of nuclei for both the bromine isotopes.

The coupling constants for the terms concerned are determined from the term values and using these, both the quadrupole moment and the magnetic moment of the bromine nucleus are evaluated.

C O N T E N T S

INTRODUCTION

The phenomena of interference have found important and increasing applications in high resolution work in spectroscopy and Astronomy since 1887, the date of invention of the Michelson interferometer. However, of all the interferometers, that developed by Fabry and Perot [1] is the most elegant and versatile. It has contributed successfully to the study of hyperfine structure in Atomic spectra and has led to important advances towards our knowledge of the nucleus. A variable gap Fabry-Perot interferometer supersedes all other high-resolution instruments by its simplicity and versatility. A well silvered interferometer varying from 1 to 10 mms. in plate separation offers a resolving power ranging from 100,000 to 1,000,000 with an associated high dispersion. It is valuable in high precision wavelength determination and high dispersion studies of linewidths and line contours.

However, high resolution spectroscopic interferometry has as yet hardly found application in astrophysics, apart from solar studies. The reason is to be attributed to the question of available light intensities. It is first necessary to disperse the spectrum to be examined, either before or after crossing with the interferometer and then, as is well known, the interferometer itself leads to

additional considerable loss of light. If it were not for this, one could readily see considerable application to astrophysics.

The Fabry-Perot interferometer is invariably used in transmission (i.e. all the multiple beams transmitted through the interferometer are collected by a lens to form fringes in the focal plane) and not in reflection. (i.e. all the multiple beams reflected on the same side as the incident beam are collected to form fringes.) Although the use of two beam reflection fringes in metrology is a commonplace, the reflected Fabry-Perot multiple beam fringes have not apparently been used in high resolution spectroscopy; and there appears to be no mention in the literature of their use apart from a note by Tolansky[2]. In it, he gave an approximate theory and calculation for the reflected system. The particular feature distinguishing this reflection technique is that the interferometer introduces practically no light loss at all.

It is the aim of this report to give a more complete theory of the reflected system and to show how such a technique can be adapted to the spectroscopic measurements, particularly to the precision evaluation of the line-widths of weak lines.

Chapter I.

GENERAL THEORY

FABRY-PEROT INTERFEROMETER

This instrument, developed in 1897, consists usually of two plane parallel glass or quartz plates (worked optically flat to $\lambda/40$) kept accurately parallel by spacers, and enclosing an air gap between them. The reflecting power of the surfaces is enhanced by putting down a thin semi-transparent highly reflecting layer of silver.

Fringes arise from multiple reflections between the two silvered faces. The principle is the same as that associated with Haidinger[3] fringes seen with thick plates near normal incidence.

These are fringes of equal inclination. If light of wave-length λ from an extended source falls upon such a pair of plates separated by an air gap 't' cm. thick, all the light incident along the surface of a cone of semi-vertical angle θ contributes to form a single circular fringe when

$$n\lambda = 2\mu t \cos\theta$$

n being the order of interference and μ the refractive index of the medium between the plates. The emergent rays

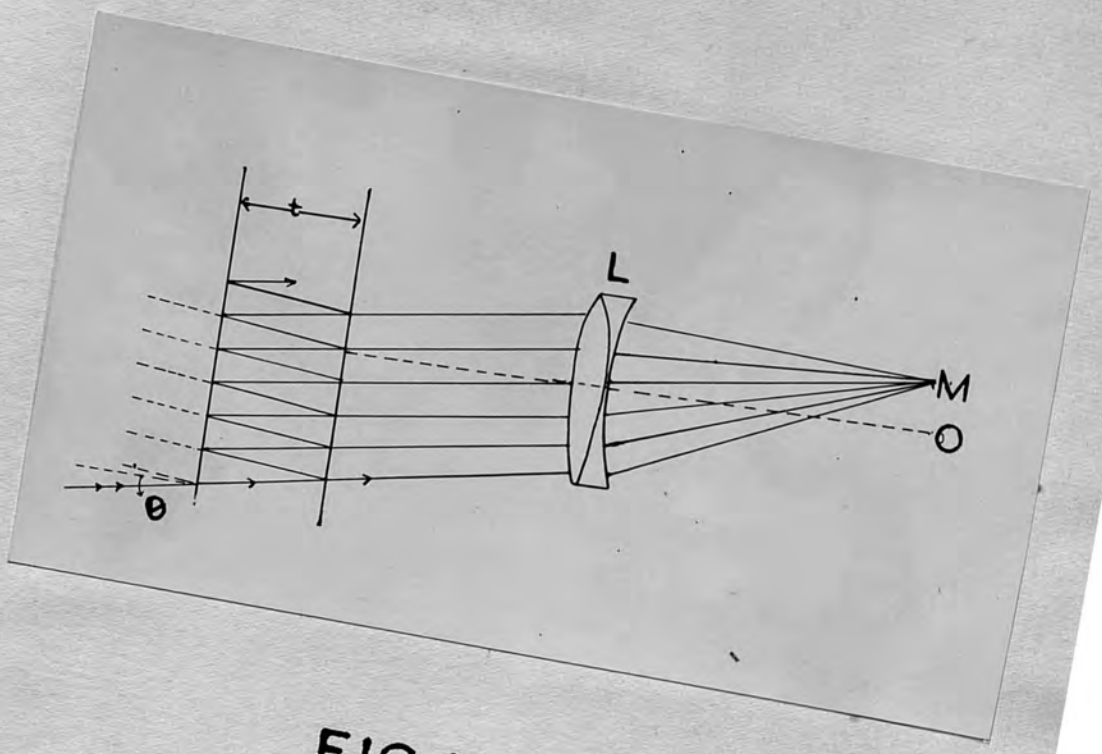
t
L
M
O
θ

FIG. 1

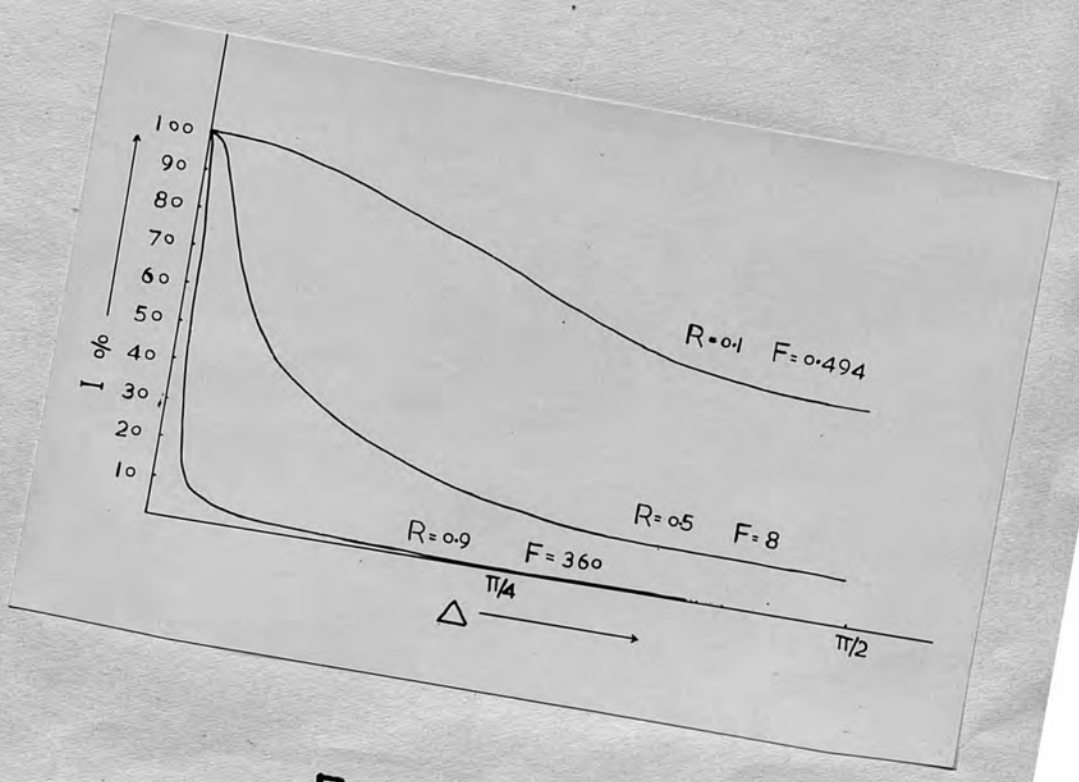
100
90
80
70
60
50
40
30
20
10
I %
R=0.1 F=0.494
R=0.5 F=8
R=0.9 F=360
π/4
π/2
Δ

FIG. 2

are collected by a lens and form the fringe system in its focal plane. The ray trace is illustrated in Figure 1.

The multiple reflections have a profound effect on the character of the fringes, as is illustrated in Figure 2. With low reflectivity the intensity gradually varies from the maximum to the minimum and back to the maximum again, giving broad fringes of $\cos^2\theta$ type as in the case of a Michelson interferometer (dark and bright rings of equal width). Multiple reflections, however, concentrate the light, when the reflectivity is high, almost entirely near the maxima, the intensity falling off rapidly on either side, and thus giving rise to very narrow fringes.

The expression for the intensity distribution will now be given for both the transmitted and the reflected system and the two systems will then be compared.

Theory

Let 1, 2 and 3 (Figure 3) represent three isotropic dielectric media separated by two plane parallel bounding surfaces AB and CD. The two surfaces are highly reflecting and semi-transparent. This is achieved by putting down semi-transparent films of silver or aluminium some 100 to 500 A° units thick, on a glass support. The medium 2 enclosed between AB and CD , has a refractive index μ

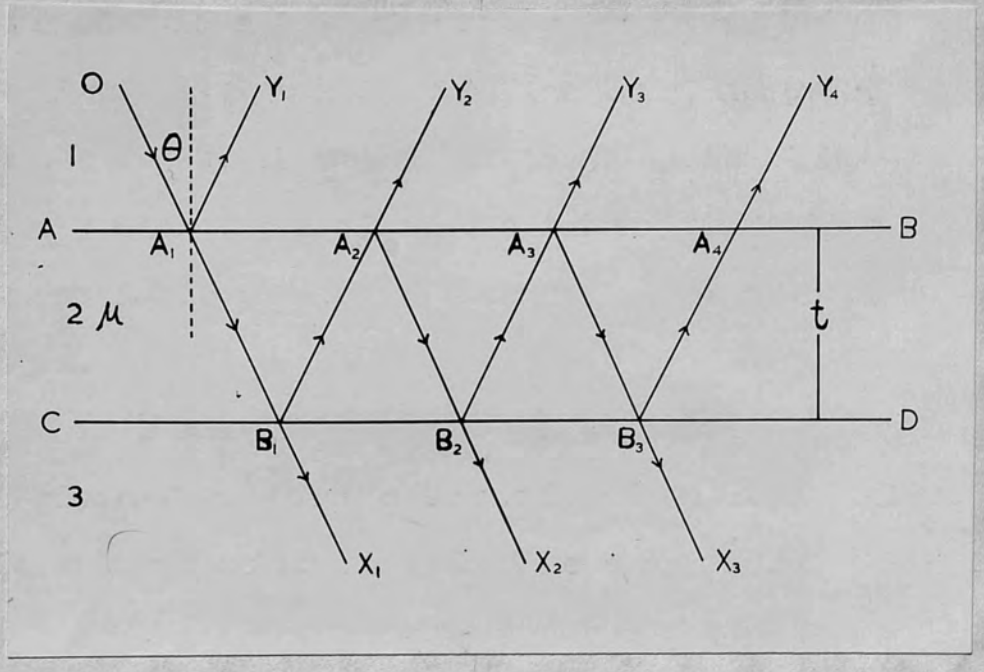

FIG. 3

and thickness t . Let r_1 , and t_1, denote the fractions of light reflected and transmitted when a ray of unit amplitude is incident on AB in medium 1. For a ray incident on AB in medium 2, let r_2 and t_2 be the corresponding magnitudes. Similarly let r_3 and t_3 represent the reflected and transmitted fractions for a ray incident on CD in medium 2. The phase changes on reflection at AB and CD are denoted as follows:-

β is the phase change on reflection for a ray incident on AB in medium 1. (glass-metal).

β_1 the phase change on reflection for a ray incident on AB in medium 2. (air-metal).

β_2 the phase change on reflection for ray incident on CD in medium 2.

γ_1 , and γ_2 the phase changes on transmission through AB and CD respectively.

Let a plane wave of wave-length λ and of unit amplitude be incident at an angle θ on AB in medium 1. The incident wave-front represented by the ray OA_1 , is partially reflected and transmitted at A_1 , giving rise to the reflected ray A_1Y_1 , and the transmitted ray A_1B_1 The ray A_1B_1 undergoes a partial reflection and transmission at B_1 . By repeated reflections between AB and

CD , there arise a series of transmitted and reflected wave-fronts represented by rays B_1X_1 , B_2X_2 etc. and A_1Y_1 , A_2Y_2 etc. respectively.

Transmitted System

This is formed by collecting all the transmitted wave-fronts by a lens.

The successive transmitted wave-fronts are of decreasing amplitude and there is a constant phase difference between successive wave-fronts given by,

$$\Delta = \frac{2\pi}{\lambda}(2\mu t \cos\theta) + \beta_1 + \beta_2$$

These wave-fronts are coherent and the state of interference at any point in the focal plane of the collecting lens is given by the vector sum of all the disturbances. The resultant amplitude A_T is given by the sum

$$A_T = t_1t_3 e^{i\omega t} + t_1t_3 r_2r_3 e^{i(\omega t-\Delta)} + t_1t_3 r_2^2r_3^2 e^{i(\omega t-2\Delta)} + \cdots\cdots$$

$$= \frac{t_1t_3}{1 - r_2r_3 e^{-i\Delta}} e^{i\omega t}$$

Here $e^{i\omega t}$ represents the incident wave-front of unit amplitude. A_T is complex and is of the form $a+ib$. So the intensity is given by A_T^2 or $|a^2+b^2|$.

Therefore,

$$I_T = \frac{t_1^2 t_3^2}{1 - 2r_2 r_3 \cos\Delta + r_2^2 r_3^2}$$

$$= \frac{T_A T_C}{1 - 2\sqrt{R_A R_C}\cos\Delta + R_A R_C}$$

$$= \frac{T_A T_C}{(1-\sqrt{R_A R_C})^2} \cdot \frac{1}{1 + \frac{4\sqrt{R_A R_C}}{(1-\sqrt{R_A R_C})^2}\sin^2\frac{\Delta}{2}} \qquad 1.1$$

where $T_A = t_1^2$, $T_C = t_3^2$, $R_A = r_2^2$, and $R_C = r_3^2$

The intensity is maximum for $\Delta = 2n\pi$, where n is an integer.

Therefore

$$I_{max} = \frac{T_A \cdot T_C}{(1-\sqrt{R_A R_C})^2} \qquad 1.2$$

The minimum intensity occurs at $\Delta = (2n+1)\pi$ and is given by

$$I_{min} = \frac{T_A \cdot T_C}{(1+\sqrt{R_A R_C})^2} \qquad 1.3$$

In practice, the interferometer is symmetrical. This means that the two media 1 and 3 are similar, say glass and AB, CD have the same reflecting powers. Thus for a symmetrical interferometer,

$$R_A = R_C = R, \quad T_A = T_C = T.$$

This gives the familiar expression for the Fabry-Perrot interferometer in transmission.

$$I_T = \frac{T^2}{(1-R)^2} \cdot \frac{1}{1+\frac{4R}{(1-R)^2}\sin^2\frac{\Delta}{2}}$$

$$= \frac{T^2}{(1-R)^2} \cdot \frac{1}{1+F\sin^2\frac{\Delta}{2}} \qquad 1.4$$

where $F = \frac{4R}{(1-R)^2}$ is known as the coefficient of finesse as it determines the sharpness of the fringes.

Reflected System

A detailed analysis was first given by Hamy[4] as early as 1906 but his paper seems to have been much neglected.

If the system of reflected wave-fronts represented by rays A_1Y_1, A_2Y_2, etc. are collected by a lens, the fringes of the reflected system are formed in its focal plane. The phase difference between the rays A_1Y_1 and A_2Y_2 is

$$\frac{2\pi}{\lambda}(2\mu t\cos\theta) + \beta_2 - \beta + \gamma_1 + \gamma_2$$

$$= \frac{2\pi}{\lambda}(2\mu t\cos\theta) + \beta_1 + \beta_2 - \beta_1 - \beta + \gamma_1 + \gamma_2$$

$$= \Delta + K$$

where $K = \gamma_1 + \gamma_2 - \beta_1 - \beta$

Similarly the difference of phase between A_1Y_1 and A_3Y_3 is $2\Delta + K$ and so on for other rays.

If $e^{i\omega_1 t}$ represents the first reflected wavefront (A_1, γ_1), the resultant reflected amplitude A_R is given by

$$A_R = r_1 e^{i\omega_1 t} + r_3 t_1 t_2 e^{i(\omega t - \Delta - K)} + r_3^2 \cdot r_2 t_1 t_2 e^{i(\omega t - 2\Delta - K)} + \cdots\cdots + \cdots$$

$$= \left[r_1 + \frac{r_3 t_1 t_2 e^{-i(\Delta + K)}}{1 - r_2 r_3 e^{-i\Delta}} \right] e^{i\omega_1 t}$$

Reflected intensity I_R is given by

$$I_R = r_1^2 + \left[\frac{r_3^2 t_1^2 t_2^2 - 2 r_1 r_2 r_3^2 t_1 t_2 \cos K + 2 r_1 r_3 t_1 t_2 \cos(\Delta + K)}{1 + (r_2 r_3)^2 - 2 r_2 r_3 \cos \Delta} \right] \qquad 1.5$$

Let $x = r_3^2 t_1^2 t_2^2$, $y = 2 r_1 r_3 t_1 t_2$,

$z = 2 r_1 r_2 r_3^2 t_1 t_2$, $\omega = r_2 r_3$

Then

$$I_R = r_1^2 + \frac{x + y \cos(\Delta + K) - z \cos K}{1 + \omega^2 - 2\omega \cos \Delta} \qquad 1.6$$

To determine the maximum and the minimum of the reflected intensity, the condition is given by $\frac{\partial I_R}{\partial \Delta} = 0$.

It is assumed that x, y, z, ω, and K, are independent of Δ . This is an approximation as there

is a small variation of these quantities with Δ . The above condition furnishes the relation

$$\left[\cos K(y - wz) + 2xw\right]\sin\Delta + (y\cos K + wz\cos K)\cos\Delta + 2wy\sin K = 0$$

This can be put in the form,

$$m\sin\Delta + n\cos\Delta = p$$

or

$$\sin(\Delta + \phi) = \sin\psi \qquad 1.7$$

where $\tan\phi = n/m$ and $\sin\psi = p/\sqrt{m^2+n^2}$

The solutions of this equation are

$$\Delta + \phi = N\pi + (-1)^N\psi$$

According as N is even or odd,

$$\left.\begin{aligned}\Delta + \phi &= 2n\pi + \psi \\ \Delta + \phi &= (2n+1)\pi - \psi\end{aligned}\right\} \qquad 1.8$$

and

One series of roots corresponds to the maxima and the other to the minima. The quantities ϕ and ψ depend on the values of the optical constants of the reflecting surfaces.

The first interesting point about these solutions is that though the two series of roots are periodic of period 2π they are not equidistant because of the presence of the quantity ψ . This means that the minima are not half-way between consecutive maxima. Thus in contrast to the transmitted system, the reflected fringes, in general, are asymmetrical. Only under special conditions, the reflection fringes are symmetrical.

It is clear that the condition for symmetry (maximum half way between the minima) is that ψ should be zero. This gives the condition for symmetry as

$$\left.\begin{array}{ll} 1. & K = 2n\pi \\ 2. & K = (2n+1)\pi \end{array}\right\} \quad \begin{array}{l} n \text{ - an integer} \\ \text{or zero.} \end{array} \qquad \ldots\ldots 1.8a$$

For the symmetrical fringes

$$\Delta = 2n\pi \quad \text{or} \quad \Delta = (2n+1)\pi$$

where n is an integer or zero. The sign of $\frac{\partial^2 I_R}{\partial \Delta^2}$ determines which of the two sets of values determines the maximum and which gives the minimum. The results are summarised below.

When K is an even multiple of π, (case 1) $\Delta = 2n\pi$ gives a maximum and $\Delta = (2n+1)\pi$ gives a minimum. This means that the reflection maxima and minima occur at the same values of Δ as in transmission, and the reflected fringes have an appearance similar to the transmission fringes - <u>bright</u> maxima on a <u>dark</u> background.

On the other hand, when K is an odd multiple of π, (case 2) maxima occur at $\Delta = (2n+1)\pi$ and minima at $\Delta = 2n\pi$. Thus where there are maxima in transmission, there occur minima in reflection and vice versa. The fringes are <u>dark</u> minima on a <u>bright</u> background.

<u>Experimental observations</u>

The conditions mentioned above represent limiting cases to which actual conditions can tend. Holden[5] has

experimentally verified these conclusions using a wedge interferometer, studying the localised Fizeau fringes. [Multiple-beam Fizeau fringes developed by Tolansky[6]]. Experimental results obtained with Fabry-Perot fringes of equal inclination will be described now.

It is clear from the above discussion that the factor K governs the nature of the reflection fringes. K involves β_1, and β and hence essentially depends on the properties of the first reflecting surface i.e. the surface on which light is incident. By varying the optical constants of the first surface (changing R controls β_1, and β and hence K as well), the conditions 1 and 2, (eq 1·8a) for symmetrical fringes are achieved.

From eq. (1·5) it will be clear that the expression for the reflected intensity is not symmetrical in optical constants of the two surfaces AB and CD. The nature of the fringes will change, therefore, according to which of the two surfaces first receives light.

If the reflectivity of the front surface is changed, one obtains the following sequence described in Table I, starting with an uncoated glass as the first surface. Then according to Stokes Theorem, for this case $\beta_1+\beta = (2n+1)\pi$ Hence this falls in line with case 2. (eq 1·8a). The table I, applies to the particular case of silver and wave-length λ 5461.

TABLE I

Reflectivity of the first surface.	K	Position of the Maximum Δ	Position of the Minimum Δ	The nature of the fringes.
Glass (4%)	$(2n+1)\pi$	$(2n+1)\pi$	$2n\pi$	Symmetrical minima. Broad dark fringes on a bright background.
$4\% < R < 15\%$	$2n\pi < K < (2n+1)\pi$	$(2n+1)\pi \pm \psi$		Asymmetrical minima-maxima.
$R \sim 15\%$	$2n\pi$	$2n\pi$	$(2n+1)\pi$	Symmetrical maxima. Broad bright fringes on a dark background.
$15\% < R < 60\%$	$(2n+1)\pi < K < (2n+2)\pi$	$(2n+1)\pi \pm \psi$		Asymmetrical maxima-minima.
$R > 60\%$	$(2n+1)\pi$	$(2n+1)\pi$	$2n\pi$	Symmetrical minima. Narrow dark fringes on a bright background.

Fringes obtained with a Fabry-Perot interferometer in reflection under some of the conditions described in Table I, are shown on the opposite page. These are photographed with the green line λ 5461 from a vacuum mercury arc. Fig. 4 shows fringes obtained with the first surface having a reflectivity of about 15%. The gap is 6 m.m. These are bright maxima and have an appearance similar to the transmission fringes.

Fig. 5 shows fringes with the first surface having a reflectivity of about 25%. The asymmetry is clearly visible. The maxima and minima have approached one another closely, the minimum lying nearer to the maximum of the ~~higher~~ lower order than to those of the ~~lower~~ higher order. Fig. 6 shows the microphotometer trace showing the asymmetry. The gap is about 1·5 mms. and the fringes are near the centre.

Fig. 7 shows fringes obtained with a first surface having a reflectivity of about 80%. The fringes are sharp minima on a bright background. The gap is about 2 mms.

Fig. 8 shows the variation of K with R, the reflectivity of the first surface, for λ 5461.

This is in accordance with the results of Rouard[7] for silver and gold. He found a sudden jump in the value of β_1 at a value of the reflectivity of about 15% for silver. This explains the similar change in K.

FIG. 4

FIG. 5

FIG. 7

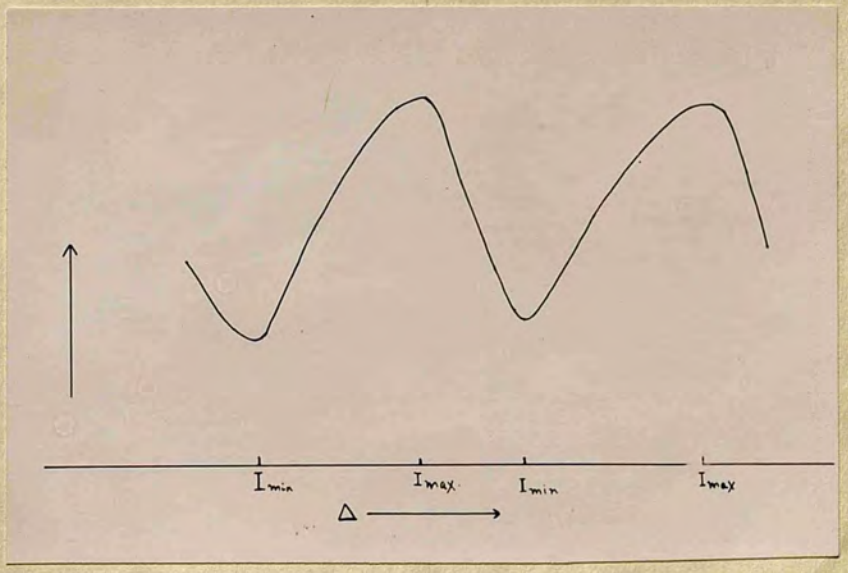

FIG. 6

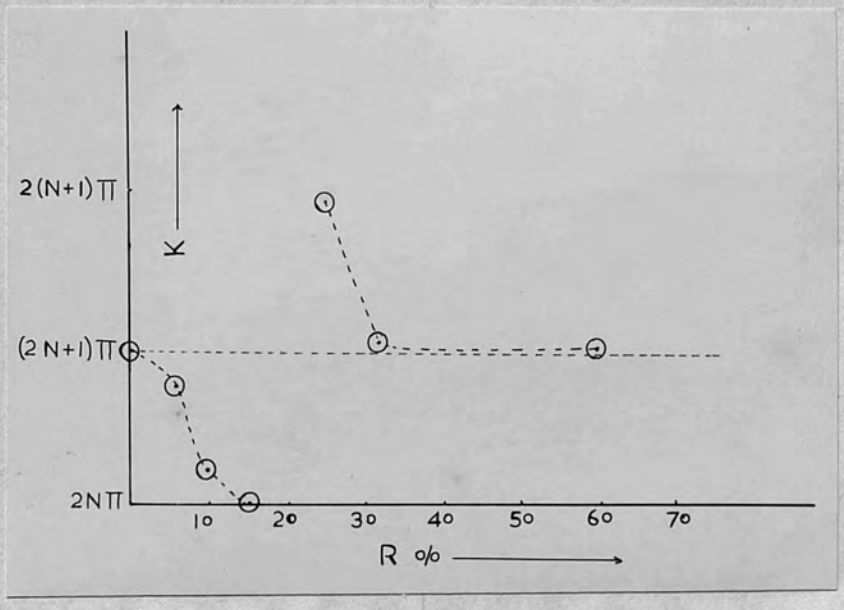

FIG. 8

From the above discussion about the reflection fringes, it is clear that only symmetrical fringes are of value from the point of view of using them for high resolution spectroscopic studies. As will be shown below, out of the three possible regions where symmetrical fringes occur, the last one for which the reflectivity of the first surface is greater than 60%, is of value for high resolution studies.

Consider first the "transmissionlike" reflection fringes which occur in the region of the first surface reflectivity of about 15% (silver). It is clear from Fig. 4, that they are not of use for high resolution work being broad. The gap is 6 mms. and the fringes are off-centre. This is of course exactly as one would expect. Even if the back surface has a reflectivity of 90%, the effective reflectivity of the interferometer plates, as far as resolution is concerned, would be $\sqrt{R_1 R_2}$ i.e. only 37%. This is in any case too low for a Fabry-Perot interferometer. It would be of interest if one could obtain a reflecting layer of a metal for which the transmission like fringes would occur at a higher value of the reflectivity of the first surface. As judged from Rouard's data, for gold this would occur at about $R = 20\%$.

Thus, it seems that the region of interest for a Fabry-Perot interferometer in reflection is between

$0{\cdot}6 < R < 1{\cdot}0$. Under these circumstances the expression for the intensity in the reflected system is much simpler.

This aspect will now be considered.

The Reflected System at High Reflectivities

When the reflection coefficient of the first surface exceeds 0·60, the fringes appear as fine minima (dark lines) on a bright background and these become sharper with increasing reflectivity.

It is clear from the previous discussion that in the range $0{\cdot}6 < R < 1{\cdot}0$, it can be taken as a good approximation that

$$K = (2n+1)\pi$$

As a further simplification, assume that the interferometer is symmetrical. Even if the two surfaces differ in reflectivity (say, first surface 80% and back surface 90%), one can still treat it as a symmetrical interferometer of reflectivity $R = \sqrt{R_1 R_2}$. It follows then from Eq 1·5, that

$$I_R = R\left[1 + \frac{T^2 + 2RT - 2T\cos\Delta}{1 - 2R\cos\Delta + R^2}\right] \qquad 1{\cdot}9$$

I_R is maximum for $\Delta = (2n+1)\pi$ and is given by

$$I_{R\text{-}max} = \frac{R}{(1+R)^2}(1+R+T)^2 \qquad 1{\cdot}10$$

Minima are given by for $\Delta = 2n\pi$, by

$$I_{R\text{-}min} = \frac{R}{(1-R)^2}(1-R-T)^2 \qquad 1.11$$

In the next chapter the properties of these fringes will be considered. They will be compared with the usual transmission Fabry-Perot fringes.

Chapter II.

COMPARISON BETWEEN THE TRANSMITTED AND THE REFLECTED SYSTEM

Transmitted System - Effect of Absorption

The expression for the intensity distribution within the transmitted fringes has been shown to be

$$I_T = \frac{T^2}{(1-R)^2} \cdot \frac{1}{1 + \frac{4R}{(1-R)^2} \sin^2 \frac{\Delta}{2}}$$

with

$$I_{max} = \frac{T^2}{(1-R)^2} \quad \text{and} \quad I_{min} = \frac{T^2}{(1+R)^2}$$

If there is no absorption, then $R+T = 1$. This gives $I_{max} = 1$, which means that the peak intensity is equal to that of the incident light, and is independent of R. This holds strictly for a symmetrical interferometer. If the reflectivities of the two surfaces differ, the peak intensity is less than unity, even in the absence of absorption. This can be easily seen from eq^{n} (1·2). Thus it is desirable to have the two surfaces of the same reflectivity.

This state of affairs is, however, far from what actually is realised. In practice, the silver films absorb light according to their thickness.

It is essential for the production of sharp fringes to have a high reflectivity but the increase in R can only be easily achieved by putting on thicker films. This, naturally, leads to greater absorption. It may be possible to push up the reflectivity without unduly increasing the absorption by deposition of suitable films of high and low refractive index upon the silver film. Such a technique is complex but Dafour[8] has succeeded in achieving a reflectivity, as high as 94%, by using the multilayer technique.

In Fig. 9, the curve on the right shows the intensity distribution for no absorption ($R = 0{\cdot}85$), while the curve on the left shows the effect of absorption of 4%.

If A is the fraction of light intensity absorbed during transmission through a film, then instead of $R+T=1$ one has to write $R+T+A=1$. This gives the peak intensity as

$$I_{max} = \frac{T^2}{(1-R)^2} = \frac{1}{(1+A/T)^2} \qquad 2{\cdot}1$$

The values of A and T are clearly determined by the value of R , and thus are also functions of the wave-length.

Table II gives the values of the reflection and the transmission coefficients as percentages measured for

FIG. 9

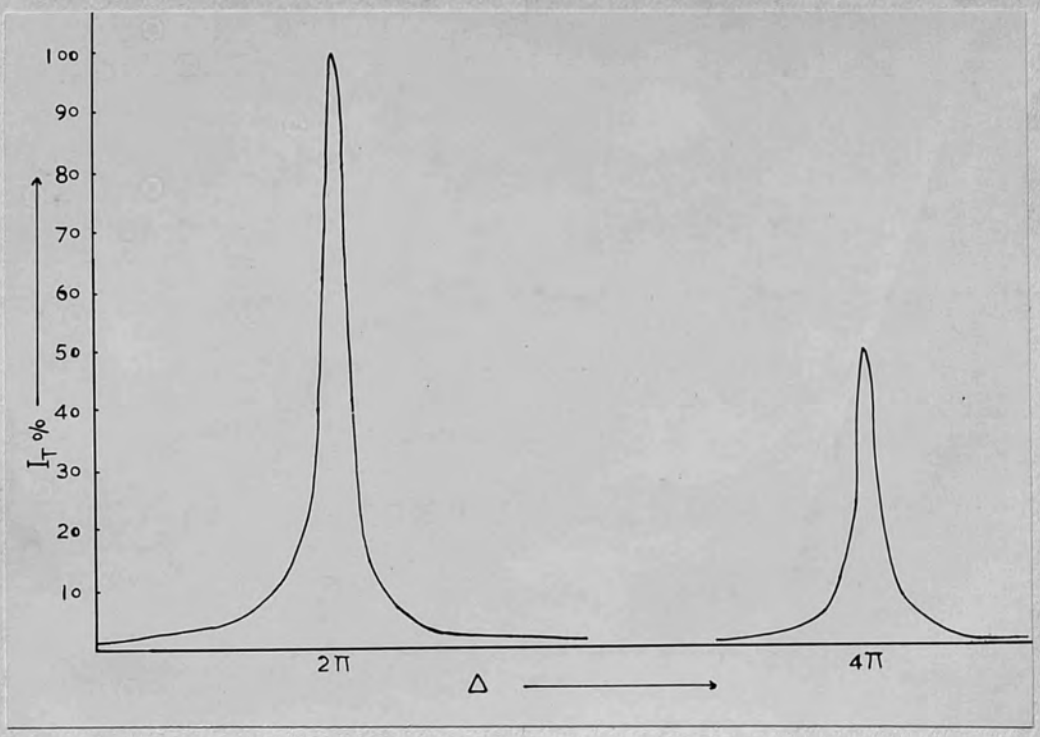
100
90
80
70
60
50
40
30
20
10
I_T %
2π
4π
Δ

FIG. 10

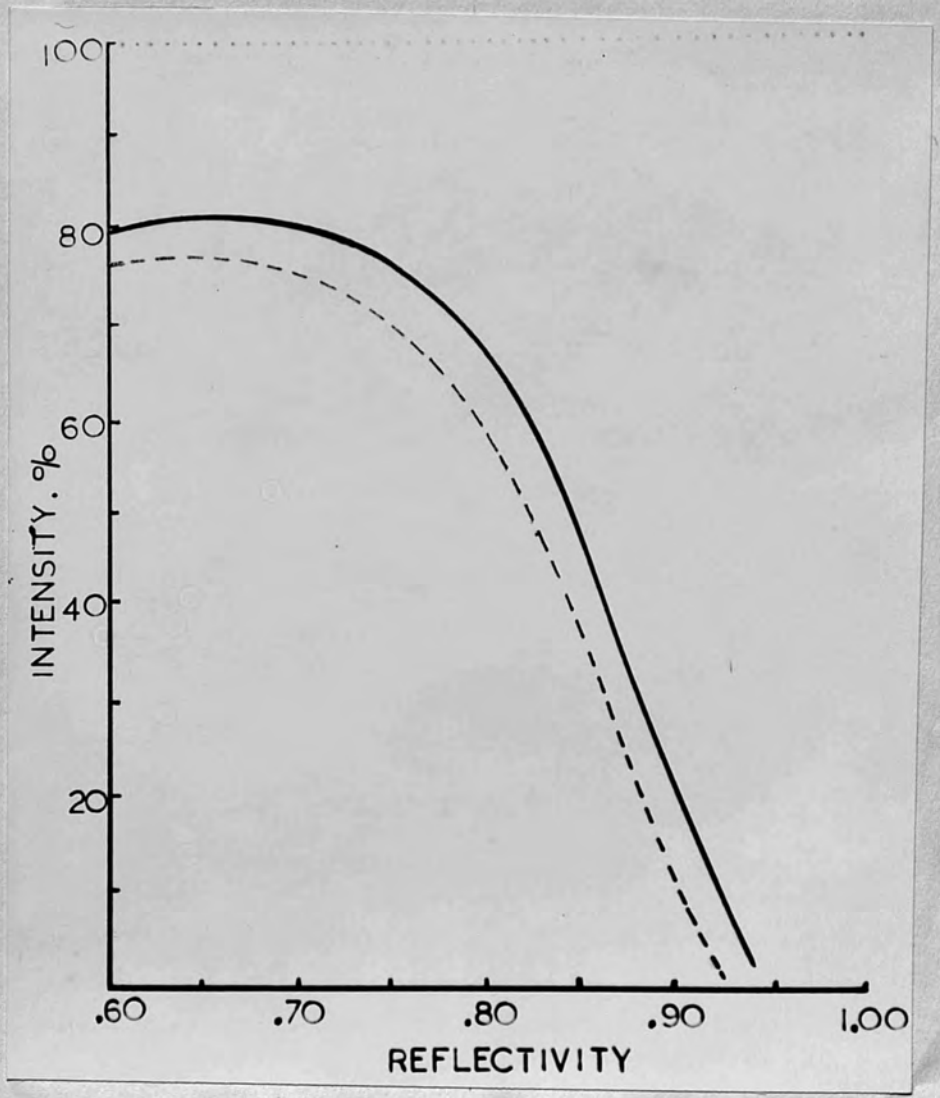
100
80
60
40
20
INTENSITY. %
.60
.70
.80
.90
1.00
REFLECTIVITY

silver films for λ 5461, as reported by Tolansky[2]. The last row gives the values of I_{max}.

TABLE II

R	60	70	75	80	85	90	94
T	35·5	27	22	16·5	10·5	4·5	0·7
A	4·5	3	3	3·5	4·5	5·5	5·3
$100 \times (1+A/T)^{-2}$	79	81	76	68	49	20	1·3

These values refer to fresh films produced by evaporation in vacuum. There are other data available in the literature and they are closely similar.

The manner in which I_{max} varies with R is shown in Fig. 10. The importance of absorption is clear, for with $A = 0$ the plot would have been the straight line parallel to the R -axis through the point corresponding to intensity of 100%.

The effect of a one per cent increase in absorption on intensity is shown by the dotted curve in the same Figure.

To achieve adequate fringe sharpness, it is necessary to have reflectivities in the region of 85 to 95% and it is apparent from the above mentioned graph, that there is a very rapid fall in intensity in this very important region. In practice, matters are often more than

those indicated in Fig. 10. Any increase in A displaces the curve to the left and quite a small addition to A makes a large alteration in the intensity at the critical end region. It is experimentally more difficult to produce silverings with low values of A than with high values of R . Indeed, technically, production of high R is an easy matter; mere increase of thickness is enough. To get films of low absorption, the conditions of deposition have to be critically regulated. There are several factors that go to increase the absorption of the film. Surface films on the flats, inadequate vacuum, impurities on the filament, atmospheric corrosion etc., all contribute to the increase in A . The figures quoted in Table II, refer only to freshly prepared films deposited under best conditions. Experience shows that such surfaces age quickly. This causes only a small percentage reduction in R , but the corresponding increase in A is often considerable.

Thus one finds that a good high definition Fabry-Perot interferometer rarely transmits more than a few per cent of the incident light, and a reduction by a factor of 30 is a common experience. At R = 90%, the peak intensity is 15% of that of the incident light, but at R = 94%, it is reduced by a further factor of 10. The corresponding decrease in fringe width is from $1/30$ to $1/50^{\text{th}}$ of an order.

This is the principle objection to this versatile instrument and often precludes its use for faint light sources. To this difficulty must be added the sensitivity of the instrument to variations in temperature, pressure, shock, and mechanical changes in the springs holding the flats etc. These are such that exposures over more than say, four hours, usually exhibit disturbances. Hence the importance of increasing the transmitted intensity and reducing the exposure time.

The Reflected System. Absorption.

It has been shown already that the maximum reflected intensity is given by

$$I_{max} = \frac{R}{(1+R)^2}(1+R+T)^2$$

This reduces to $\frac{4R}{(1+R)^2}$ in the absence of absorption

However, for an actual case, there is absorption and one has to use the relation $R+T+A = 1$. This gives,

$$I_{max} = \frac{R}{(1+R)^2}(2-A)^2$$

$$= \frac{4R}{(1+R)^2}(1-A+A^2/4)$$

$$= \frac{4R}{(1+R)^2}(1-A) \qquad 2.2$$

as a good approximation.

This is valid since A is small compared with unity. In the data quoted above, the maximum value of absorption is of the order of 0·05 and $A^2/4 << A$

Thus the value of I_{max} obtained in the absence of absorption, is decreased by an amount $4AR/(1+R)^2$ on account of the presence of absorption.

The effect of absorption on the minima is much more pronounced. The value of I_{min} is

$$I_{min} = \frac{R}{(1-R)^2}(1-R-T)^2$$

This reduces to zero for $A = 0$. For values of A , other than zero, it is given by

$$I_{min} = \frac{R}{(1-R)^2} \cdot A^2 \qquad 2.3$$

using the relation $R+T+A = 1$.

In Fig. 11 the curve on the left shows the intensity distribution for no absorption ($R = 0{\cdot}85$). It is complimentary to the intensity distribution in transmission. The curve on the right depicts the effect of absorption.

In Table III, are given the values of I_{max} and I_{min} for various values of the reflectivity R . The second column gives I_{max} as calculated from values of R , T and A taken from Table I. The third column gives the values of I_{min} while the fourth column gives the values of I'_{min} calculated assuming an increase of one per cent in absorption.

FIG. 11

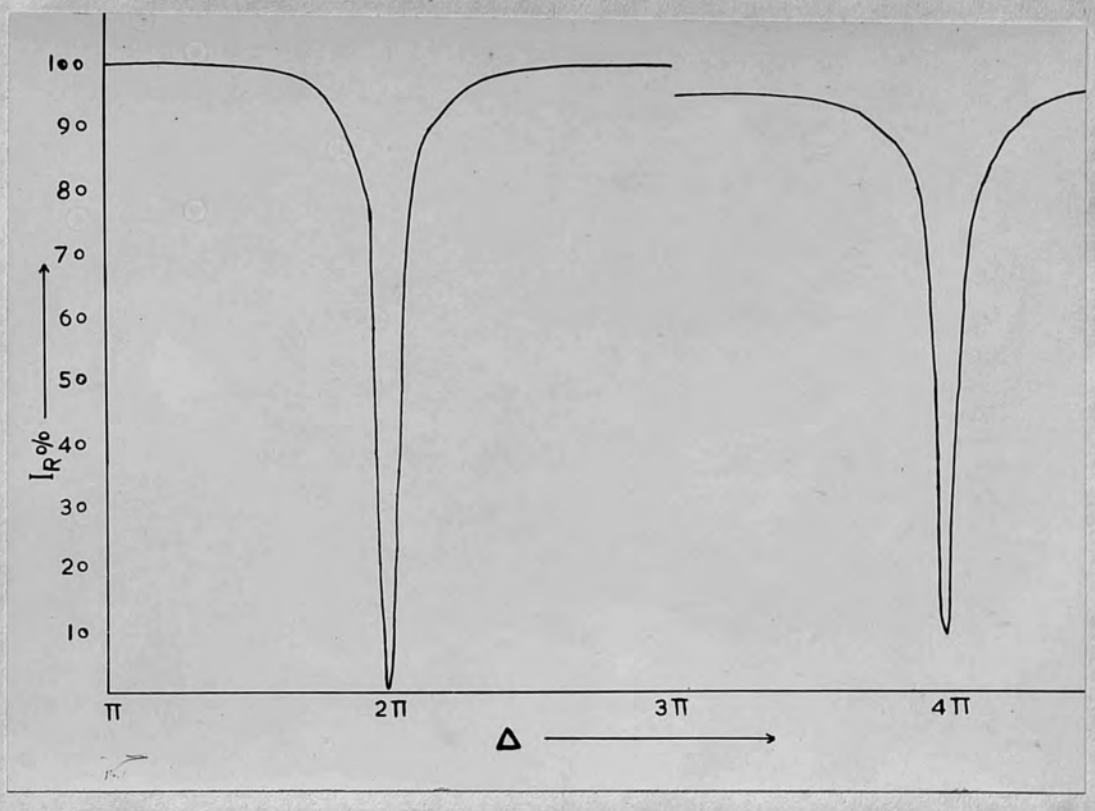
100
90
80
70
60
50
40
30
20
10
I_R%
π
2π
3π
4π
Δ

FIG. 12

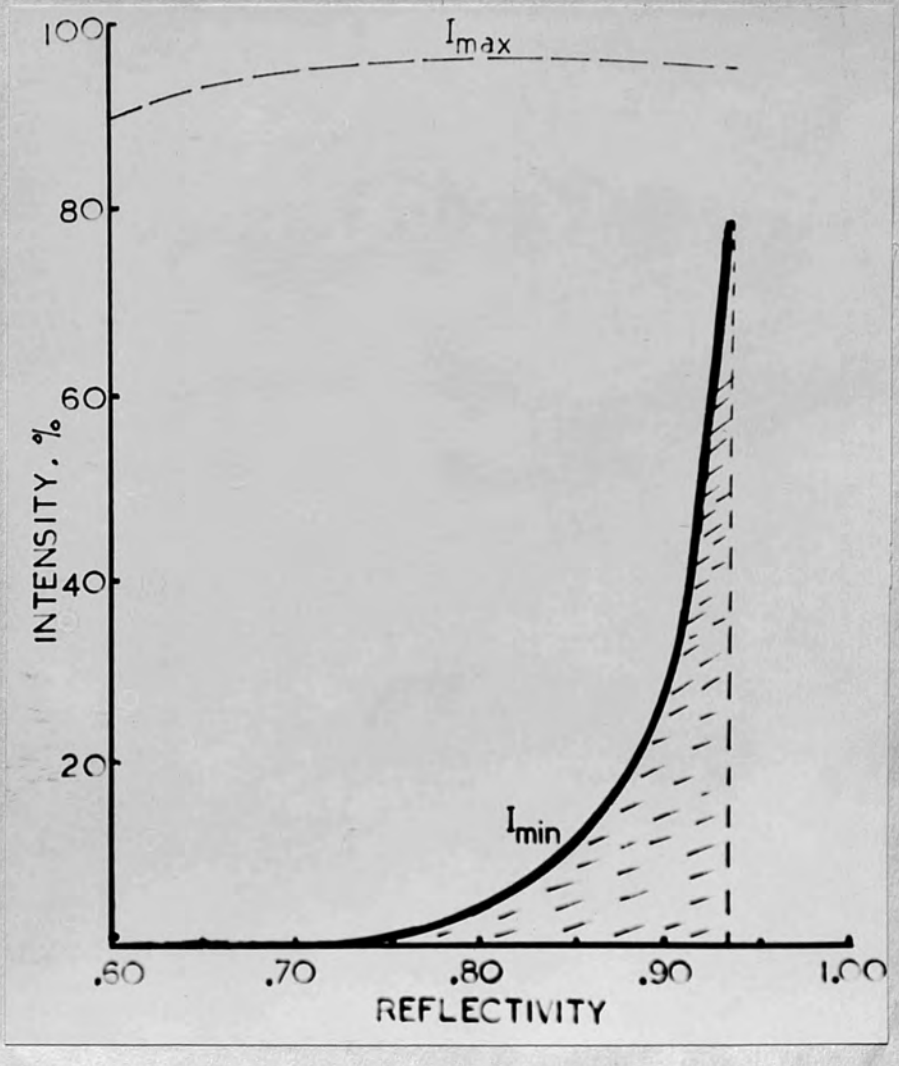
100
80
60
40
20
INTENSITY, %
I_{max}
I_{min}
.60
.70
.80
.90
1.00
REFLECTIVITY

TABLE III

R	60	70	75	80	85	90	94
I_{max}	·89	·94	·94	·95	·95	·93	·93
I_{min}	·007	·01	·01	·02	·08	.27	·76
I'_{min}	·01	·01	.02	·04	·13	·38	·93

In the absence of absorption, I_{max} is very nearly unity for high reflectivities. Indeed even if R is as low as 70%, I_{max} has only fallen to 0·97. The maximum in the presence of absorption is then not much different from unity. Table III shows that for 80 to 85% reflectivity, the maximum intensity is merely some 5% less than that of the incident light while in transmission the maximum for the same case is reduced by at least 50%. This clearly shows the light efficiency of the reflection fringes. The interferometer introduces practically no loss of light. These results are graphically represented in Fig. 12. The dotted line shows the plot of I_{max} against R while the full line shows the plot of the values of I_{min} against R

Visibility of the Fringes

The 'visibility' or contrast is defined, as is customary, by the expression

$$V = \frac{I_{max} - I_{min}}{I_{max} + I_{min}} \qquad 2.4$$

For transmission fringes, it is given by

$$V = \frac{2R}{(1+R^2)} \qquad 2.5$$

The change of visibility with R is shown in Fig. 13 - curve A . It is a parabolic curve with the visibility only increasing from 0·8 to 1 as the reflectivity increases from 50 to 100%. Thus the visibility is not much affected by R and is independent of the absorption.

On the other hand, the visibility of the reflection fringes is sensitive to absorption. Though absorption has very slight effect on the intensity of the maximum, it has a considerable effect on the visibility.

In Fig. 13 curve B shows the variation of the calculated values of the visibility with R . It is clear that for values of R above 80%, the drop in visibility is rather rapid. From Fig. 12 or Table II, it is seen that whereas the minimum is of the order of only 1% of the intensity of the maximum for reflectivities below 75%, it rises rapidly and at a reflectivity of 94% it is as great as 80% of the maximum. This can be interpreted as meaning that as the reflectivity increases the effect of absorption is to decrease the visibility of the fringes. The fringes are dark lines on a bright background. It is as if, the dark fringes are diluted by the addition of light represented

FIG. 13

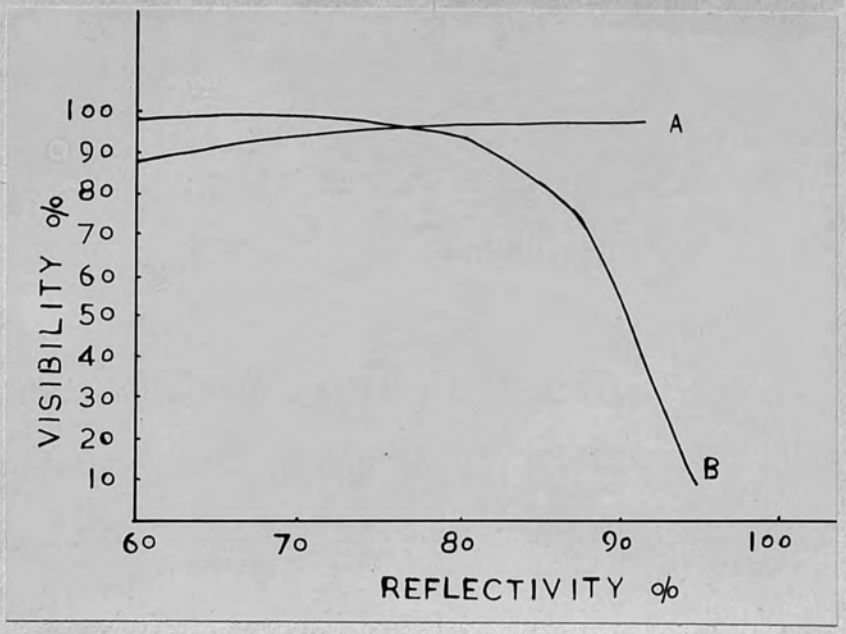
VISIBILITY %
100
90
80
70
60
50
40
30
20
10
A
B
60
70
80
90
100
REFLECTIVITY %

FIG. 14

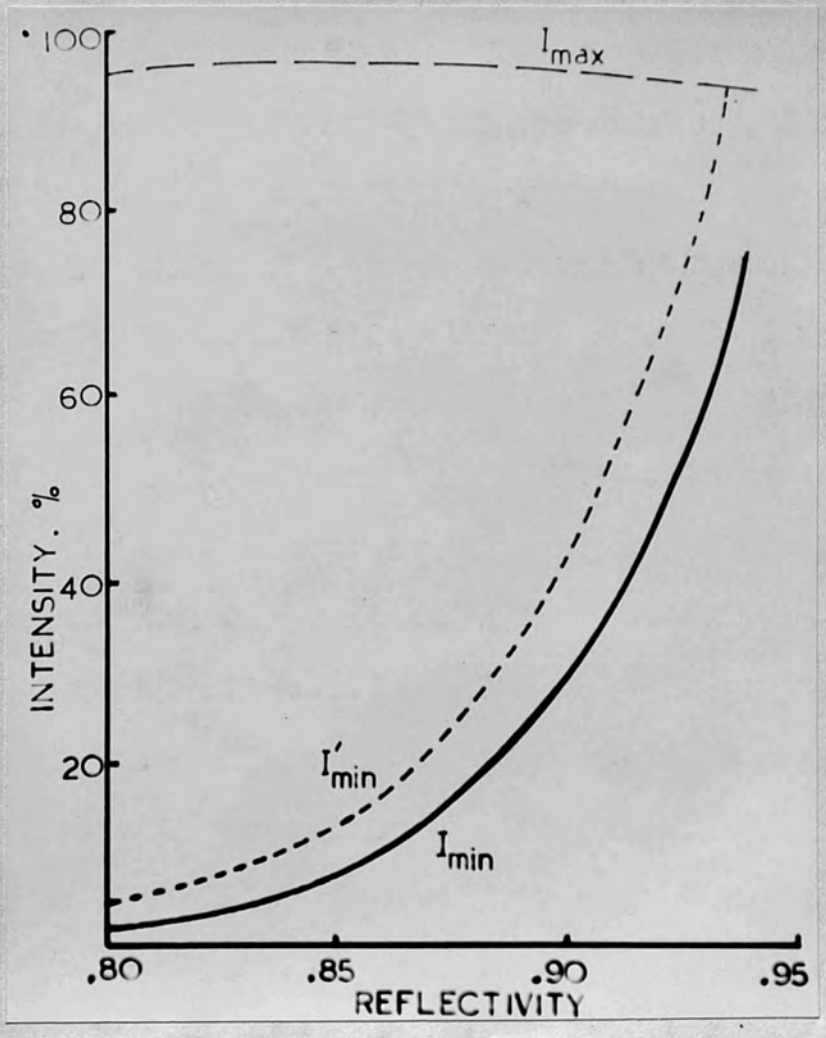
100
80
60
40
20
INTENSITY. %
I_{max}
I'_{min}
I_{min}
.80
.85
.90
.95
REFLECTIVITY

by the shaded region below the curve of minima in Fig. 12. It can also be said that the intensity in a dark fringe approaches that of the background as R increases, and hence contrast suffers. Fig. 14 shows the higher reflectivity region of Fig. 12, with an additional curve shown dotted. This is to show the effect of a one per cent increase in absorption on the visibility. In this case the increased absorption may make the fringes for R above 90% not visible at all. This point is emphasised to show that great care is needed to avoid undue absorption in the preparation of silver films for reflection technique.

Sharpness of the Fringes

It is usual to assess the sharpness of the fringes in terms of their half-width. By the half-width of a fringe is meant the width (which may be expressed as a fraction of an order) between two points on the intensity distribution curve (shown in Fig. 9 and 11) where the intensities are half that of the maximum intensity.

Half-width in transmission

The intensity distribution is

$$I = \frac{I_{max}}{1 + F \sin^2 \frac{A}{2}}$$

where

$$F = 4R/(1-R)^2$$

If Δ corresponds to a point where

$$I = I_{max}/2$$

we have

$$1 + F \sin^2 \frac{\Delta}{2} = 2$$

If Δ is small, (this is usually the case for high reflectivities) one gets as a good approximation

$$\text{Half-width} = 4/\sqrt{F}$$

Thus in transmission sharpness depends only on R and is independent of absorption. We follow a similar method to calculate the half-width in case of the reflection fringes.

Eq. (1-9), which gives the intensity distribution in reflection fringes, can be written in the form

$$I_R = R\left[\frac{1 + (R+T)^2 - 2(R+T)\cos\Delta}{1 - 2R\cos\Delta + R^2}\right]$$

with

$$I_{max} = \frac{R}{(1+R)^2}(1+R+T)^2$$

Again, if Δ corresponds to a point for which $I = I_{max}/2$ we get

$$\frac{R}{(1+R)^2}(1+R+T)^2 = 2R\left[\frac{1 + (R+T)^2 - 2(R+T)\cos\Delta}{1 - 2R\cos\Delta + R^2}\right]$$

This gives

$$\cos\Delta = \frac{(1+R)^2\left[1 - (A - A^2/2)\right] - (1+R^2)\left[1 - (A - A^2/4)\right]}{(1+R)^2\left[1 - A\right] - 2R\left[1 - (A - A^2/4)\right]}$$

after the substitution $R+T+A = 1$. Here again, if A is of the order of ·05, $A^2/2$ or $A^2/4$ will be small compared to A and can be neglected.

Then

$$\cos\Delta = \frac{2R}{1+R^2}$$

This gives the half-width as

$$\text{Half-width} = \sqrt{\frac{4R}{1+R^2}} \cdot \frac{4}{\sqrt{F}}$$

The above approximation is only valid, provided A is small and hence this emphasises again the necessity of great care to keep down absorption. In this case, the sharpness is independent of A and depends only on R as in the case of the transmission fringes.

Choice of Proper Reflectivities for the Reflection Technique.

The above discussion makes the following points clear. Firstly, to get sharp fringes the reflectivity should be as high as possible. Secondly, in order to have good visibility, the absorption should be low, and hence the first surface reflectivity cannot be increased much. From the visibility curve it is seen that a reflectivity of about 75% gives maximum visibility. Thus the two considerations are in opposition and a compromise is to be

achieved. It is clear that at low reflectivities one obtains broad fringes with excellent contrast while at high reflectivities one obtains narrow fringes with a poor contrast.

The fact that, for good visibility it is necessary to keep the reflectivity of the first mirror low, can be to some extent compensated for by making the reflectivity of the back surface as high as possible, - higher than that permissible in a transmission instrument. If a Fabry-Perot interferometer consists of two different mirrors with reflectivities R_1 and R_2, then the resolving power of the combination is, as a good approximation, equal to that of a symmetrical interferometer with reflectivity

$$R = \sqrt{R_1 R_2}$$

Thus, by making the back mirror so thick as to be practically opaque, a reflectivity $R_2 = 95\%$ may be obtained. This, when combined with a first surface with reflectivity $R_1 = 80\%$, would be equivalent to a symmetrical interferometer having a reflectivity of 87%. This is adequate for many purposes and gives excellent fringes. Even if one chooses R_1 to be 75% in order to have best visibility, the combination gives a reflectivity of 84% which is quite good.

With either of these values for R_1, it is seen that the conditions of visibility are good, whereas with the normal values $R_1 = R_2 = 90\%$, used in transmission, visibility in

reflection is poor. That is the reason, why an ordinary transmission instrument does not give good reflection fringes.

Chapter III.

EXPERIMENTAL TECHNIQUE

The Experimental Arrangement.

There are three possible methods which can be adopted for using the interferometer in reflection in conjunction with a spectrograph. These are shown in Figs. 15, 16, and 17.

In Fig. 15 an image of the source is formed by an achromatic lens on to a prism which is either above the spectrograph slit or to the side of it. A parallel beam of light is thrown on the interferometer by another achromat. The same achromat returns the light back to the spectrograph slit and focusses the fringes on to it. This may be described as an external beam mounting.

Fig. 16 shows, what may be called, an internal mounting. It is a Littrow mount in which the usual mirror is replaced by the interferometer. This arrangement is difficult to make with the usual built in type of spectrograph available in the laboratory.

Fig. 17 illustrates a most economical form of mounting. In this, a 30° Littrow prism is used and the silvered face of it forms one of the plates of the interferometer. Thus only one flat is required. However, the

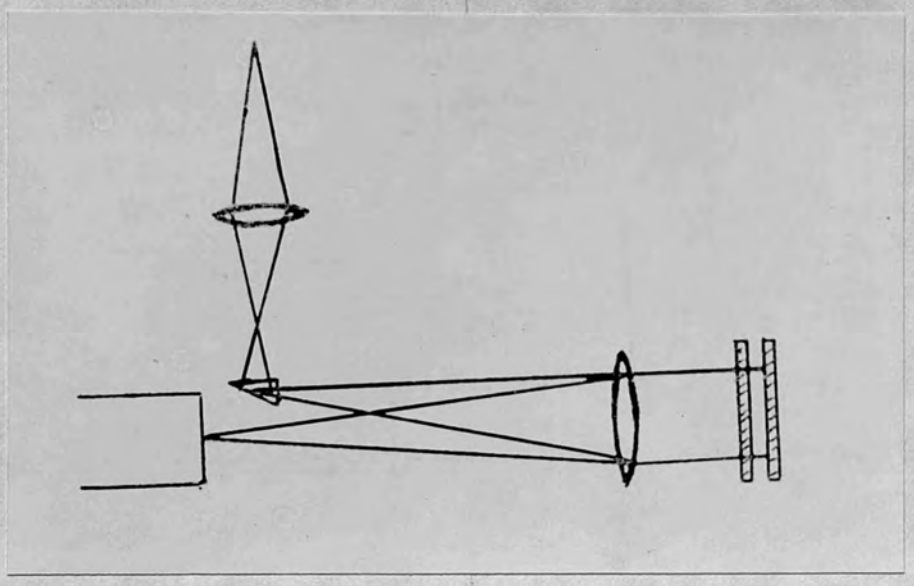

FIG. 15

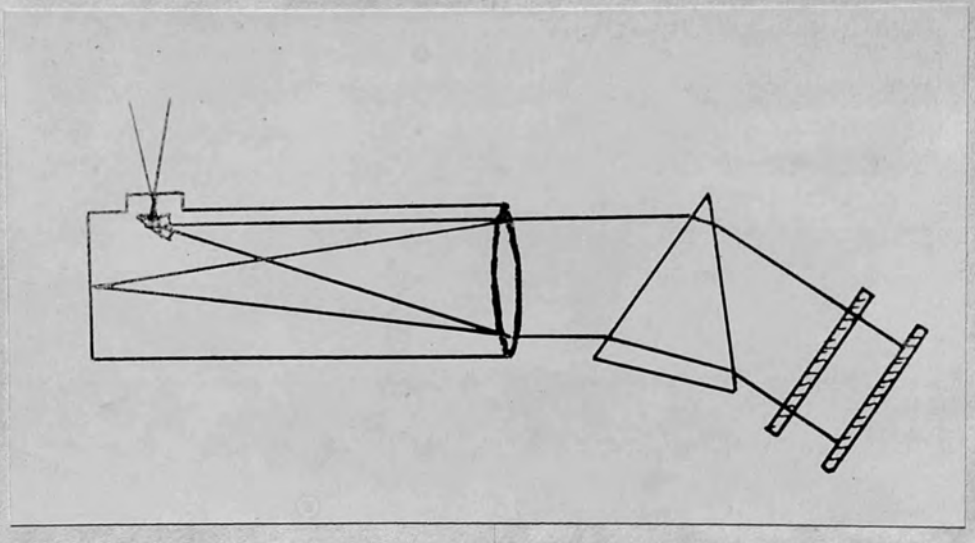

FIG. 16

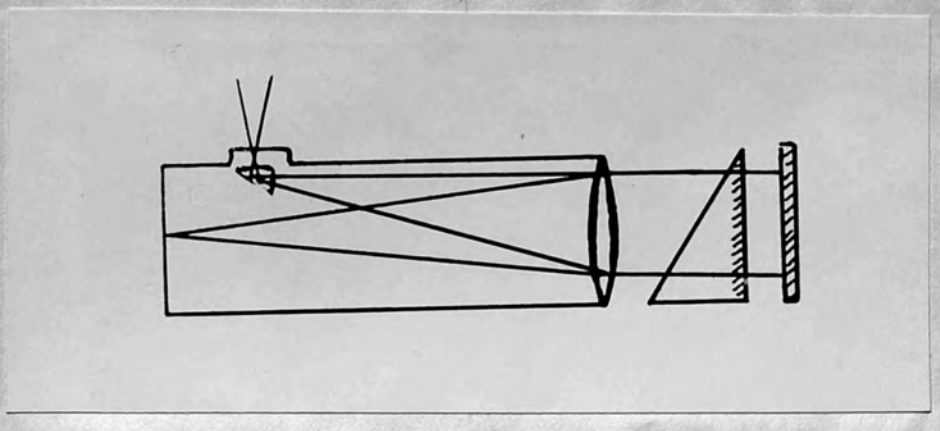

FIG. 17

prism face will have to possess the high degree of flatness demanded by an interferometer. The faces of prisms, generally used in spectrographs, are not sufficiently accurate to act as a good optical flat. Both the arrangements, shown in Figs. 16 and 17, suffer from the defect that only wave-lengths at minimum deviation show a symmetrical fringe pattern. In addition, one cannot tilt the interferometer to get fringes off centre.

In the present work, the arrangement shown in Fig. 15 is used with slight modification in detail. Instead of one, two prisms are used above the spectrograph slit so as to turn the beam from the source through 180°, and then it is thrown as a parallel beam by an achromat on to the interferometer slit. This enables the source to be kept on the same axis as the interferometer itself, except that it is displaced vertically upwards so that its image is thrown on to the top prism. The achromat which serves the double purpose of producing a parallel beam, and focussing the fringes on to the slit has a focal length of 40 cms.

The Fabry-Perot mount is of the standard type and is shown in Fig. 18. The different parts are clearly marked. One of the flats rests on three equidistant pressure points. Over this is placed, a ring spacer in the form of a brass ring with three equidistant projecting invar rods fixed in

1. OPTICAL FLATS
2. SPACER
3. BRASS RING. 3 PT. CONTACT.

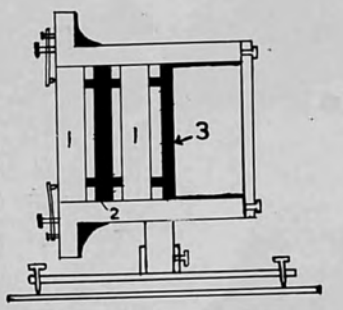

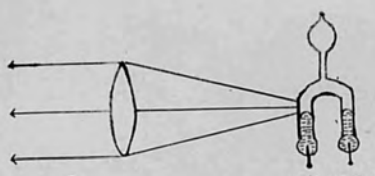

FIG. 18

it. For small separations, selected steel balls serve as well. The second flat rests on this with its silvered surface facing that of the first one. A brass ring with three plane projecting studs is lightly pressed against this so that the projecting points are in line with the spring contacts. Finally a brass ring and a top ring screwed in the outer metal casing hold everything in position. The metal case can be rotated about a vertical axis. The interferometer can be tilted off the horizontal axes by adjusting the levelling screws in the base plate.

The interferometer plates are adjusted to be accurately parallel to each other by the usual method, using a mercury arc as a source.

Spectrograph

In the present work as well as for the work described in the second part, a Hilger automatic Quartz-glass spectrograph is used.

The instrument is of a Littrow type with two interchangeable optical trains, one, a quartz prism with a quartz lens and the other a glass prism with a glass lens. The slit and the focal plane are at the same end of the housing whilst at the other end there is an objective which serves as both a collimator and a camera lens. The prisms are of angle 30° and have a reflecting back face. Each of the lenses has a focal length of about 170 cms., and a diameter of about 75 mms. The aperture is f/24.

The slit is symmetrical and is adjustable by a thimble drum having 50 divisions marked on it, each division being equal to 0·005 mm. This permits a very accurate setting. The slit tube can be adjusted by means of a capstan ring. This moves the slit relative to the camera head, thus providing a focussing adjustment. A millimetre scale can be photographed as a reference and serves as a wave-length scale in conjunction with a dispersion curve. The plate holder takes plates 25 cms. long and can be moved up and down, its position being set every mm. In all spectrographs of the Littrow type, a certain amount of fog is caused by the reflection of light from the two surfaces of the lens. A narrow mask is placed in front of the lens to avoid this.

The range of the spectrum obtained with the glass prism is from λ 3700 to 12000 A°. and is covered in two settings. The average dispersion at λ 6200 A° is 20 A° per mm. The quartz prism gives a spectrum from λ 1900 to 8000 A°, the average dispersion at λ 4000 being 13 A° per mm.

Since neither of the lenses is achromatic, the following adjustments are necessary in order to obtain a given region of the spectrum in good focus.

a. The focus of the lens.

b. The inclination of the prism to the lens axis.

c. The tilt of the plate-holder.

In this spectrograph, all these adjustments are done automatically in one operation by turning a single wheel at the camera end of the spectrograph. This wheel works a rack and pinion which makes all the three adjustments simultaneously for a given setting. Near the wheel is a drum marked with two sets of wave-length scales, one for quartz and the other for glass. One can also change easily from quartz to glass or vice versa by turning a handle.

The instrument was adjusted in the usual way. The wave-length range scale was set so as to photograph the spectrum up to λ 8000 A$^{\circ}$ with the quartz optic and the slit was illuminated with an iron arc. A series of exposures were taken corresponding to different positions of the slit as controlled by the capstan ring. From this, the position of best focus was determined. A similar procedure was followed for the glass optic.

The base of the spectrograph takes a bar which forms a rigid support upon which accessories such as a condensing lens, a Fabry-Perot interferometer or a Lummer-plate could be placed in exact alignment with the spectrograph axis. This bar is fitted with bolts to the base of the main instrument and forman integral part of it. The spectrograph is mounted on a solid foundation consisting of a slate bed supported on strong brickwork piers. This reduces vibration troubles.

Microphotometer

A Hilger microphotometer is used to determine the shape of fringes. The instrument is shown in Fig.19.

The image of a 6 volt-18 watt lamp with a straight filament is focussed on to the photographic plate with a microscope objective. A second objective projects an image of the line on the plate on to a slit with a magnification of ten diameters. Behind the slit, is a selenium barrier layer photo cell.

The slit has symmetrically opening jaws controlled by a peripheral milled ring, calibrated in divisions of $1/50$ mm. Thus a single division on the scale corresponds to two microns on the image on the plate.

The plate can be moved by a accurately worked screw and the movement can be read on a drum up to $1/200$ mm.

The recording galvanometer has a sensitivity of 5×10^{-10} amp/mm. The readings can be noted on a screen with a magnification equivalent to that of a scale at a distance of two metres in an ordinary mirror-scale arrangement. The galvanometer is supported on an allegedly vibrationless support. However, it is found that operation of the plate carriage causes a vibration of the image if the microphotometer and the recording unit are on the same table. It is preferable to have two separate supports or alternatively a very rigid support in the form of a slate bed supported on brick piers.

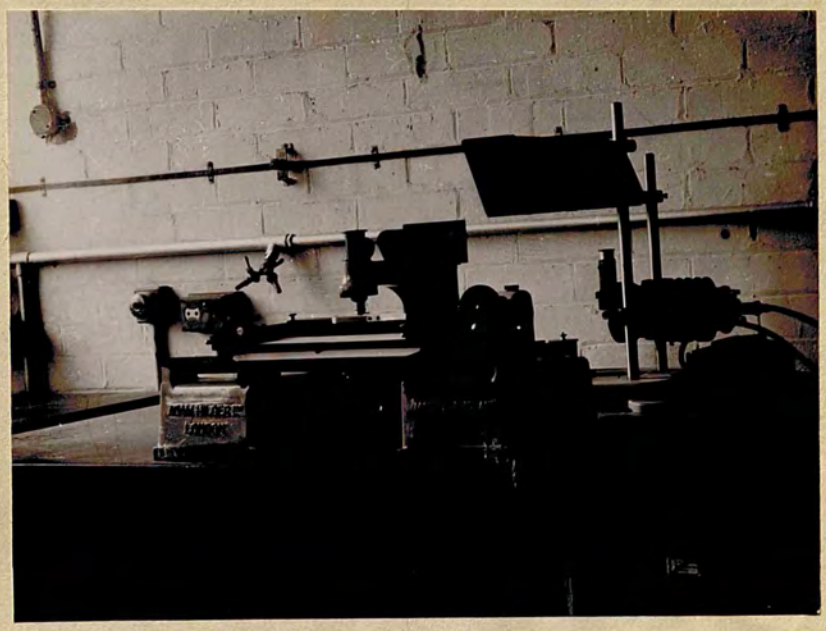

FIG. 19

It is essential that the intensity of light given by the photometer lamp should remain constant during a set of readings. A large capacity (6 volt) accumulator was directly connected to the microphotometer terminals. It was charged at about 5/6th of the discharge rate during the operation.

The lamp takes some time to settle down and so it was always switched on at least 15 minutes before starting a set of readings.

Preparation of Reflecting Surfaces

In this and the work to be described in Part II, the semi-transparent highly reflecting mirrors are prepared by evaporation in vacuum. In the evaporation process, the coating material is heated in a vacuum and the evaporating molecules, unimpeded by gas molecules, radiate in straight paths until they strike a surface upon which they condense to form a thin film. High vacuum is essential for the process in order (a) to avoid oxidation or decomposition; (b) prevention of random distribution of evaporating molecules by gas collisions.

A commercial evaporation plant supplied by W. Edwards & Co., is used in the present work. Fig. 2D(a,b) shows the essential parts of the plant. It consists of a pyrex glass work chamber 46 cms. in diameter and 60 cms. high. This rests upon a plated steel base A and makes a

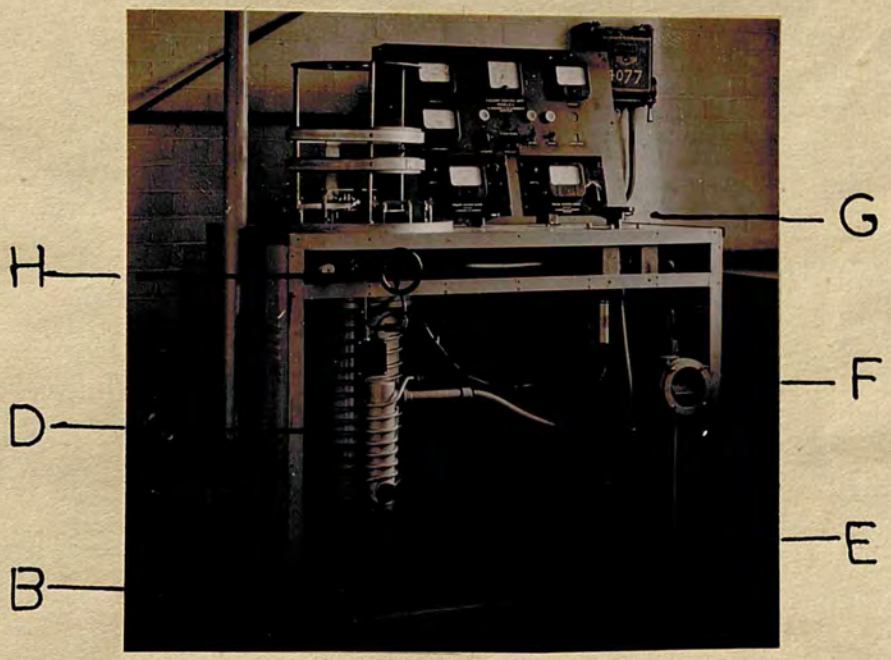

FIG. 20 a

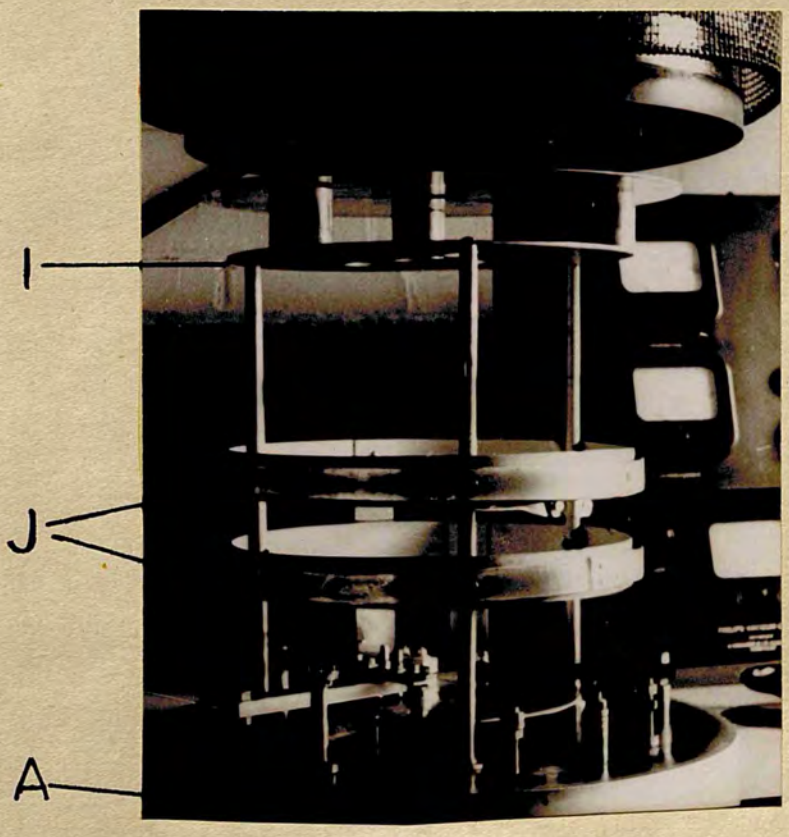

FIG. 20 b.

vacuum seal by an L -shaped gasket. The chamber can be lifted by a hand winch B.

The pumping system consists of a high speed oil diffusion pump D with a pumping speed of 1000 litres/second. This is backed by a mechanical pump E with a speed of 10 litres/sec. There is a moisture trap ($P_2 O_5$) F, and a three way bypass valve G which allows the mechanical pump to be directly connected to the chamber for preliminary evacuation. It also serves to isolate the rotary pump from the chamber and the diffusion pump. The chamber is connected to the diffusion pump through a vacuum valve H. There is an air release valve and a needle valve to serve as a fine leak, if required.

The evaporating sources are heated by a transformer (20 volts-150 amps.) whose output is controlled by a Variac, and an ammeter gives the heating current. High tension for ionic cleaning is provided by an H.T. transformer, (3300 volts-500 milliampers) the input to which is also controlled by a variac, and an ammeter records the current in the primary.

The work-table itself consists of an aluminium disc I held by vertical bench supports. The disc carries various sized holes on which specimens can be placed. The distance of the specimen is 35 cms. from the source.

Aluminium is used for all construction inside the chamber to avoid sputtering. On top of the work table, rests a disc of glass supported on three aluminium cylinders. This helps to keep the top of the chamber clean, and by looking through it estimation of reflectivities can be made. The aluminium rings J serve as electrodes for the high tension discharge used for cleaning.

The vacuum is tested by two gauges, - a Pirani gauge in the backing line which serves as a check on the pump performance, whilst the pressure in the work chamber is given by a Phillip's ionisation gauge of the cold cathode type having a range from 0·1 to 5 microns. The lowest pressure reached is less than 0·05 micron.

Evaporation Process

The glass or quartz flats have to be thoroughly cleaned since absorption depends so much on traces of impurity. As the flats are accurately worked, drastic chemical cleaning must be avoided, and caustic agents should not be employed. After preliminary cleaning with soap and water, the flats are further cleaned by Hydrogen Peroxide. This is an excellent solvent for many organic materials and also removes silver coatings from mirrors which require re-silvering. The cleaning is best done by gentle rubbing with absorbent cotton using a circular motion. A sensitive test of the state of cleanliness of the surface is afforded by the

"breathing test". If one breaths gently on to the surface, a clean surface, free even from monomolecular fatty acid films, condenses the moisture in a continuous invisible film. Slightest trace of grease gives a grey appearance to the film. This is the condition usually present after cleaning. The monomolecular layer is removed by ionic bombardment only. Thus ionic discharge is of importance as the most reliable and final cleanser. To remove aluminium from aluminised quartz flats, hydrochloric acid is useful.

For silver molybdenum filaments are suitable while for aluminium, tungsten is preferable as a filament material. The final cleaning is done by ionic bombardment. When the pressure is down to about 5×10^{-5} mm. of mercury, the material is evaporated using a current of 100 to 130 amperes. The material is prefused before final evaporation and during this process a screen is inserted between the filament and the specimen. Prefusing helps to remove the oxide layers on the filament, if any.

The rate of evaporation is also of consequence. If the material is evaporated rapidly, it is found that the film has higher reflectivity than for one formed by slow evaporation. This aspect has been studied in detail for aluminium by Crawford and Gray[9]. They find that films evaporated quickly, say in 10-20 sec., show higher

reflectivity though an electron microscopic study reveals a non-uniform mottled appearance. In contrast, films formed slowly (30 min. to two hours) are uniform but of low reflectivity. It is found that films of silver deposited quickly (10 to 15 sec.) are superior.

Chapter IV.

APPLICATIONS

It is the object here to discuss the possible applications of the reflection fringes to various problems where high resolution instruments are commonly used. The primary advantage of the reflection fringes, as has been shown by comparison with the transmission fringes, is their light efficiency - the intensity of the maximum being practically the same as that of the incident light.

The possible applications are:

(a) Hyperfine structure in spectral lines.

(b) Wave-length determination and line width estimation.

Fig. 21 shows the reflection fringes with neon. The source is a discharge tube filled with pure neon at a pressure of about 1 mm. The excitation is by means of an external electrode connected to a high-frequency oscillator generating a wave-length of some 20 metres. The oscillator is described in part II. The slit is broad and the lines in the region λ 5800 to λ 6400 A^{o} are photographed. The lines appear with dark reflection fringes crossing them. The interferometer gap is 3 mms. and the exposure time is less than one second. In contrast to this the corresponding

Ne

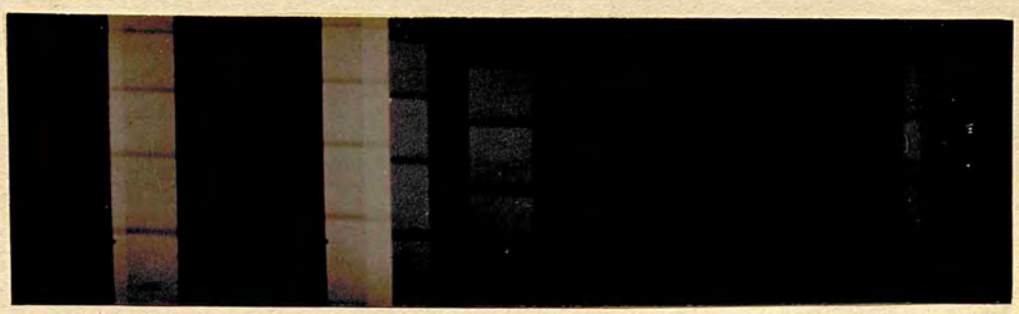

FIG. 21

Ne

FIG. 22

transmission fringes obtained with the same source and shown in Fig. 22, require an exposure of 40 sec. to 1 minute at least. The light efficiency of the reflection fringes is about 40 times as great.

As is seen from the picture, there is an excellent contrast (good visibility) and the fringes are sharp. For the gap used (3 mms.) the resolving power is a quarter of a million and the separation between orders is 1·66 cm.$^{-1}$ or 0·4 of an angstrom unit approximately. Neon has no effective nuclear spin hyperfine structure.

In Fig. 23, fringes given by the green and yellow lines of mercury (λ 5461, 5770 and 5790 A°) are shown. The source is a high frequency discharge in mercury vapour. The fringes are sharp and single for the line λ 5461. It is known that this line has a structure due to the nuclear spin. However, the picture does not reveal the structure. The reason is as follows: When a line consists of more than one component, the bright backgrounds of the different fringes are super-posed and the minima are lost in the bright background except that which belongs to the central brightest component. Thus it seems that the reflection fringes are not capable of revealing hyperfine structure in general. However it may be possible to observe a structure in a very limited manner. The first condition would be that the components should have comparable intensity. Secondly, the

FIG. 23

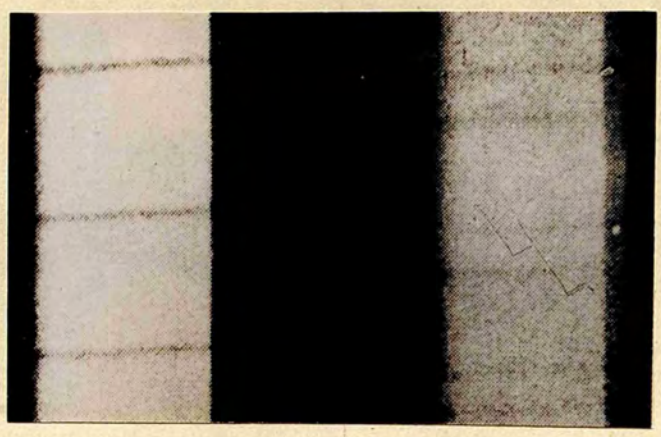

Hg.

FIG. 24

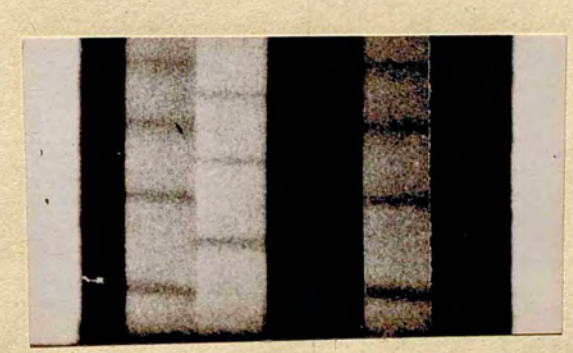

Fe.

number of components should be small otherwise, the superposition would be complex and the visibility would suffer. It should be possible to detect a neighbouring component of comparable intensity. In the illustration showing mercury fringes with the two yellow lines the slit width has been deliberately increased so that the two lines overlap. This corresponds to a condition where the preliminary dispersion of the spectrograph fails to resolve the lines. In the region of overlap twin fringes corresponding to the two yellow lines are visible.

Wave-length Determination and Line Widths.

With sharp fringes as are obtained with neon, it should be possible to determine wave-lengths with a precision to better than 0·001 A.U. Of course, for comparison, standard wave-lengths have to be used in the usual manner. The fringes will require to be photographed with their centres thrown on to the slit and then the method of exact fractions can be followed. Even when the line happens to be complex, by making the interferometer gap small enough, the structure can be compressed into a single fringe and that will give the average wave-length of the line concerned. In Fig. 24, are depicted the fringes given by some lines from an iron arc spectrum. Provided the preliminary dispersion is sufficient, reflection fringes can be easily

obtained with a many lined complex spectrum. It is also well known that the wave-lengths of iron arc lines are many a time used as secondary standards, to calculate the separations of the interferometer. Of course, the primary standard is the red cadmium line. The fringes, as is clear from the plate, are much broader than those obtained with neon and mercury sources. This brings out another quality of these fringes. They are quite sensitive for showing the line-width inherent in the nature of the source of the lines. This aspect is discussed in detail below. It is important to note here that these fringes are not meant to replace the versatile transmission fringes wherever they are available. It is only in cases, where the intensity considerations preclude the use of a transmission Fabry-Perot interferometer, that the reflection fringes should be tried. The first possible field of application seems to be astronomical spectroscopy.

Line width measurement is of great importance in astrophysical work. It may be possible to derive information regarding temperatures in the upper atmospheric regions if reliable line width data can be obtained from auroral lines, or night sky spectra. These are, of course, feeble sources and would not yield to a transmission interferometer technique. In order to see whether the reflection fringes

are sensitive enough to detect changes in line width, the following experiments were done using mercury sources excited under different conditions.

Three types of sources are used:

1. Water-cooled vacuum arc.
2. Hot vacuum arc.
3. Hot high pressure discharge lamp. Three different series of photographs were taken.

a. With a fixed interferometer gap, the fringes were photographed with a hot vacuum mercury arc carrying a current of 3 amps., and with a water-cooled mercury arc carrying the same current.

b. Keeping the interferometer gap fixed, a series of photographs of the fringes were taken while the current supplied to the hot vacuum mercury arc was varied. The values of current used were 1, 2, 3, and 4 amperes respectively.

c. With a fixed interferometer gap, photographs were taken of fringes from a high pressure mercury discharge lamp at successive stages in its warm-up to normal running pressures. This is possible only because, the exposure times are less than a second. This fact enables one to have a succession of photographs during the normal warming up time.

All these photographs were studied with the help of the microphotometer described already. The corresponding

traces depicting the fringe shape are shown in Figs. 25, 26, and 27. In each figure the different traces are superposed, but displaced in the vertical direction for clarity.

Fig. 25 corresponds to case (a). The curve marked A gives the fringe shape for the water-cooled arc while B gives the fringe shape for a hot arc. The sharpness produced on account of cooling is clearly evident. The interferometer gap is 2·29 mms. and the separation between order is 2·185 $cm.^{-1}$.

The shape of fringes given by a hot mercury arc carrying different currents is shown in Fig. 26. The curves A, B, C and D correspond to currents of 1, 2, 3, and 4 amperes respectively. The broadening of the fringes with increasing current is clearly marked. The arc does not normally run below a current of some 3 amperes. By using a large inductance in series with the arc, (although it is being run by a direct current) it is possible to reduce the working current to less than 1 ampere and this has a striking effect on the line widths as is seen from the microphotometer traces.

Fringes obtained with a high pressure mercury discharge lamp, during its successive stages of warming up, are shown in Fig. 27. Curve A corresponds to the moment immediately after switching on the lamp, while B

FIG. 25

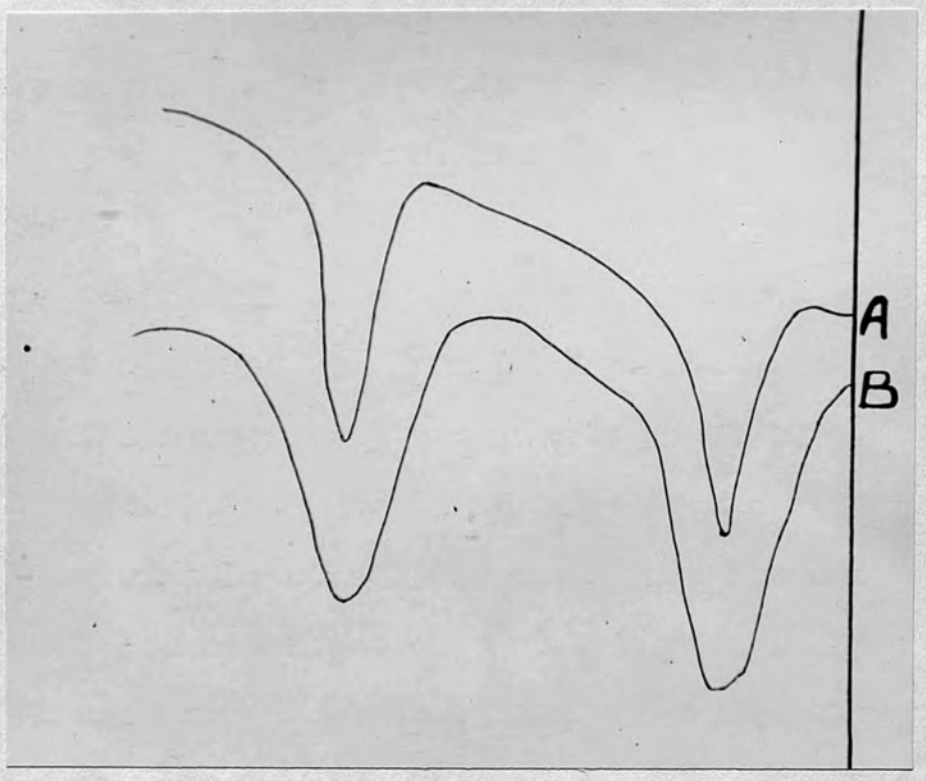

A WATER COOLED ARC

B HOT ARC

FIG. 26

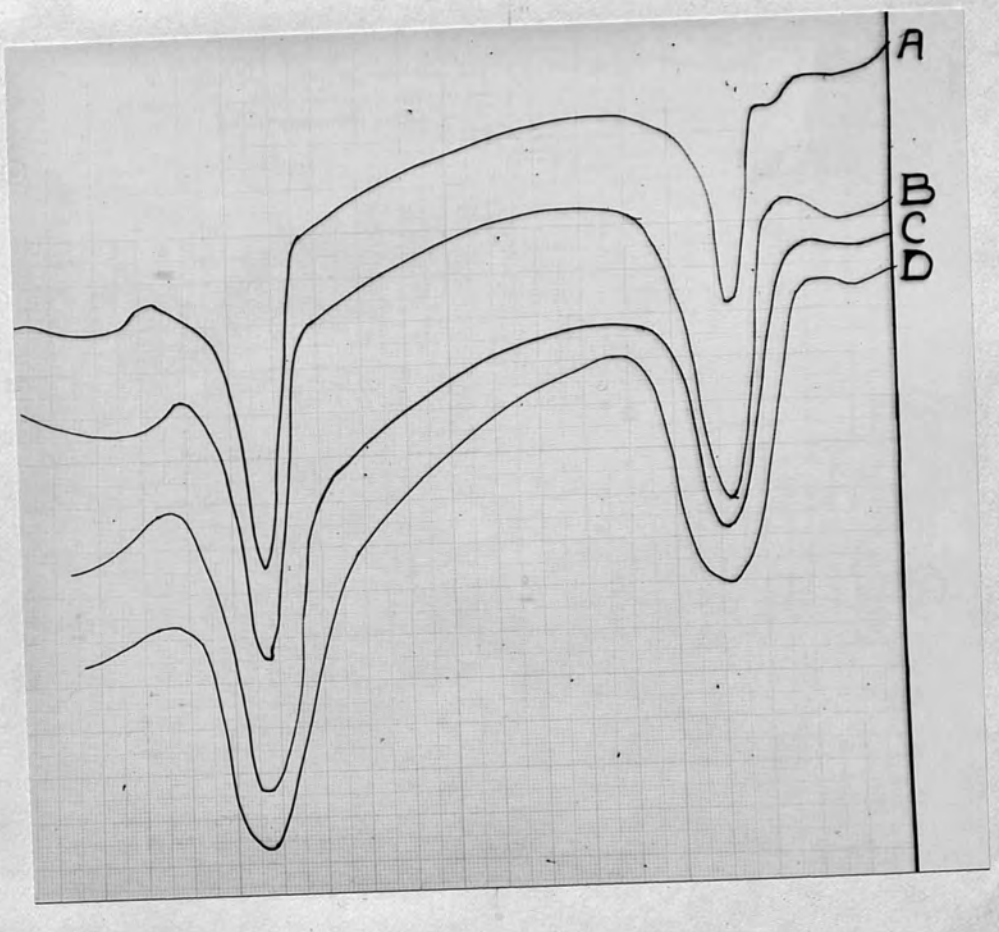

A CURRENT 1 AMP.

B " 2 "

C " 3 "

D " 4 "

FIG. 27

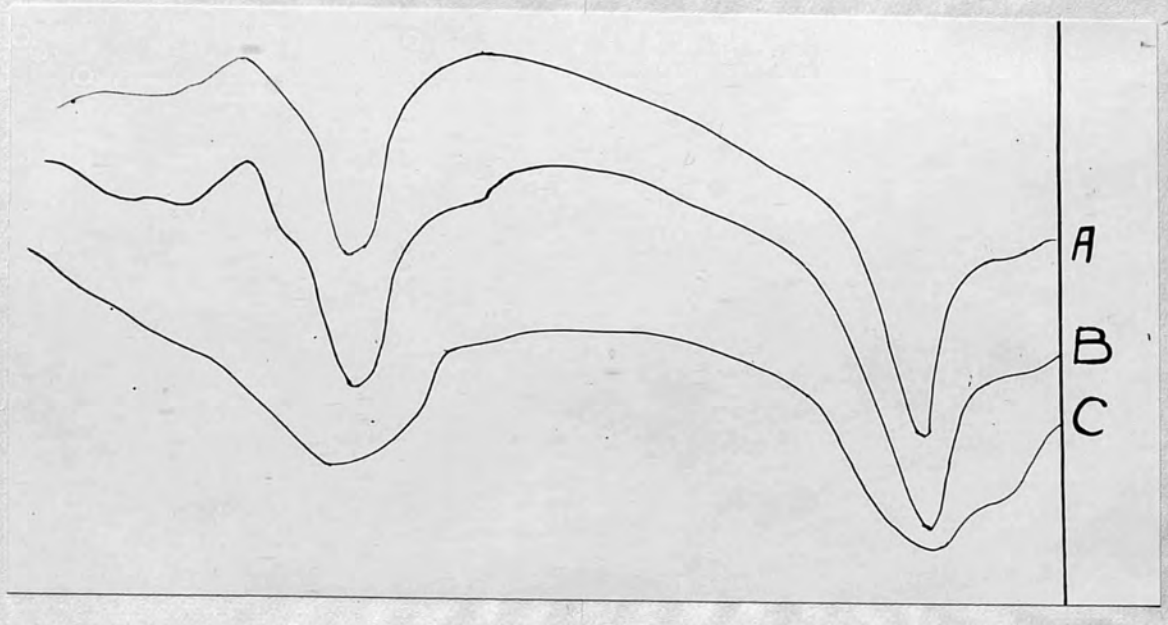

and C correspond to further stages. Eventually the fringes become so broad, that the gap used is too high to enable fringes to be recorded at all. This means that the fringe width now exceeds the order separation, and the fringes cannot be seen. In a high pressure discharge lamp, there is a small quantity of mercury and at the beginning the vapour pressure is low. As the lamp gradually warms up, more and more of the mercury is evaporated and the pressure rises. When the lamp is fully running, all the mercury is vaporised, and the pressure reaches a value of several atmospheres. (The pressure is between 20 to 40 atmospheres according to the makers). So, here, the broadening is essentially due to a pressure increase and can be described as resonance and collision broadening. It is well known that in addition to broadening, the effect of pressure is to produce an assymetry. The curve C has begun to show assymetry in addition to broadening.

The fringe widths shown here are not the true line widths but represent the combined instrumental and true line widths. The Fabry-Perot interferometer produces its own intensity distribution depending upon the reflecting coefficient, even when a truly monochromatic radiation is incident on it. No attempt is made to assess the true line widths, as the object of this work is not a specific determination of line widths in mercury but rather to

investigate the use of the reflected fringes for such measurements. The true line width can be determined from a knowledge of the observed line width and the instrumental width by using a method given by Burger and Van Cittert[10]. They give a relation between the true width, the observed width and the instrumental width. Minkowski and Bruck[11] have extended the analysis of the above authors and have given a useful general graphical relationship which can be applied to most cases.

The instrumental line width can be determined from a knowledge of the reflection coefficient by using the formulae already given, while discussing the sharpness of the fringes. This procedure is not advisable. It requires a precision determination of the reflecting coefficient, a matter of some difficulty. Inevitable errors in the flats also affect the instrumental fringe width.

It is much easier to determine the instrumental width experimentally. While the instrumental line width is inversely proportional to the plate separation, the true line width is independent of it. Thus, if the line width is observed with two different separations, it provides two expressions in terms of relations given by Berger and Van Cittert and these can be solved to give the true line width as well as the instrumental width.

In view of the sensitivity of the visibility of the reflection fringes the plate separation must be properly chosen according to the type of line under examination. Just as the presence of hyperfine structure affects visibility, so line broadening itself appreciably reduces the visibility. For the broader the line i.e. the greater the fraction of an order occupied by the line, the more is the visibility affected. Fortunately, the flexibility of the variable gap Fabry-Perot interferometer is of great value in this connection. By decreasing the plate separation, the fringes can be made narrow so that their widths are reduced to a small fraction of an order. This way, by a proper choice of the plate separation, the visibility can be retained as desired, whatever may be the type of line studied. This also helps to give the true instrumental fringe shape. As is suggested by Tolansky and Heard[12], by continuously decreasing the gap, one approaches the true instrumental fringe shape which is in this case large compared with the true line width.

Lastly, it must be mentioned that evaluation of line width is more difficult experimentally than the determination of wave-length differences.

Continuous Spectra.

We shall now consider the nature of the reflection fringes obtained with a continuous spectrum. The fringes

observed with a transmission Fabry-Perot with white light have been studied in detail by Tolansky[13]. Meggers and Burns[14] reported these in studying the Fraunhofer lines in the solar spectrum with the help of a Fabry-Perot interferometer crossed with a powerful grating. They can also be observed when using a Lummer plate in the study of the Solar spectrum.

These fringes are formed under the condition

$$n\lambda = 2t\cos\theta \quad (\mu = 1 \text{ for air})$$

when both θ and λ vary continuously. They are formed at infinity like the usual Fabry-Perot rings and can be focussed by collecting with a lens, all the rays of the same inclination. The fringes are curved.

There is however one important condition governing the successful observation of these fringes. The separation of the plates of the interferometer must be properly chosen according to the available dispersion of the spectrograph. The value of t must be so selected that the difference between successive orders ($\Delta\nu$) can be resolved by the spectrograph. Thus if one uses a gap of about 1 cm., as was done by Meggers and Burns, the value of $\Delta\nu$ is 0·5 $cm.^{-1}$. A very good grating shows the fringes as close fine lines. If one desires to observe the fringes with an ordinary spectrograph, such as a Hilger

medium quartz instrument, a convenient value for t is about 1/7th millimeter or less.

As in transmission, one can obtain these white light Fabry-Perot fringes in reflection as well. The experimental arrangement was the same as previously described with the difference that a pointo-light was used as a source of continuous radiation. Because of the greater dispersion of the big spectrograph, a gap up to 1 mm. could be used. With such small gaps, the fringes are of large angular diameter and in order to project a number of orders on to the slit a short focal length lens must be used. White-light reflection fringes obtained with a gap of 0·5 mm. and focussed with a lens of 12 cm. focal length, are shown in Fig. 28.

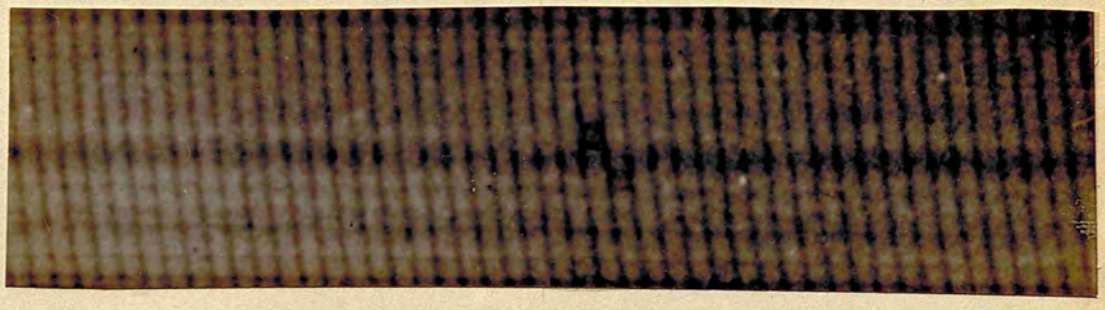

FIG. 28

PART II

HYPERFINE STRUCTURE IN BROMINE

Chapter V.

HISTORICAL REVIEW

The Bromine arc and spark spectra have frequently been studied. Kimura[15] excited the bromine spectrum in a Geissler discharge tube, in 1920, and investigated the nature of the discharge under different conditions of excitation, varying the pressure of the bromine gas, the current density, and the potential gradient. He noted the changes in the colour of the glow and its spectrum. The simple criterion that spark lines require more energy than arc lines allowed him to distinguish between the arc and the spark lines. He[16] also investigated the hyperfine structure of some of the lines and the Zeeman affect of others using an echelon grating. In 1927, Asagoe[17] excited the spectrum at a high gas pressure with a strong discharge and observed an apparent red shift in the wave-length; and an asymmetrical broadening of the red lines. He[18] interpreted this as due to the stark effect produced by intra-atomic fields caused by the large current density. In 1926, Hori[19] studied the structure of the lines emitted in a spark discharge with a small transmission echelon. He found similar quartet structures in four strong red lines, with the intensity and intervals degrading towards the shorter wave-lengths. In 1930, de Bruin[20] discussed these four lines and noted

that the ratio of intervals (4: 2·7: 1·7) was close to the theoretical values 4: 3: 2 required by a nuclear spin $3/2$. He proposed $3/2$ as the value of the spin moment of the bromine nucleus.

In 1930, Kiess and de Bruin[21] excited the arc spectrum in a Geissler tube at various pressures, the lines covering the spectrum region from the ultra-violet to the infra red. They carried out a multiplet analysis, and listed all the strong lines including those observed by Turner[22] in the Schumann region. The lines are classified as combinations between the terms of the doublet and the quartet systems. The observed multiplet structures were in complete agreement with those predicted by Hund's theory for an atom with seven valence electrons.

Lacroute[23] in 1935, excited both the arc and the spark spectra and studied the Zeeman effect. He verified the accuracy of the classification of Kiess and de Bruin[21] except for a few changes in term allocations. He partially classified the spark spectrum. He could not make full use of the Zeeman effect observations due to lack of Hyperfine structure data.

Tolansky[24, 25] studied the hyperfine structure in about 18 lines, excited by an elctrodeless discharge, and using a Fabry-Perot interferometer of variable gap. He found that the structures in the four strong red lines (λ 6632,

6560, 6351, 6148) were not equal as was assumed by de Bruin[20]. He, however, confirmed that the nuclear spin of bromine nucleus was $3/2$ and showed that both the isotopes of Bromine (79 and 81) possessed the same nuclear spin and identical nuclear magnetic moments. Schmidt[26] using Tolansky's data for the $4P_{5/2}$, $4P_{3/2}$ and $3P_{3/2}$ terms, calculated the magnetic moment of the bromine nucleus.

Tolansky and Trivedi[27] carried out a further study of the bromine arc spectrum using a Fabry-Perot interferometer. They gave the structures of 76 lines from λ 8700 down to λ 4360. The structures in many lines were completely resolved and the interval factors for 38 terms were determined. They demonstrated the existence of deviations from the interval rule in one term and attributed it to the existence of a nuclear quadruple moment (Q^0_λ) which has approximately the same value for both the isotopes. It was found that, one of the intervals utilised by Schmidt[26] for the determination of the nuclear magnetic moment, was much smaller than the value previously reported.

The present work was undertaken in order to extend the observations in the arc spectrum of bromine, below 4360 with a view to determine with certainty some intervals previously given as not being accurately known. It was also the aim to check the previously observed deviation from the interval rule and to calculate the quadruple moment (Q^0_λ) and the magnetic moment of the bromine nucleus by determining the nuclear coupling constants for bromine.

Another important object was to study the hyper-fine structure in the first spark spectrum of bromine which has not as yet been investigated and it is hoped that this will help in the further classification of the spark spectrum which is only as yet partially classified.

Chapter VI.

GENERAL THEORY

Nuclear Spin

A large number of spectral lines when examined by high resolving power instruments, are found to consist of several narrow, closely packed components. Such an appearance is termed hyperfine structure (H.F.S). It is now known that at least two distinctly different effects are responsible for the existence of the H.F.S.

The first type of hyperfine structure is described as magnetic H.F.S., while the second is due to the presence of isotopes. The magnetic H.F.S. was first explained for Bismuth by Goudsmit and Back[28]. Bismuth has no isotopes and so it could only be explained on Pauli's postulate that the nucleus possessed a spin angular momentum with an associated magnetic moment. Nuclear magnetic moment is quantised and denoted by I measured in units of $h/2\pi$

To the electrons in the various atomic orbits is ascribed a total angular impulse, J ($h/2\pi$), which is the resultant quantised vector due to the orbital motions and the spins of all the electrons. The resultant of the nuclear spin I and the total electron moment J, is the total angular momentum of the atom and is denoted by the vector F, such that

$$\vec{F} = \vec{I} + \vec{J}.$$

The resultant of I and J obeys quantisation rules, the possible number of values of F being $(2I + 1)$ or $(2J + 1)$ according to whichever is less. Thus each energy level, characterised by a given J value, is split into $(2I + 1)$ or $(2J + 1)$ levels of slightly different energy. It is the transitions between these various levels that give rise to the magnetic H.F.S. The selection rule $\Delta F = 0, \pm 1$ holds, the change $F = 0 \rightarrow 0$ being forbidden.

The Interval Rule

Goudsmit and Bacher[29], Hargreaves[30], Fermi[31], Fermi and Segre[32], showed that the energy due to the coupling of I and J is given by

$$W = AIJ \cos IJ \qquad \ldots\ldots 6.1$$

The interaction energy in quantum terms reduces to

$$W = \frac{A}{2}\left[F(F + 1) - I(I + 1) - J(J + 1)\right] \qquad \ldots\ldots 6.2$$

Here A is known as the interval factor. This shows that the Lande interval rule as obeyed by gross multiplets, should hold good for H.F.S. levels. The separation between two levels with quantum numbers F and $(F - 1)$ is given by

$$A/2\left\{F(F + 1) - (F - 1)F\right\} = AF.$$

Thus the successive intervals in an H.F.S. level should be proportional to the greater of the two adjacent quantum

numbers. H.F.S. multiplets usually obey this rule, but many exceptions are known. These will be discussed later.

The Interval Factors

The ratio of the intervals between the levels is a function of F, the actual separations depending upon the value of the interval factor A. Further, the character of the structure, whether it is regular or inverted depends upon whether A is positive or negative.

The value of the interaction constant, A, depends on three factors.

(a) The mechanical moments J and I are coupled through the magnetic fields they produce. So the interaction constant involves the nuclear magnetic moment $\mu = I \cdot g(I)$, where g(I) is the nuclear g-factor. It is the ratio of the nuclear magnetic moment to the nuclear mechanical moment both expressed in quantum units.

(b) The coupling energy between J and I depends on the degree of ionisation.

(c) It depends upon the probability of the electrons being near the nucleus, coupling energy for a penetrating s-electron being greater than that for a p-electron.

In the calculation of the interval factor, it is assumed as a simplification that the nucleus behaves as a small magnet and that the interaction takes place between

the electron magnetic field and the field of the nuclear magnetic dipole.

The interaction energy between a single electron and a nucleus has been given by Breit[33] and Goudsmit[34]. According to Goudsmit, the interaction constant a(s) for an 's' electron is given by

$$a(s) = \frac{g(I)}{1838} \cdot \frac{8R\alpha^2 Z_i Z_o^2}{3 \cdot n_{eff}^3} \qquad \ldots\ldots 6{\cdot}3$$

where g(I) is the nuclear g-factor, and

R, the Rydberg constant,

α, the fine structure constant,

Z_o, the effective nuclear charge outside the core of the closed electron shells,

Z_i, the effective nuclear charge inside the core of the closed electron shells,

n_{eff}, the effective quantum number. In general $Z_i = Z$ for 's' electrons and $Z_i = Z - 4$, for 'p' electrons.

For any other electron, the interaction constant is

$$a(l) = \frac{g(I)}{1838} \cdot \frac{R\alpha^2 Z_i Z_o^2}{n_{eff}^3 (l+1/2) j(j+1)} \qquad \ldots\ldots 6{\cdot}4$$

Breit[35] and Racah[36] have shown that a relativity correction must be applied by multiplying 'a' by F/H, where

$$F(l,z) = \frac{4j(j+1/2)(j+1)}{(4e^2-1)e}, \quad e^2 = (j+1/2)^2 - (\alpha z_i)^2 \quad \ldots 6.5$$

$$H(l,z) = \left[\frac{2l(l+1)}{(\alpha z_i)^2}\right]\left[\{(l+1)^2-(\alpha z_i)^2\}^{1/2} - 1 - \{l^2-(\alpha z_i)^2\}^{1/2}\right] \quad \ldots 6.6$$

For two or more valence electrons, Goudsmit[36] expresses the total interval factor in terms of the separate constants for the individual electrons. There is an approximate agreement with observed results.

Breit and Wills[37] have discussed and revised the theory using Dirac's equations for an electron. They give interval factors in the general case of an intermediate coupling, because in practice neither pure L-S nor pure j-j coupling is common. In addition to Goudsmit's constant a', and a'' corresponding to $j = l \pm 1/2$, a third constant a''' is given for each electron corresponding to different j-values.

Intensity of H.F.S. Components

The intensity rules obeyed by the H.F.S. components were given by Hill[38] and tabulated by White and Elliason[39]. According to these rules, the sum of the intensities of all the components coming to a level of a given F value is proportional to (2F + 1), the quantum weight of that level. Measurement of intensities is many a time helpful in the analysis of H.F.S.

Nuclear Magnetic Moments

The nuclear spin moment I is related to the nuclear magnetic moment μ by the relation

$$\mu = I \cdot g(I), \qquad 67$$

in which g(I), is the nuclear g-factor already defined.

The number of H.F.S. levels in a term depends on the value of I, if $I < J$ but the total width of the structure depends on the magnetic moment. The calculation of 'μ' from the observed hyperfine structure pattern involves the determination of g(I). We have already seen, that the interval factor contains the nuclear g-factor. So in the determination of the magnetic moment, it is necessary to evaluate all the factors in the expression for A, except g(I) and then use the observed size of H.F.S. pattern to find 'μ' .

For the simple case of a single electron in the field of the nuclear magnetic dipole with charge ze , the results are for "s" electron $a(s) = \frac{4}{3} g(I) \cdot \mu_0^2 R^2(0)$

and for a non-s electron $a(l) = 2 g(I) \mu_0^2 \cdot \overline{r^{-3}} \left[\frac{l(l+1)}{j(j+1)}\right]$

From the above formulae, it is clear that for the evaluation of 'μ' , in addition to a knowledge of the interval factors, one must be able to determine $R^2(0)$ or $\overline{r^{-3}}$, in the neighbourhood of the nucleus. Knowledge of accurate wave-functions is rather meagre. They must be calculated either by the statistical method of Thomas[40]

and Fermi[41] or by the more exact method of self-consistent field due to Hartree[42]. In either case, since the formulae are sensitive to small changes in the wave-function, values of μ obtained from these are often not consistent.

It is desirable, therefore, to have some approximate method which would lead to consistent results and which could be applied even when wave-functions are not available. Such formulae were given by Goudsmit[43].

With the relativity correction given in eqs. 6·5, 6·6 these formulae are for 's' electron,

$$\mu = \frac{a(s)\cdot 1 \cdot n_{eff}^3 \; j(j+1)(l+1/2)}{R\alpha^2 Z_i Z_0^2 \; F(l,Z_i)} \cdot 1838 \qquad \cdots 6.8$$

and for a non-s electron

$$\mu = \frac{a(l)\cdot 1 \cdot j(j+1)(l+1/2)}{\delta \cdot l(l+1)} \frac{Z_i \cdot H(l,Z_i)}{F(l,Z_i)} 1838 \qquad \cdots 6.9$$

The meanings of the various symbols except δ are already given in the discussion of the interval factors. δ is the spin-orbit interaction doubling.

The above relations cannot be directly applied if the atom has more than one valence electron. Frequently the interaction is mainly due to the presence of a

penetrating s-electron in a group of valence electrons and then μ can be determined in terms of the interval constant of the 's' electron.

When all the valence electrons have considerable interaction with the nucleus, it is possible to find relations which give the size of the H.F.S., in terms of the separate interval constants of the individual electrons. In this connection, the paper by Breit and Wills[37], already referred to, is of great value and in it are given results for various configurations.

It is well-known that perturbations between states are often prevalent in atomic spectra. This means that the wave-function representing a particular state contains the pure wave-functions not only of that state but of others which are found to perturb it. Exact calculation of such perturbations is difficult and since they have great influence on the value of μ, it is desirable to avoid any such perturbed state in the determination of the magnetic moment. States having wide H.F.S., and which are not subject to perturbation must be selected. States having the same value of J and of the same parity, perturb each other.

Deviation from the Interval Rule

In general the hyperfine multiplets obey the interval rule better than gross multiplets but this very regularity makes exceptions more striking.

When the interval rule is not obeyed, the interaction between the nucleus and the electron shells is no longer proportional to the scalar product of the two vectors and the cosine law breaks down. Perturbations can arise under four distinct circumstances:

1. Perturbations arise due to a configuration interaction between two terms having the same L, S, and J values and of the same parity, even if the terms are far apart. This may be visualised as a sort of resonance action. [Russel and Shenstone(44)]

2. When the gross-structure multiplet separation is comparable with the fine structure due to the nuclear moment, the intervals in the latter are distorted. Two H.F.S. levels having the same F value perturb each other; the general effect being a repulsion between them [Paschen(45)]

3. When two terms fall accidentally close to each other, a perturbation takes place. Such an effect was observed by Schuler and Jones(46) in the Hg I spectrum.

4. Perturbations are also caused by the presence of a nuclear electric quadrupole moment. [Schuler and Schmidt(47)]. This effect will now be considered in detail.

Nuclear Quadrupole Moment

Schuler and Schmidt[47] observed a breakdown in the interval rule in the spectrum of Europium, which could not be accounted for by the presence of an interaction between electron configurations. They correctly interpreted this as indicating that the electric charge distribution of the nucleus was no longer spherically symmetrical. The nucleus is, then, said to exhibit an electrical quadrupole moment. The interaction between a spherically symmetrical nucleus and the electron charge distribution is given by the cosine law,

$$E = a_0 + a_1 \cos(ij), \qquad \cdots\cdot 6.10$$

where a_0 is the displacement of the centre of gravity from its position corresponding to a zero spin and a_1 is the H.F.S. interval factor. The interaction between a non-spherically symmetrical nucleus and a non-spherically symmetrical electron charge distribution obeys a different law, given by,

$$E = a_0 + a_1 \cos(ij) + b \cos^2(ij)$$
$$= a_0 + \frac{a_1}{2}.C + b.C(C+1), \qquad \cdots\cdot 6.11$$

where $C = f(f+1) - i(i+1) - j(j+1)$

i, j, and f having the usual meanings. As in equation eq 6.10 $a_1 \cos(ij)$ represents the energy of a nuclear magnetic dipole in the magnetic field of the electrons. The constant, b,

is a measure of the departure of the nucleus from spherical symmetry. No deviations can be observed for S-terms, since the electric charge distribution of the electron in this state is spherically symmetrical and the electrostatic energy due to the nuclear asymmetry is the same at all points.

The exact quantum mechanical expression was given by Casimir[48] as

$$\left\{ e\overline{\varrho^2(3\cos^2\theta-1)} \right\}_i \cdot \left\{ -e/_{2^3}\,\overline{(3\cos^2\delta-1)} \right\}_j \left[\frac{3/_8\, e(e+1) - 1/_2\, i(i+1)\, j(j+1)}{i(2i-1)\, j(2j-1)} \right] \quad \ldots\ldots 6.12$$

The first term $\left\{ e\overline{\varrho^2(3\cos^2\theta-1)} \right\}$ is denoted by q and represents the average over the charge density of the nucleus. ϱ is the distance of a volume element from the point nucleus and θ is the angle between ϱ and the z-axis (z axis being along the direction of the nuclear spin). q is called the nuclear electric quadruple moment. The term $\left\{ e/_{2^3}\,\overline{(3\cos^2\delta-1)} \right\}$ is a measure of the deviation of the electron charge distribution from spherical symmetry. For S-states, it is zero. It is positive for a prolate distribution and negative for an oblate distribution in the direction of J.

Comparison between eqs. 6·11 and 6·12 gives

$$q = \frac{-b \cdot 8i(2i-1)j(2j-1)}{3e^2\left\{\frac{1}{r^3}(3\cos^2\alpha - 1)\right\}} \qquad \cdots 6\cdot13$$

$\overline{(1/r^3)}$ is given in terms of the spin-orbit interaction doublet separation.

We shall use this formula later in determining the quadrupole moment of bromine. The average of $\overline{(3\cos^2\alpha - 1)}$ can be determined in terms of the theoretical coupling constants and the method is illustrated in the actual calculation carried out.

The sign of 'q' is important. A positive value of q signifies that the nucleus is elongated (charge distribution) in the direction of the nuclear spin axis. On the other hand, a negative value of q indicates a charge distribution which is flattened in the direction of the spin.

Isotope Effect

So far the main features of the magnetic H.F.S. have been considered. There can however be a hyperfine structure due purely to the presence of isotopes even in the absence of any nuclear spin effect. The two effects are often mixed up and the structure then becomes complex. Isotope effect is different according to whether the

element is light or heavy. In case of light elements, it is simply a mass effect arising from the finite mass of the nucleus. This modifies the simple Bohr formula, derived on the assumption of an infinite nuclear mass. Spectral lines of the heavier isotope are shifted in the direction of higher frequency. In many-electron spectra, the effect becomes complex, the solutions having been given for two or three-electron systems by Hughes and Eckart[49], and Bartlett and Gibbons[50]. In general, the isotope shift is inversely proportional to the square root of the nuclear mass and is therefore exceedingly small for heavy elements.

The typical isotope effect for heavy elements was first interpreted by Schuler and Bruck[51], in cadmium which has four even and two odd atomic weight isotopes. Even atomic weight isotopes show no magnetic H.F.S. and hence all fall together while the odd isotopes show magnetic H.F.S. splitting. Schuler and Keystone[52] have found in the Thallium spectrum that the structure of one isotope is bodily shifted with respect to that due to the other isotope. More complex effects have been observed by Schuler and Keystone[53] in mercury, by Tolansky and Lee[54] in Platinum and by Schuler and Schmidt[55] in Samarium. The even isotopes do not fall together and to add to the complexity, the odd isotopes may possess different nuclear spins. These

isotopic shifts can be explained approximately on the basis of a non-coulombic nuclear field. For a true point nucleus, the field is everywhere a coulombic field. But the finite nuclear size modifies this situation. There is a certain distance r from the nucleus (nuclear radius) beyond which the field is purely a coulombic one, but inside it departs from it. The value of r depends on the nuclear mass and is different for different isotopes. The relation obeyed is in general, $r \approx M^{1/3}$

Racah[56], Breit and Rosenthal[57] and Breit[58] have attempted a theoretical explanation based on the above idea. For Samarium, Schuler and Schmidt[55] associate the difference of behaviour between Sm^{150} and Sm^{152} with the α-ray activity of Sm^{150} Kopfermann[59] believes that a possible link up may be found between the isotope shift and the nuclear quadrupole moment.

Nuclear Structure - Origin of Nuclear Magnetic Moment and Spin.

All nuclei fall into four classes according to whether Z, the atomic number and M, the atomic mass are even or odd. This seems to be a reliable system of classification, since it is independent of any particular nuclear model. We shall, in what follows, consider the neutron-proton nuclear model. The most important result for a general theory of the nuclei is that the spins of

all nuclei of odd atomic weight seem to be half integer multiples of $h/2\pi$, while all nuclei of even atomic weight have integer spins most of them probably having a zero spin. [Bethe and Bacher[60]] . The total spin of a nucleus is the resultant of all the angular momenta due to the orbital motions of all particles inside the nucleus, and of all the spins of the nuclear particles. The resultant has to be taken according to the vector model of the quantum theory. Now the orbital angular momenta are always integers (in units of $h/2\pi$). Thus the appearance of half-integer values for the total spin of some nuclei must be attributed to half-integer values for the spins of the individual nuclear particles. The empirical rule connecting atomic weight and nuclear spin must thus be interpreted as showing that both the proton and the neutron have half-integer spin. The spins of the proton and the neutron are $1/2$. Experimentally proton spin has been shown to be exactly $1/2$. If both proton and neutron have spin $1/2$, then the resultant spin of A elementary particles, neutrons and protons, will be integer or half-integer according to whether the atomic weight A is even or odd.

The magnetic moment of the proton was assumed to be $1/1840^{th}$, that of the electron. A nuclear magneton (μ_N) has a value,

$\mu_N = \frac{he}{4\pi Mc} = 5{\cdot}02 \times 10^{-24}$ gauss cm^3 where M is the

mass of the proton. But the work of Rabi, Kellog, Ramsey and Zacharias[61] has shown that the accurate value of the proton magnetic moment is $2 \cdot 789 \mu_N$. It is also found that the magnetic moment points in the same direction as the angular momentum due to the proton spin, as would be expected from a positive charge.

The magnetic moment of the neutron has been given by Arnold and Roberts[62] and has the value 1·91. The magnetic moment of the neutron has that direction which it would have if the neutron had a negative charge. The spin of the neutron is presumed to be $1/2$, from the evidence given below. A Deuteron consists of one proton and one neutron. The magnetic moment of the Deuteron was determined by Farkas and Farkas[63] and the value is 0·85. It is also directed in the same direction as the spin. The Deuteron magnetic moment should be equal to the sum of the magnetic moments of the proton and the neutron. Agreement between the theoretical and the observed values can only be achieved by assuming that the neutron spin is $1/2$

The nuclear model is visualised as follows[64]. Out of the total number of the nuclear particles, an even number of protons and neutrons (nucleons) form a core. Any excess nucleon goes round this in an orbit with angular momentum l which is an integer and an inherent spin which is $1/2$ for both the proton and the neutron. The properties

of the nucleus are in the main, determined by this excess nucleon.

Explanation of the isotope shift is on the following lines. Consider a nucleus of even charge Z and of even mass M. To this nucleus, a neutron is added, thus giving rise to an isotope of odd mass number. The added neutron does not enter the nucleus but rotates round it. In the absence of any interaction between the neutron and the nuclear charge distribution, the nuclear field will remain unchanged, and there will be no observable isotope shift. In practice, however, this is not quite the case. Perhaps, some neutron-nucleus interaction does exist, slightly altering the nuclear field.

On this theory, one can consider the shape of the nucleus about which the odd nucleon revolves[65]. Experimentally it is found that the nuclear quadrupole moments of large numerical value are always positive, the measured values lying between -0.5×10^{-24} to $+6 \times 10^{-24}$ units. But a revolving proton should create a negative quadrupole moment and one can therefore postulate that the nucleus, itself, is elongated in the direction of the axis, which lies perpendicular to the plane in which the proton rotates. The nucleus no longer possesses spherical symmetry, and the proton's orbital motion is about the major axis of the nucleus.

If elements with known quadrupole moments are chosen and the calculated effect of the circulating nucleon is taken into account, it is possible to estimate the quadrupole moment of the nucleus alone. The quadrupole moment is then found to be positive or zero, with a pronounced maximum at $Z \approx 71$, the region of the rare-earths. Schmidt[55] associates the isotope shift in the rare earths with this. The non-spherical shape of the nucleus brings about a new charge distribution and consequently the nuclear field will differ from that employed by Rosenthal and Breit[57], namely a spherically symmetrical charge distribution.

Recently attempts have been made to explain the nuclear magnetic as well as quadrupole moments in terms of a nuclear shell model with some success. The interest has been revived, particularly, on account of the new data obtained with the micro-wave technique[66].

As has been pointed out by Meyer[67], the exceptional stability of nuclei which have proton or neutron numbers of 2, 8, 20, 50, 82 and 126 suggests the existence of shell structures in nuclei. Schemes have been proposed by Nordheim[68] and by Feenberg[69] for assigning orbital quantum numbers to the last odd nucleon.

Hill[70] and Townes and Low[71] have tried to interpret the asymmetry of the nucleus as arising, as a

first order approximation, through incomplete proton or neutron sub-shells. By assigning orbital quantum numbers to the odd nucleon, the sign of the electric quadrupole moment can be predicted. The conclusions are based on the following assumptions.

1. The shapes of nuclei are determined by the probability distribution ($\psi\overline{\psi}$) of the independent nucleons in the incomplete shells.

2. Completely closed shells or sub-shells, which are spherically symmetrical, do not contribute towards q, the quadrupole moment. Just as pairs of nucleons make no contribution to the spin I, so also sub-shells with even number of nucleons do not contribute towards q.

3. In an unfilled shell having an odd number of nucleons, the "unpaired" nucleon has an m_j value equal to I (nuclear spin) and the other nucleons distribute themselves in pairs among the remaining values of Mj. Here Mj is the magnetic quantum number with respect to the nuclear magnetic field.

4. A sub-shell with only one nucleon in the state $m_j = |I|$, endows the nucleus with a negative q value. A sub-shell with an odd number of nucleons in states $m_j = |I|$, $\pm 1/2$, $\pm 3/2$ etc. will, in general, produce a nucleus of a positive q value.

The signs of q, predicted according to this scheme are in good agreement with the observed values. We shall see later how the signs of the observed quadrupole moments of hologens agree with the above predictions.

However, the nuclear shell model does not give the correct magnitude of the quadrupole moment in contrast with the situation regarding the nuclear magnetic moments which can all be accounted for by a suitable admixture of states of a single nucleon.

The Analysis of the Hyperfine Structure

Nuclear spin is determined by a number of methods apart from Hyperfine structure studies. Some of them are:

1. Zeeman effect.
2. Atomic and Molecular beam.(72)
3. Alternating intensities in B-and spectra.
4. Specific heat.(73)
5. Polarisation of resonance radiation.(74)
6. Certain nuclear reactions.(75)
7. Microwave spectra.(66)

However the study of hyperfine structure is widely applicable to almost all elements whose spectrum can be excited. The successful analysis of the H.F.S. in the atomic spectra can lead to the evaluation of the nuclear spin, and in suitable cases, of the nuclear magnetic moment.

On account of the intensity and interval rules, the line patterns fall into two types. They are known as regular and irregular patterns respectively.

Often, only one of the terms involving a line is associated with a penetrating s-electron and this results in a much wider structure than that of the other term. The line pattern, then, has often an appearance of a regular degraded series and is known as a regular pattern (sometimes a "Flag" pattern). If both the upper and lower term interval factors are of comparable order, the line pattern may be complex and is then known as an irregular pattern.

A regular and an irregular pattern is illustrated in Fig. 29. This is for the $5s^4P_{5/2} - 5p^4D_{5/2}$, transition in Br I. The interval factor for the upper term is assumed to be $^4/_5$ ths that of the lower term. The spin is $^3/_2$. The pattern is complex with no apparent regularities.

If the interval factor of the upper term is only $^1/_{20}$th of that of the lower, then the same line pattern becomes regular. Since experimentally the closely packed components cannot be resolved, a regular quartet pattern is observed.

This regular pattern shows the approximate structure of one of the terms only, the lower term in this case. The number of components in a pattern is $2I + 1$ or $2J + 1$ according to whether $I < J$ or $J < I$. Since this line is a quartet, I cannot be greater than J and the only possible value for I is $^3/_2$. This illustrates, how, a single pattern can give the nuclear spin directly.

The analysis of an irregular pattern is more difficult. If the resolution is good, analysis can be carried out by seeking for common wave-number differences. In the case where many line structure components crowd together and cannot be experimentally resolved, the line pattern is analysed by looking for wave-number differences and fitting them between the F levels by a trial and error

FIG. 29

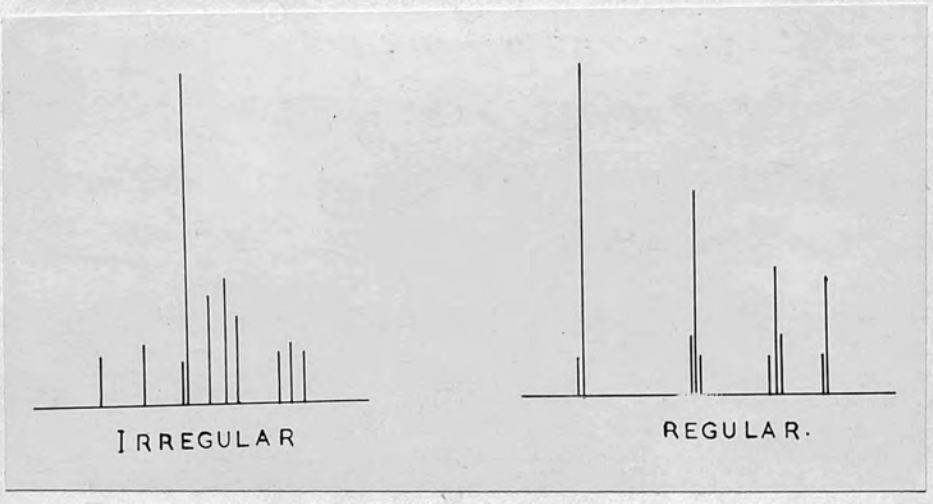

FIG. 30

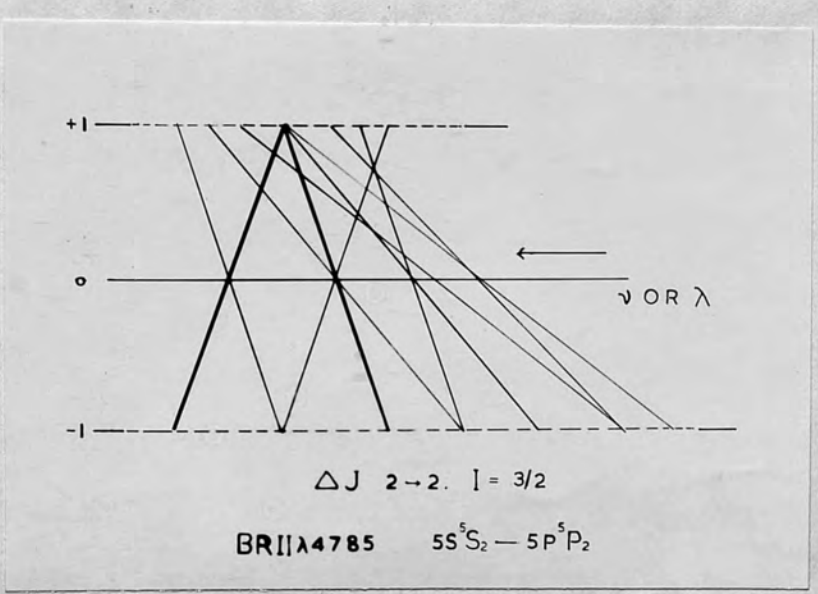

method. In this way, the pattern is built up and provided enough checks are available, the analysis can be tested for validity.

Graphical Analysis

Fisher and Goudsmit[76] have proposed a graphical method which is of value in analysis of patterns where the resolution is incomplete. The method is based on the interval rule as well as on the intensities.

Both I and J values must be known and the method is valid only for cases where there are no deviations from the interval rule.

Firstly, the interval factors for the upper and lower terms are made equal and the complete multiplet drawn. The position of each component of the pattern is plotted as a point along a line using the value of λ or ν for a scale. The graph is illustrated in Fig. 30. The positions of components for equal interval factors are shown along a line marked +1. Then, the upper term is completely inverted and with the same interval factor, the new resulting multiplet is drawn. The position of each component of the new line pattern is plotted as a point along the line marked -1. Points representing the same F transitions are joined up by straight lines whose widths may preferably be made proportional to the intensities of the components

as calculated from the intensity rules. The points along the top line represent the line pattern given by two terms having identical interval factors. The points along the bottom line, represent, on the other hand, the pattern for two terms having the same interval factor but one of which is inverted. The middle line marked ○ corresponds to the case where the upper or initial level has no effective separation. The whole region below the central line, gives patterns for cases where one of the terms is inverted. One can draw a line at a level corresponding to a given ratio of the two interval factors. Each of the lines joining points representing the same F transitions, cuts this line in a point. These points represent the line pattern given by two terms having the above chosen interval ratio. The graph shown here corresponds to the analysis of the line λ 4785 of Br II. It is a transition $\Delta J = 2 \rightarrow 2$. $\left[5s\,^5S_2 - 5p\,^5P_2\right]$. The arrow indicates the position where a line is to be drawn to get the observed pattern. The corresponding ratio of the intervals of the upper and lower terms is $1/5$. The procedure is valid because the term $5S_2$ having the large interval factor, is spherically symmetrical and therefore does not show any deviations from the interval rule on account of the existence of a nuclear electric quadrupole moment.

Chapter VII.

EXPERIMENTAL TECHNIQUE

(GENERAL)

The hyperfine structure separations are small varying from 2 cm^{-1} down to quantities at present unobservable. Hence apparatus of high dispersion as well as of high resolving power is necessary for these studies. As the high dispersion tends to reduce the intensity, bright sources must be used. This introduces serious complications for in general, the procedures adopted for increasing the brightness of a source usually simultaneously lead to an increased line width. Line sharpness is a prime consideration in H.F.S. studies.

Line Broadening

The factors leading to a line broadening will now be considered.

1. Natural Width

Every spectral line has a natural width because of the fact that an energy level is not infinitely narrow but has a finite width depending upon the average time an electron remains in that particular level. The natural width is usually very small.

2. Doppler Width

The atoms responsible for the emission of the radiation have a Maxwellian distribution of velocities. All atoms emit the same frequency but that emitted by atoms moving towards the observer is increased while that for atoms receding from the observer is decreased according to the Doppler effect. This leads to a line broadening. The width depends directly on the square root of the temperature and inversely on the square root of the molecular weight. The broadening is serious for light atoms.

3. Self-Reversal.

When the radiation from a hot source passes through a cooler layer of the same vapour, it is partially absorbed. In a line originally single, self-absorption at first tends to broaden it. With further absorption a false doublet appears. Such a spurious doublet will cause serious errors if not detected.

4. Collision and Pressure Broadening

When an atom which may be absorbing or radiating energy collides with another atom, the phase and the amplitude of the radiation change. The effect is complex and leads to effective broadening and asymmetry. The effect depends to a marked degree on the pressure and the nature of the perturbing gas. When the perturbing atoms are the

same as those emitting the radiation the effect is known as resonance broadening.

5. Stark Broadening.

With high current densities, many ions are formed which upon collision with other atoms produce strong electric fields. The interatomic fields cause a stark broadening of the lines.

Sources

Doppler broadening is considerably reduced by cooling the source and thus keeping down the temperature of the emitting vapour. Various methods of cooling may be adopted - from a blast of cold air, or circulation of water to a drastic cooling by liquid air. The choice depends upon the form of the source and upon the element whose spectrum is being investigated. Water cooling suffices usually for heavier elements. To overcome the pressure broadening the only way is to run the source at as low a pressure as possible. To reduce stark broadening, one must avoid high current densities and steep electric gradients.

The following are the common types of sources now employed to excite sharp lines.(77)

1. The cooled Geissler discharge tube.
2. The cooled low pressure arc.
3. Hollow cathode discharge.

4. High frequency electrodeless discharge.

5. Atomic beam.

The fourth type is suited when internal electrodes cannot be used as in case of active vapours like the hologens. It is excited at low pressures and the electric fields involved are not strong. It gives sharp lines.

High Resolution Instruments

The instruments employed are either a large diffraction grating, a grating crossed with an interferometer or a spectrograph of reasonable dispersion crossed with an interferometer of high dispersion. Interferometers occupy an important place in H.F.S. work and those employed are the Echelon grating, the Fabry-Perot interferometer and the Lummer-Gehrcke plate, each having special advantages. In this investigation, the Fabry-Perot interferometer and the Lummer plate were used. These, therefore, will now be considered in detail.

The Lummer Plate

This was first devised by Lummer[78] in 1901, and was improved and developed in conjunction with Gehrcke[79]. It essentially consists of a plane parallel plate of glass or quartz. The one used in this investigation is of crystalline quartz, about 3·42 x 30 x 200 mm. in dimensions and is of exceptional quality. A beam of monochromatic light enters a prism and is then incident obliquely on the

plate near to grazing incidence. The ray trace is shown in Fig. 31. The ray suffers internal reflections and there emerge beams on either side of the plate with successive constant retardation in phase and gradual reduction of intensity. These, when collected by a lens, interfere and fringes are formed in the focal plane, there being two systems one on either side of the plate. These are fringes of equal inclination formed at an angle $i \sim 90^\circ$ instead of at $i \sim 0^\circ$ as in the case of a Fabry-Perot interferometer. An extended source is necessary. Since the reflection coefficient is high near the critical angle, the fringes are very sharp.

The range of the plate $\Delta\lambda$, the largest wave-length difference that can be detected without overlap is

$$\Delta\lambda = \frac{n\lambda^2}{n^2\lambda - 4t^2\mu\frac{\partial\mu}{\partial\lambda}} \qquad \ldots 7.1$$

and the resolving power is

$$\lambda/\partial\lambda = \frac{l}{\lambda \sin i}\left[\mu^2 - \sin^2 i - \lambda\mu\frac{\partial\mu}{\partial\lambda}\right] \qquad \ldots 7.2$$

where l is the length of the plate and μ the refractive index of the material of the plate. At $\lambda 5000$, the

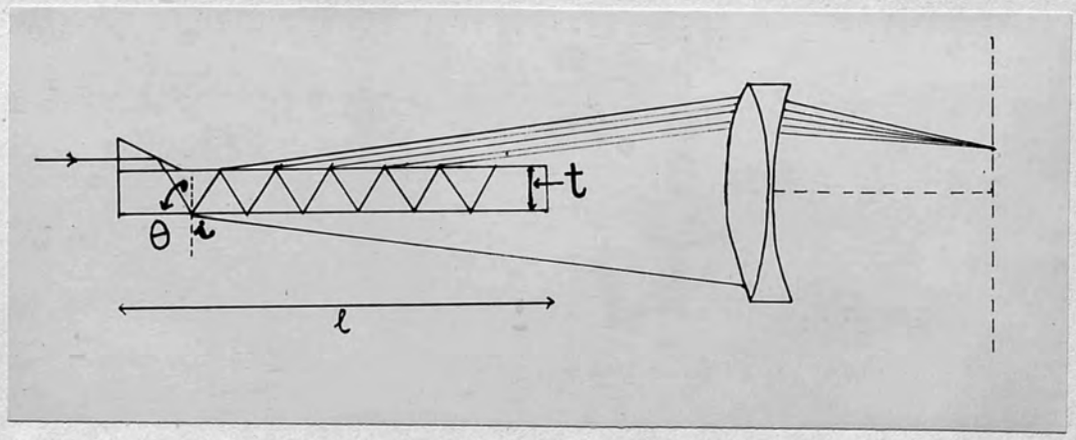

FIG. 31

resolving power of the plate employed, is equivalent to that of a Fabry-Perot interferometer of gap 4·24 mms.

Since quartz is doubly refracting, two sets of fringes are produced, one due to the ordinary and the other due to the extraordinary image. These should be separated and the extraordinary image of the source must be selected. This was achieved by the following method. A small horizontal aperture of vertical height of 3 to 5 mms. is placed before the source. This is not necessary with a narrow capillarly source. By adjusting the tilt of the plate it is then possible to throw one of the images outside the slit. The length of the slit is cut down to facilitate this.

The plate used here is free from ghosts which arise through slight imperfections in the plate. The plate requires careful handling if the best results are to be obtained. The surfaces must be clean and free from grease and dust. Since it is very sensitive to temperature changes, it takes some hours to attain temperature equilibrium after being handled. A quartz plate attains equilibrium more quickly than one of glass.

Fabry-Perot Interferometer

We have already considered the theory of this interferometer in detail in Part I. If λ is the wavelength of the incident light, θ the angle of incidence and n the order of the fringe, then

$$n\lambda = 2\mu t \cos\theta$$

$$= 2t \cos\theta \quad (\mu \simeq 1 \text{ for air}) \qquad \ldots\ldots 7.3$$

In going away from the centre, θ increases and hence n decreases. At the centre, $\theta = 0$ and if n_0 is the order of interference at the centre,

$$n_0\lambda = 2t$$

using relation(73), the distance between successive orders is given by

$$d(\cos\theta)/dn = \lambda/2t$$

and the dispersion by

$$d(\cos\theta)/d\lambda = \frac{n}{2t} = \frac{\cos\theta}{\lambda}$$

which is independent of t.

If one considers fringes near the centre, θ is small and one gets the relation

$$\lambda/d\lambda = -n/dn$$

Thus the resolving power for a given n, depends on the smallest change of order that can be detected. Using the Rayleigh Criterion for resolution, Meissner(80) has given an expression for the resolving power as

$$\lambda/d\lambda = -n \times 1{\cdot}49 \cdot F^{1/2}$$

where $F = 4R/(1-R)^2$

The resolving limit dV is given by

$$d\nu = -\frac{d\lambda}{\lambda^2} = \frac{1}{2t \times 1.49 F^{1/2}} \qquad \ldots\ldots 7.4$$

The resolving limit is thus inversely proportional to the plate separation and depends also on the reflection coefficient.

The spectral range or the largest wave-number separation that can be detected without overlapping is given by

$$\Delta\nu = \frac{1}{2t} \qquad \ldots\ldots 7.5$$

It varies inversely as the separation t and hence can be controlled as required.

The sharpness of the fringes depends on the reflecting coefficient of the silver coatings. The resolving power cannot be increased beyond a limit by using thicker and thicker coatings of high reflectivity since this leads to increased absorption. The gain in resolution is not much compared with the consequent decrease in the intensity. Therefore, in practice, theresolving power is increased by making t large if this is possible; and overlapping is not prohibitive.

Selection of Either of the Above Interferometer

The selection of one or the other of the above interferometers depends upon the spectral region to be investigated. The Lummer plate is especially good for

violet and ultra-violet regions. The only defect is its fixed dispersion and limited resolving power. For reasonably wide patterns it proves valuable in conjunction with an aluminised Fabry-Perot. At times, ambiguity may arise due to overlapping. With a Fabry-Perot interferometer, this ambiguity is entirely avoided by varying the spacing between the plates.

Chapter VIII.

EXAMINATION OF THE BROMINE ARC AND THE SPARK SPECTRUM

Experimental

This chapter will be divided into five sections.

1. Description of the circulating system used to maintain a constant supply of pure bromine vapour at a desired pressure through the discharge tube.
2. Excitation of the arc and the spark spectra.
3. Description of the high frequency oscillator employed to excite the spectrum.
4. Description of the spectrograph and the interferometer.
5. Preparation of Fabry-Perot mirrors and the photography of the spectrum.

The Circulating System

The layout of the system is produced in Fig. 32, on the opposite page, various parts being lettered and named. For preliminary vacuum in the system, a rotary oil pump is used; while the circulation of the bromine vapour in the discharge tube, is maintained at the necessary low pressure by a triple-jet mercury diffusion pump P. This

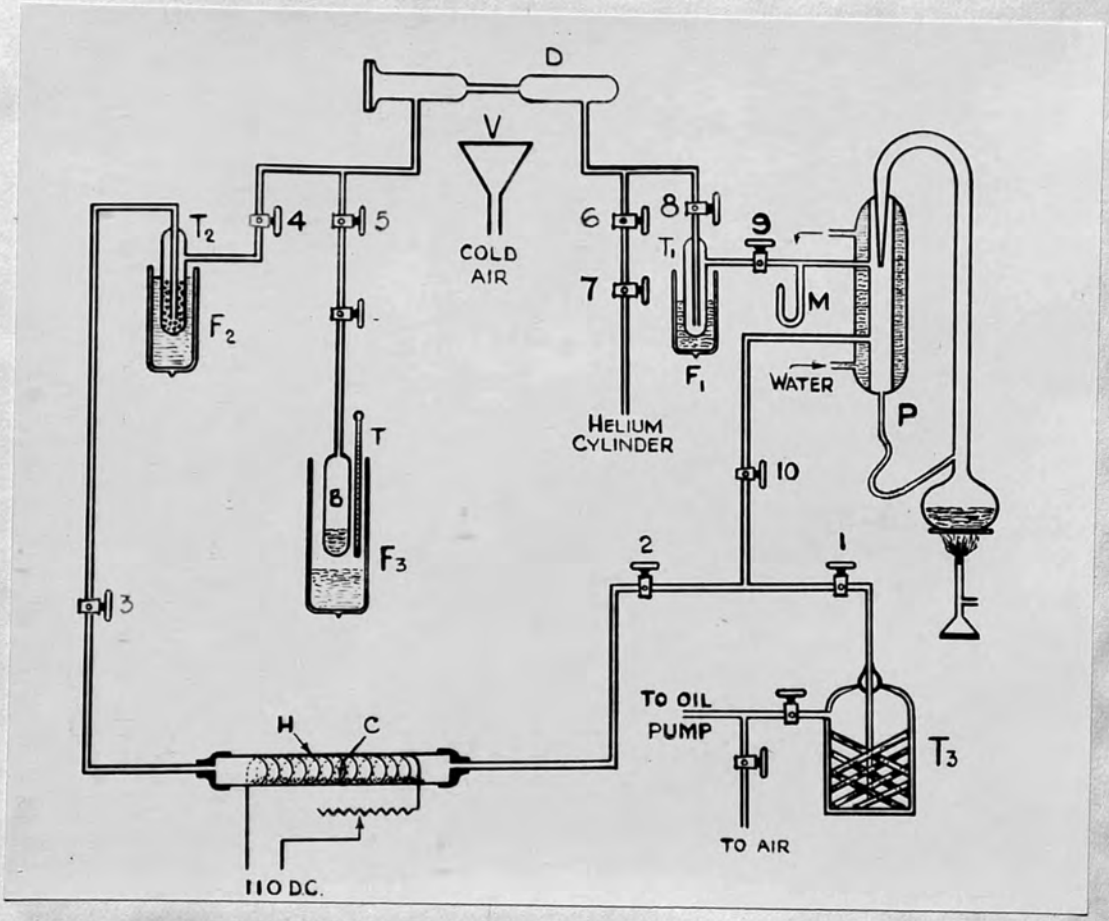
D
V
COLD
AIR
T2
4
5
6
8
9
T1
7
M
F2
F1
WATER
P
T
HELIUM
CYLINDER
10
B
F3
2
1
3
TO OIL
PUMP
H
C
T3
TO AIR
110 DC.

FIG. 32

pump functions properly, once an initial vacuum is produced, even when the backing pump is cut off and can maintain the circulation up to a pressure difference of 1·5 cms., if desired. The pressure in the system is measured with the mercury manometer M. There are four traps in the system. The trap T_1, which merely consists of a tube through which the vapour circulates, is cooled with liquid oxygen in a thermos flask F . This trap serves two purposes: It prevents the mercury vapour from the diffusion pump diffusing backwards to the discharge tube and also condenses and solidifies the bromine vapour circulating through it, thus avoiding the contamination of the hot mercury in the diffusion pump. The trap T_2 contains activated charcoal and is cooled by liquid oxygen in the flask F . The charcoal absorbs any impurity gases given off during the discharge. It efficiently removes the main impurities - nitrogen, oxygen, CO_2, and H_2O. Some of the mercury vapour which is carried over by the circulating gas, is also removed, so also, any water vapour that may be present. When the bromine vapour is circulating in the tube D, some of it diffuses backwards and condenses on the inner glass walls of the charcoal trap.

The charcoal trap requires occasional baking out and the gases given off during this process are filtered by passage through the trap T_3, containing KOH sticks,

before they seach the oil pump. This safeguards the pump oil. Bromine vapour if allowed to enter the pump, attacks even the metal parts.

The tube C forms a trap incorporated to eliminate the hydrogen which is generally produced in a tube running at low pressure. Another source of impurity may be the HBr formed by the action of bromine on the tap grease. This trap consists of a fused silica tube packed lightly with copper oxide filings, and provided with glass-wool stops at both the ends. The tube is surrounded by an electric furnace H and is maintained at red heat (500° - 600°C). As the gases stream through the hot copper oxide, any hydrogen present reacts to produce water which is eventually trapped by the charcoal trap.

The tube B contains pure bromine, redistilled before use. A little P_2O_5 placed in the tube before the introduction of the bromine, absorbs any water vapour present in the tube. The bromine reservoir can be maintained at different temperatures by surrounding it with freezing mixture contained in a flask F . The temperature is registered by the thermometer T. Bromine having a vapour pressure of about 62 mms. at room temperature, must be cooled to a temperature of the order of -45°C , the pressure at this temperature being a little less than 2 mms. At this pressure, an intense arc spectrum was excited. To get

a spark spectrum, the pressure must be reduced further and cooling below -80^{oc} is necessary. The method of cooling then, was to surround the reservoir by a flask containing liquid oxygen, and adjust the position of the bottom of the tube B above the liquid oxygen surface in order to achieve any desired temperature. This works quite well. Down to -80^{oc}, a slush of alcohol and solid CO_2 can be used.

The discharge tube D was of pyrex glass, about 30 cms. long and 25 mms. wide. The capillary was about 10 cms. long with a 5 mm. bore for the arc spectrum and of about 1·5 mm. bore for the spark spectrum. One end of the tube was sealed, while the other end which was flanged and ground, had a quartz window attached to it. The discharge was kept cool by a cold air blast from an air blower.

The system can be connected through taps 6 and 7 to a helium cylinder, and any desired amount of the gas can be introduced into the system. Helium is not absorbed by the charcoal trap and becomes very pure on continuous circulation.

The method of operation was as follows: The tap 2 was set to close the left hand side and the system was thoroughly evacuated for about half an hour. Then the tap 1 was set to cut off the rotary pump. On opening the tap 2, the circulation starts and the impurity gases are

absorbed by the traps. Bromine was allowed to enter through the tap 5 and a continuous supply had to be maintained as it is easily condensed in the trap T_1.

Production of the Arc and the Spark Spectrum.

Some bromine vapour was introduced into the discharge tube which was then connected to the H.F. oscillator, through external copper foil electrodes on the limbs of the discharge tube. Different pressures were tried in order to produce the most brilliant glow. The effect of different positions of the electrodes was also noted. The nature of the discharge was observed with two electrodes from the H.F. oscillatory circuit or with only one electrode while earthing the other limb of the tube. It was found that only one electrode round one limb of the tube with earthing of the other, gave a brilliant glow in the capillary. The glow had a tendency to run in the side limbs which were the inlets and outlets for the bromine vapour.

It was found that the arc spectrum was best excited at a vapour pressure of bromine corresponding to the temperature of -45°C, the pressure being about 2 mms. Helium was tried at different pressures but it did not intensify the bromine lines. However it helped to clear up the continuous background that existed below 4000 A°.

In order to excite the spark spectrum, the following procedure was adopted. In a high frequency

electrodeless discharge, the excitation is gentle and can be considered as a low voltage excitation. Because of this, arc lines tend to predominate. However, in an H.F. discharge, as the gas pressure is lowered, the increase in the mean free path enables the ions to acquire higher energies between collisions and more and more spark lines appear. Thus one gets comparitively sharper spark lines in an H.F. discharge than those excited in a Geissler discharge tube which runs at a higher gas pressure. It has been observed by Brasefield[81], in case of an H.F. discharge in mercury, helium and neon that the potential drop at the electrodes increased as the frequency of oscillation decreased, and also that the spark lines were more prominent in the region under the electrodes. With bromine, it was found that a wave-length of about 15-20 metres was suitable for the arc spectrum while a wave-length of 100 metres was better suited for the spark spectrum. Narrowing down of the capillary also helped in increasing the current density and hence lead to better excitation of the spark spectrum.

The nature of the discharge was found to change with pressure as described below: At a pressure greater than 4 mms., streaks of violet red colour appeared and gave the band spectrum. On decreasing the pressure, the discharge assumed a rosy colour and strong arc lines appeared. On lowering the pressure still further the

discharge became a whitish blue and spark lines appeared. It was found that the spark lines were strongest at a pressure of about 0·1 mm. and the capillary appeared full of a bluish white glow while the wider portions of the tube exhibited a rosy tinge. Most of the B & II lines are in the green, blue, and violet, and bands appear at the red end. Fig. 33 illustrates how a change from the arc to the spark spectrum occurs on lowering the pressure. The top strip A shows the arc lines while in the lower strip B, spark lines show up strongly in addition to the strong arc lines. Fig. 34 shows the spark spectrum only. Helium had no marked effect on the lines and therefore was dispensed with.

The High Frequency Oscillator

The circuit adopted was of the conventional Hartley type and is shown in Figure 35. The oscillating coil L was made of copper wire (S.W.G. 14). The valve was a triode, Osram TA 45, and had a dissipation of 500 watts. The filament was heated by a current of 6 amperes at 20 volts, supplied by a step-down transformer T_2. The anode voltage was 5500, supplied by the step-up transformer T_1. The supply of raw A.C. did not affect the performance. The grid leak was 52000 ohms. The high frequency currents were prevented from entering the grid side of the circuit by an air-cored choke and a condenser C_3 of capacity

FIG. 33

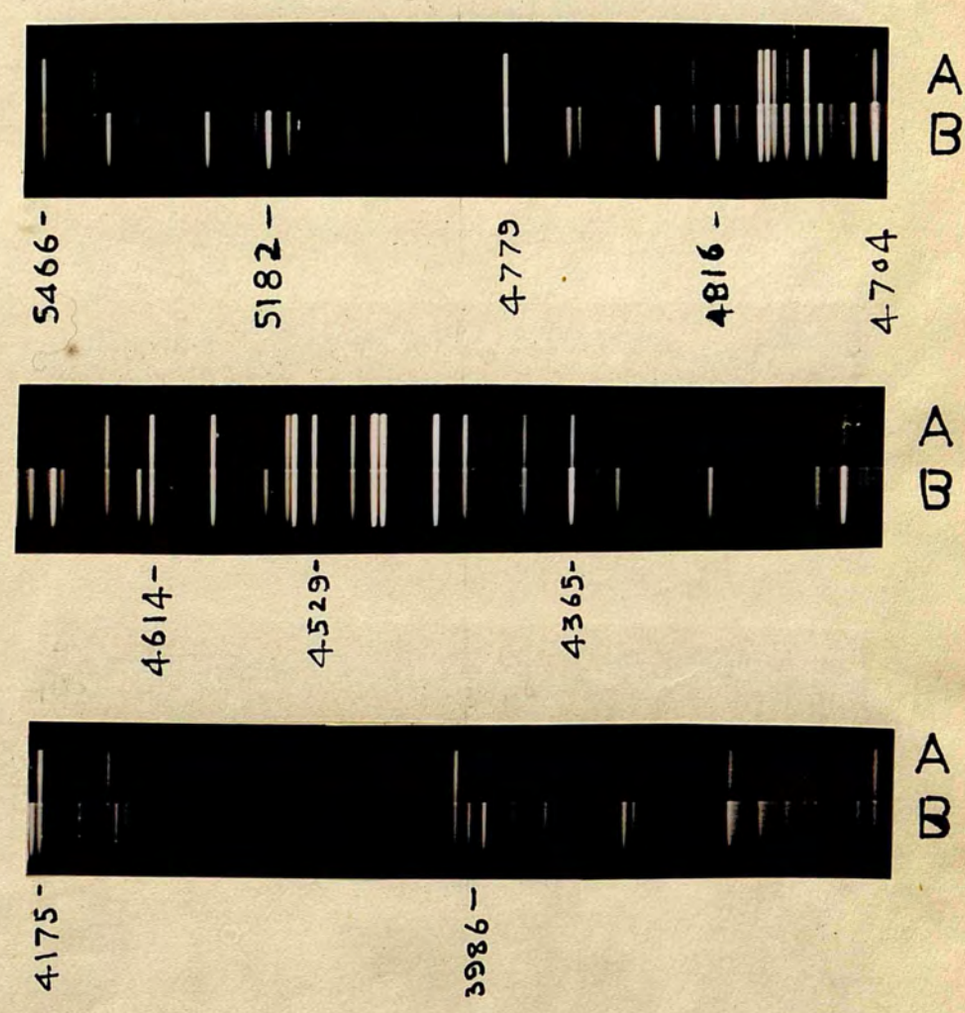

BROMINE

A ARC

B SPARK.

FIG 34

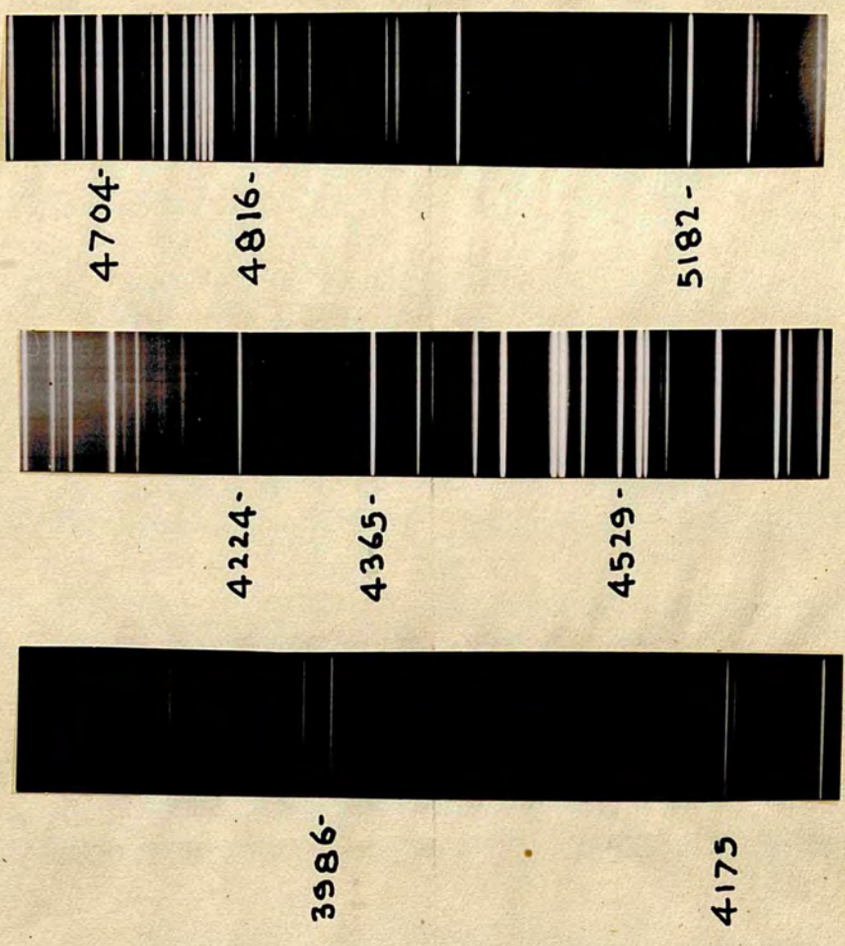

SPECTRUM OF BR II

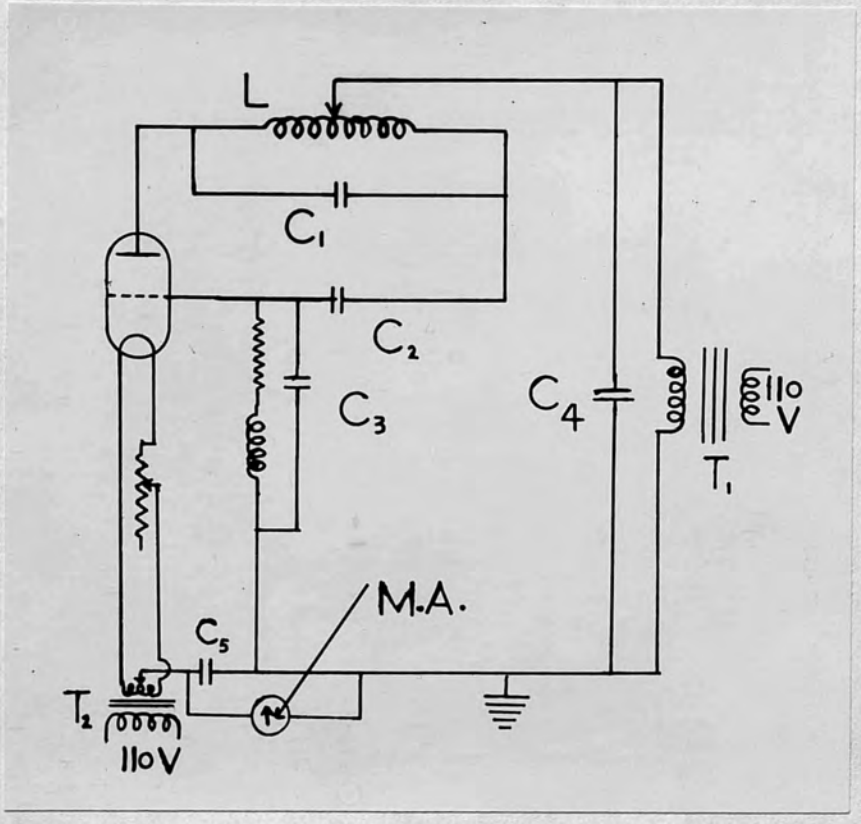

FIG. 35

0·002 μF. The condenser in the oscillating circuit (C_1) was 0·00017 μF. To reduce losses, the high frequency conductors were flexible copper braids.

A piece of copper foil about 2 cm. wide was wrapped round the discharge tube close to the capillary and was connected by a flexible braid to the anode end of the coil L. The other end of the discharge tube was earthed.

When the discharge was running the current was 60 milliamperes.

The Spectrograph

The spectrograph described in detail in Chapter III, was chosen because of its high dispersion, though it was slow as regards speed. The high dispersion separated close lines and allowed structures to be determined which would otherwise be complicated by overlapping.

As the spectrograph was completely built in, it was not possible to introduce the interferometer between the prism and the collimating lens. Hence an external beam mounting was employed. This has advantages particularly when a Lummer plate is used. It eliminates the scattered light which is particularly troublesome in the ultra-violet and the projection lens used to focus the fringes on to the slit compensates for the focal properties of the plate, if any. (These arise when the two surfaces of the plate are

not exactly parallel). Fig. 36 shows the disposition of the apparatus. The lens L_1, a quartz achromat of focal length 22 cms., threw a parallel beam on to the interferometer F. Another quartz-fluorite achromat L_2 (focal length 75 cm.) focussed the fringes on to the slit of the spectrograph P. The lens must be accurately adjusted in order to have the fringes in sharp focus. It was found that the interchange of glass and quartz flats which differed slightly in thickness, affected the position of the focus. The wedge-angle of the optical flats, the prismatic angle between them and the inclination of the interferometer also seemed to alter the focus slightly. After various trials, the different focal positions were noted on a scale attached to the base bar on which the optical system was alligned. The Fabry-Perot interferometer could be rotated about a vertical axis to receive a normal parallel beam, and the tilt of it could be altered about a horizontal axis by screws in the base plate of the holder. (See Fig. 18). The Lummer plate was mounted in an asbestos lined enclosure which helped to ensure temperature constancy.

From what has been said before, the importance of high reflecting coefficients for resolution is obvious. Absorption sets up a higher limit to the useful reflecting power. Usually claims of resolution over intensity have to be suitably balanced.

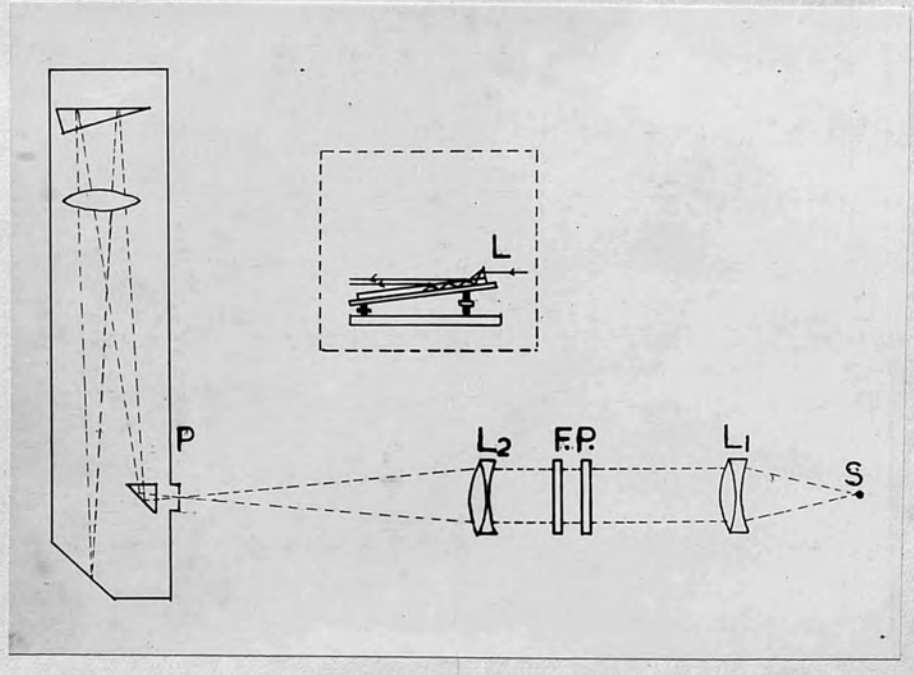

FIG. 36

Among the metals usually employed for preparation of the reflecting surfaces, may be mentioned silver, aluminium, gold and platinum. Silver deposited on glass or quartz flats is very efficient in the visible, red, and infra-red red regions. Particularly in infra-red, it reaches a high reflecting power. However, near about 3300 A°, silver has a band of almost complete ~~transmission~~ absorption and so silver is not much used below 4000 A°.

Aluminium deposited on quartz gives much higher reflectivity than silver below 4000 A°. However, before a high reflection coefficient is reached, a thick deposit of aluminium must be put on and this leads to increased absorption. The results obtained with aluminium in the ultra violet whilst better than silver are not as good as those obtained with silver in red.

Hochheim alloy is much superior to aluminium but the composition and process are not known. Edwards (82) made some observations on Al-Mg alloys. By evaporating aluminium and magnesium together the reflectivity is considerably increased. In the present work mirrors formed by evaporating Al-Mg instead of only aluminium, were employed and they were found quite efficient. Fig. 37 shows the fringes obtained with the lines λ 4077, 4046, 3662, 3654 and 3650 of mercury, the source being a water cooled arc.

Hg.

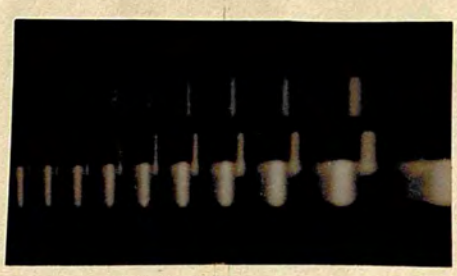

3650
3654
3662

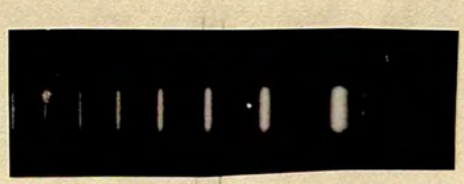

4046

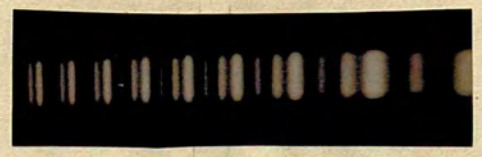

4077

FIG. 37

The evaporation plant has been already described in Chapter III. For the preparation of Al-Mg mirrors, the following procedure was adopted. It was found by Edwards that the composition of Al to Mg in the ratio 10: 1 was suitable. Even if an alloy of this composition is evaporated, the composition of the deposit may not be necessarily the same. This is because of the different boiling points of magnesium and aluminium. (Mg - 1120°C, Al - 1800°C). The rates of evaporation at a given filament temperature are therefore different. Magnesium sublimes and spurts in the filament. Therefore the magnesium ribbon was rolled inside a piece of thin aluminium foil and the whole was made into a pellet. The proportions were 10: 1 by weight. A tungsten filament was used. After evacuation, the filament was heated so as to prefuse the pellet and thus to form an alloy on the filament itself. The prefused mass was then evaporated on to the flats as usual. The mirrors thus prepared gave a reflectivity of about 86% with a transmission of about 4%. The reflectivities mentioned here and in work described in Chapter II, were measured with a Strong reflectometer.

Two pairs of flats were used - one of glass and the other of quartz. The flats are 7 cm. in diameter and 1 cm. thick. They are worked flat to $\lambda/40$ for the mercury green line. There is a small wedge angle between the two faces of the flat.

In the present work both the Lummer plate and the Fabry-Perot interferometer were used. The Lummer plate did not give enough resolution for narrow complex patterns. The Fabry-Perot interferometer was used with varying gaps from 1·5 mms. to 25 mm.

Various types of photographic plates were used, each type being specially sensitive to the region observed. For general use Ilford Hypersensitive panchromatic plates were found to be good. For green and blue region, Ilford 'Iso-Zenith' plates were used while for violet and ultra violet, Ilford "Selochrome" were found satisfactory.

The developing and drying was carried with the usual precautions. Times of exposure varied from 10 minutes for intense lines to over four hours for the faint ones. Fig. 38 shows the fringes, the gap being 8·3 mms.

FIG. 38

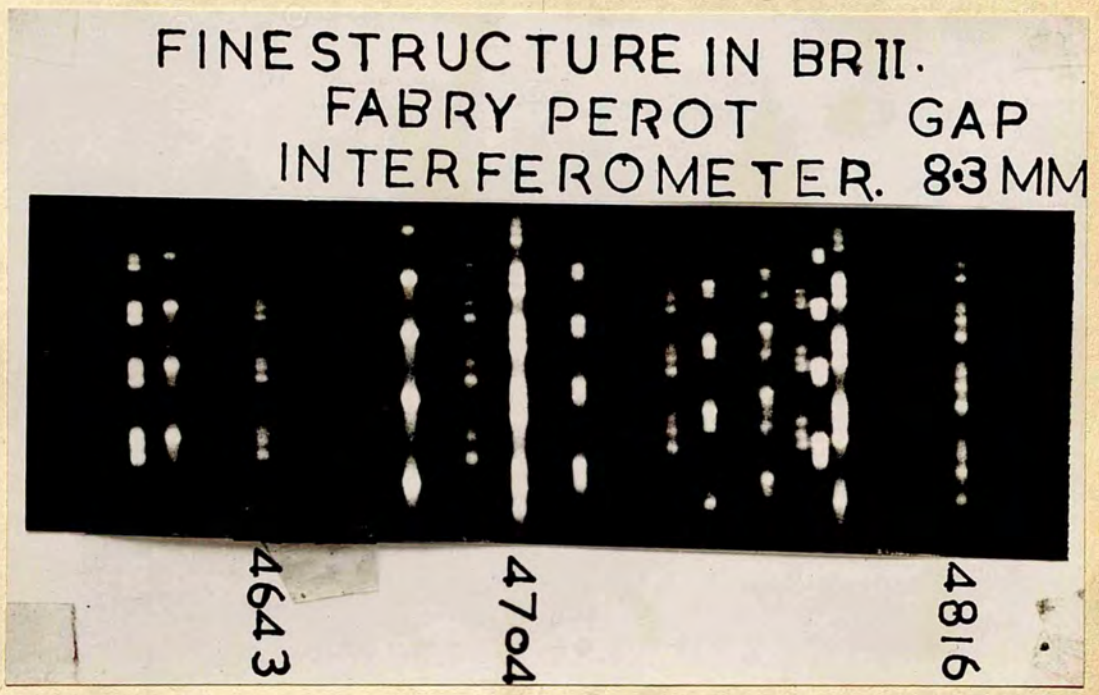
FINE STRUCTURE IN BR II.
FABRY PEROT GAP
INTERFEROMETER. 8·3 MM
4643
4704
4816

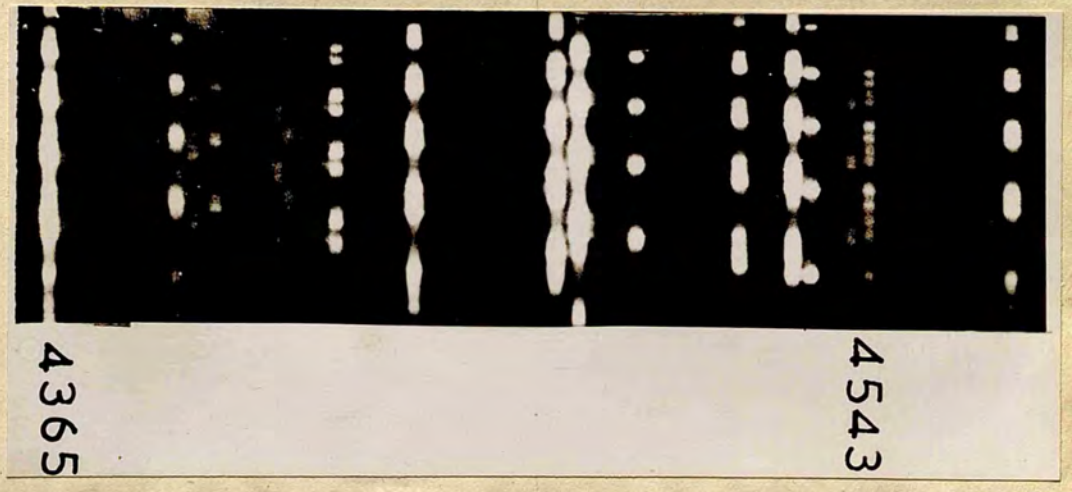
4365
4543

Chapter IX.

OBSERVATION AND ANALYSIS

Mode of Calculation of the Wave-Number Separation.

The general relation

$$n\lambda = 2\mu t \cos\theta$$

reduces to $n\lambda = 2t$

when one is working near the centre and with an air gap. ($\cos\theta \sim 1$).

Differentiation gives

$$d\lambda = -\lambda\, dn/n$$

Now if ν is the wave-number, we have

$$\nu\lambda = 1.$$

This gives $d\lambda = -\lambda\, d\nu/\nu$

Therefore

$$d\nu/\nu = dn/n$$

or $$d\nu = dn/n \cdot \nu = dn/n\lambda = dn/2t$$

If t is expressed in cms., $d\nu$ is given in cm^{-1}. Fringes are observed off-centre, say perhaps, the 5th to the 10th orders.

Consider a doublet, the components of which are denoted by x and y in Fig. 39. At least three orders must be measured. These are denoted by dashed letters.

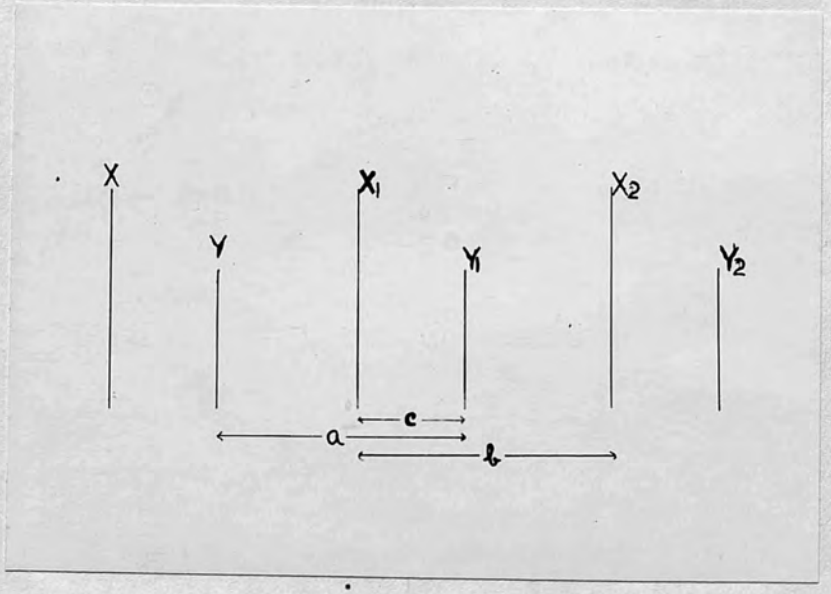

FIG. 39

The fractional order separation of $x_1 y_1$ is given approximately by $2c/a+b$. This is only a first approximation, because the fringe separations are not linear but parabolic. One has to get the average dispersion over two adjacent orders. For fringes say between the 5th to 10th orders, the errors due to this approximation is not large.

Hence $$d n = 2c/a+b$$

and $$d \nu = \frac{2c}{2t \cdot (a+b)} \ cm^{-1} \qquad \ldots\ldots 9.1$$

A few calculations of the separations are illustrated in Tables IV, V, VI and VII . The lines are chosen so as to illustrate the three classes in which they are divided according to the resolution attained. λ4704 is a line of type A (good resolution) where the errors are of the order of 1 - 2 $cm^{-1} \times 10^{-3}$. λ 4785 is a line of type B (medium resolution) where the errors are of the order of 3 - 4 $cm^{-1} \times 10^{-3}$. Lines λ 4766 and λ4614 are illustrative of type C (poor resolution) where the errors are of the order of 6 $cm^{-1} \times 10^{-3}$.

TABLE IV

Readings	a_1	c_1	$b_1; a_2$	c_2	$b_2; a_3$	c_3	b_3
30811							
32015							
32160							
32224							
			845		812		
32690		170		112			816
32860							
32972	732					68	
33040			707		691		683
33422		145		96		60	
33567							
33663	633				593		
33723							
			589				
34055							
34156							
34256							
34303							

Using the formula 9·1 and for a value of t = 8·3 mm., we get the following from Table IV

TABLE IV (A)

$cm^{-1} \times 10^{-3}$

$d\nu_1 = \frac{2c_1}{(a_1+b_1)2t}$	$d\nu_2 = \frac{2c_2}{(a_2+b_2)\cdot 2t}$	$d\nu_3 = \frac{2c_3}{(a_3+b_3)\cdot 2t}$
$\frac{340}{1577 \times 16\cdot6} = 129\cdot9$	$\frac{224}{1519 \times 16\cdot6} = 88\cdot7$	$\frac{136}{1507 \times 16\cdot6} = 54\cdot4$
$\frac{290}{1340 \times 16\cdot6} = 130\cdot4$	$\frac{192}{1280 \times 16\cdot6} = 89\cdot5$	$\frac{120}{1276 \times 16\cdot6} = 56\cdot7$
Mean 130	89	55

Thus the values for the separations are

$d\nu_1 = 130$; $d\nu_2 = 89$; $d\nu_3 = 55$

Therefore the structure of the line λ 4704 is

0 130 219 274 $cm^{-1} \times 10^{-3}$

Similar calculations are given for the lines λ 4875, λ 4766 and λ 4614.

TABLE V

Reading	a_1	c_1	b_1, a_2	c_2	b_2, a_3	c_3	b_3
30284							
30392							
30520					932		
			915				877
31026		173					
31199				125		73	
31324	774						
31397			751		723		713
31800		150		97		63	
31950							
32047	677		631		568		
32110							
32477							
32581							
32615							

TABLE VA

$cm^{-1} \times 10^{-3}$

	$\Delta\nu_1$	$\Delta\nu_2$	$\Delta\nu_3$
	123·4	89·5	55
	126·5	86·3	59·3
Mean	125	88	57

The structure of λ 4785 is therefore

0 125 213 270 $cm^{-1} \times 10^{-3}$.

TABLE VI

Reading	a_1	c_1	b_1
32090			
32192			
			910
33017		85	
33102	718		
			707
33735			
33809		74	
	593		
34328			
34428			

TABLE VI A

$cm^{-1} \times 10^{-3}$

d υ	62·9	68·6
Mean	65	

Therefore the structure of λ 4766 is

0 65 $cm^{-1} \times 10^{-3}$

TABLE VII

Readings	a_1	c_1	b_1, a_2	c_2	b_2
30370 30539 30641			922		900
31318 31461 31541	794	143	773	80	750
32112 32234 32291	614	122	579	57	
32726 32813					

TABLE VII (A)

$cm^{-1} \times 10^{-3}$

	$d\upsilon_1$	$d\upsilon_2$
	100·4	57·6
	106·1	51·7
Mean	103	54

Therefore the structure of the line λ 4614 is

0 103 157 $cm^{-1} \times 10^{-3}$

Observations

New hyperfine structures, in $cm^{-1} \times 10^{-3}$ units, were measured for lines in the region λ 4365 - 3700 in the arc spectrum of bromine. Some earlier reported lines in the region λ 6400 - 4365, were also measured along with the new ones. A number of lines in the region λλ 6000-3700, in the first spark spectrum of bromine (Br II) were measured for the first time. The structures were calculated as explained above. The observed structures are given in Table VIII for Br I and in Table IX, for Br II.

The wave-lengths and the allocations given in columns 1 and 2, are taken for Br I from the paper of Kiess and de Bruin[21] while those for Br II are taken from the paper by Lacroute[23]. The structures are given in the third column, with the visually estimated intensities below each component. Components connected by an hyphen indicate a blend. A component overlined indicates incomplete resolution.

The lines are classified according as to whether the resolution of the individual components is good or poor. The lines are classed A, B or C according to whether the resolution is good (A), moderate (B) or bad (C). This is affected by two factors, firstly the falling off in resolving power of the Fabry-Perot interferometer with decreasing wave-length and secondly, the inherent

complexity or narrowness of the pattern. The structures for a number of unclassified lines of Br II are given in Table X. In Table VII. giving the classification of the arc lines, those lines marked with an asterisk have not been previously reported.

TABLE VIII

Hyperfine structures in the lines of B II.

Units $cm^{-1} \times 10^{-3}$.

Wave-length	Allocation	Structure (Red ... Violet)				Class
6559·8	$5s^4P_{5/2} - 5p^4S_{3/2}$	0	195	323	408	A
		(6)	(4)	(3)	(2)	
6350·7	$5s^4P_{5/2} - 5p^2P_{3/2}$	0	202	341	428	A
		(4)	(3)	(2)	(1)	
6148·6	$5s^4P_{5/2} - 5p^2D_{3/2}$	0	190	318	400	A
		(5)	(4)	(3)	(2)	
5002·7	$5s^2P_{1/2} - 6p^4S_{3/2}$	0	90			A
		(4)	(2)			
4979·7	$5s^2P_{3/2} - 6p^2P_{3/2}$	0	100	173	264	A
		(4)	(2)	(6)	(1)	
4807·6	$5s^2P_{1/2} - 5p^2P_{1/2}$ (1S)	0	93	185		A
		(3)	(5)	(3)		
4614·6	$5s^2P_{3/2} - 6p^2D_{3/2}$	0	103	~157		B
		(4)	(3)	(2)		
4575·7	$5s^2P_{3/2} - 6p^2D_{5/2}$	0	84	~159		B
		(5)	(3)	(2)		
4529·9	$6s^4P_{1/2} - 6p^4S_{3/2}$	Single				
4423·0	$5s^2P_{3/2} - 7p^4P_{3/2}$	0	~54			B
		(2)	(2)			

TABLE VIII (continued)

Wave-length	Allocation	Structure (Red ... Violet)	Class
4399·7	$5s\,^2P_{3/2}$ - $5p\,^2P_{3/2}$ (1S)	0 86	A
		(2) (2)	
4369·2	$5s\,^4P_{1/2}$ - $5p\,^2P_{1/2}$ (1S)	85 0	A
		(2) (2)	
⁂ 4365·1	$5s\,^4P_{1/2}$ - $7p\,^4P_{3/2}$	122 49 - 0	B
		(4) (2) (2)	
⁂ 4175·8	$5s\,^4P_{3/2}$ - $6p\,^2D_{3/2}$	105 47 - 0	C
	($^2D_{5/2}$)	(6) (4) (3)	
⁂ 4143·9	$5s\,^4P_{3/2}$ - $6p\,^2D_{5/2}$	0 ~84	C
	($^2D_{3/2}$)	(4) (2)	
⁂ 3992·4	$5s\,^4P_{3/2}$ - $7p\,^2P_{3/2}$	~68 0 ~77	C
		(3) (5) (2)	
⁂ 3934·11	$5s\,^4P_{5/2}$ - $6p\,^2D_{3/2}$	0 180 326 403	B
	($^2D_{5/2}$)	(4) (3) (2) (1)	
⁂ 3917·8	$5s\,^4P_{5/2}$ - $6p\,^4S_{3/2}$	0 208 320 408	B
⁂ 3828·55	$5s\,^4P_{5/2}$ - $7p\,^4P_{5/2}$	0 99 181 226	C
⁂ 3815·7	. . . . .	0 66 156	C
⁂ 3794·04	$5s\,^4P_{5/2}$ - $7p\,^4P_{3/2}$	0 132 215 285	B
		(4) (3) (2) (1)	

TABLE IX

Hyperfine structure in the lines of B II.

Units $cm^{-1} \times 10^{-3}$.

Wave-length	Allocation	Structure (Red ... Violet)	Class
5238·2	$5s^3S_1 - 5p^3P_1$	0 95	C
		(1) (3)	
5182·4	$5s^3S_1 - 5p^3P_2$	0 38 93	B
		(2) (2) (3)	
5164·4	$5s^3S_1 - 5p^3P_0$	0 48	C
		(1) (1)	
4848·8	$5p^5P_3 - 6s^5S_2$	Broad single-width 50	
4816·7	$5s^5S_2 - 5p^5P_1$	0 154 264 323	A
		(5) (3) (2) (1)	
4785·5	$5s^5S_2 - 5p^5P_2$	0 125 213 270	B
		(4) (3) (2) (2)	
4766·0	$5p^5P_2 - 6s^5S_2$	0 65	C
		(2) (1)	
4735·4	$5p^5P_1 - 6s^5S_2$	0 76	B
		(2) (3)	
4704·9	$5s^5S_2 - 5p^5P_3$	0 130 219 274	A
		(5) (3) (2) (1)	
4396·4	$5p^3P_2 - 4d^5D_2$	0 - 75	C
		(1) (1)	
4356·9	$5p^3P_1 - 4d^5D_2$	Single	

TABLE IX (continued)

Wave-length	Allocation	Structure (Red ⟵ Violet)	Class
4230·0	$5s^5S_2 - 5p^3P_1$	0 ~188 270	B
		(3) (2) (1)	
4193·7	$5s^5S_2 - 5p^3P_2$	0 130 219 280	B
		(4) (3) (2) (1)	
3980·4	$5p^5P_3 - 4d^5D_4$	0 - 49	C
		(2) (1)	
3980·0	$5p^5P_3 - 4d^5D_3$	Single	
3935·2	$5p^5P_2 - 4d^5D_1$	width 50	
3914·3	$5p^5P_1 - 4d^5D_1$	Single	
3914·1	$5p^5P_1 - 4d^5D_0$	Single	

TABLE X

Unclassified lines in the B I II Spectrum

Units $cm^{-1} \times 10^{-3}$.

Wave-length	Structure (Red → Violet)			
4921·3	0	112		
	(1)	(3)		
4802·3	434	337	188	0
	(1)	(2)	(3)	(5)
4742·7	0	122	198	237
	(5)	(3)	(1)	(1)
4728·2	Single			
4719·8	0	59	119	
	(2)	(2)	(5)	
4693·3	0	144	218	384
	(6)	(3)	(1)	(1)
4678·7	Single			
4542·9	0	121	254	362
	(1)	(2)	(5)	(9)
4365·6	0	67	156	
	(2)	(2)	(3)	
4351·2	0	176	344	
	(5)	(3)	(1)	

TABLE X (continued)

Wave-length	Structure (Red → Violet)			
4297·8	0	156	246	
	(3)	(1)	(1)	
4291·4	0	158	266	364
	(9)	(6)	(4)	(3)
4223·9	118	0	215	341
	(3)	(10)	(5)	(2)
4179·6	0	146	232	
	(7)	(2)	(5)	
4140·4	Single			
4135·9	Single			
3986·3	132	0	205	338
	(1)	(10)	(3)	(5)
3970·6	Single			
3968·3	0	129	224	
	(9)	(6)	(4)	
3955·4	Single			
3950·6	Single			

ANALYSIS

Bromine Arc Spectrum

In the normal state the bromine atom has 26 electrons in closed shells in the core and seven valence electrons. The configuration of the valence electrons is denoted as $4s^2 \cdot 4p^5$ i.e. there are two electrons in 4s orbits and five in 4p orbits. The $4s^2$ electrons form a closed group and this does not take effective part in the radiation process. On excitation, one of the 4p electrons is raised to higher orbits of the s, p, d, ... type. Each separate electron configuration gives rise to a number of terms. One can build up these terms by treating the $4s^2 \cdot 4p^4$ group as a core and attaching an optical electron in either of ns, np, nd, ---- orbits. These give rise to the excited states of the atom. All these terms are predicted by Hund's theory.

In Br I, a large number of term hyperfine structures were analysed and interval factors determined by Tolansky and Trivedi[27]. It has been shown conclusively that the nuclear spin of bromine is $3/2$ and is the same for both the isotopes. Using these known structures, it is possible to analyse the new lines recorded here.

Consider the two lines λ 3794·0 and λ 4365·1. These have a common upper term, $7p\,^4P_{3/2}$. Since the structures of the lower terms $5s\,^4P_{5/2}$ and $5s\,^4P_{1/2}$ are already known,

one can obtain the upper term structure. This is shown in Fig. 40, where the transitions are shown above and the predicted and observed patterns below in units of $cm^{-1} \times 10^{-3}$. The heights of the lines representing the components are proportional to the intensity.

Fig. 41 gives the analysis of the three lines λ3934·1, λ4175·8 and λ4614·6. These have a common upper term $6p\,^2D_{5/2}$. [de Bruin gives this as $^2D_{3/2}$. The reason for adopting the present classification will be discussed later.] Using the known lower term structures, this common upper term structure is determined. In these lines it is not possible to resolve the closed group of components because of the limit set on resolution due to line width caused by doppler effect. Further, the narrowing of the capillary necessary to excite the spark spectrum also leads to some broadening on account of the increased current density. The other line structures are determined by the same method as is used in the cases illustrated here.

<u>First Spark Spectrum of Bromine</u> (Br II)

The analysis of the Br II lines is new and exemplifies the systematic method of analysis as applied to a complex spectrum.

The singly ionised bromine atom contains 26 electrons in closed shells forming a core and six valence

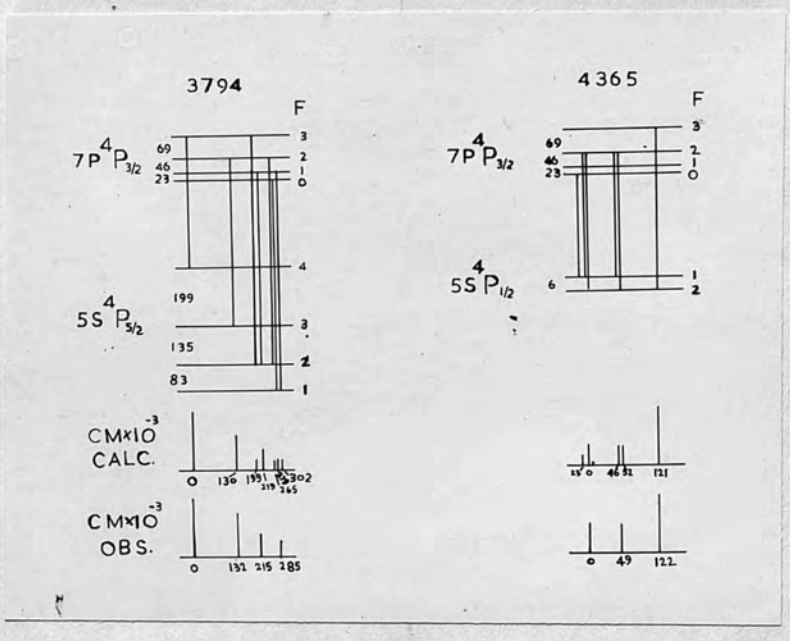
3794
F
$7P\,^4P_{3/2}$
69
46
23
3
2
1
0
4
$5S\,^4P_{5/2}$
199
135
83
3
2
1
CM×10^{-3}
CALC.
0 136 195 215 265 302
CM×10^{-3}
OBS.
0 132 215 285
4365
F
$7P\,^4P_{3/2}$
69
46
23
3
2
1
0
$5S\,^4P_{1/2}$
6
1
2
15 0 46 82 121
0 49 122

FIG. 40

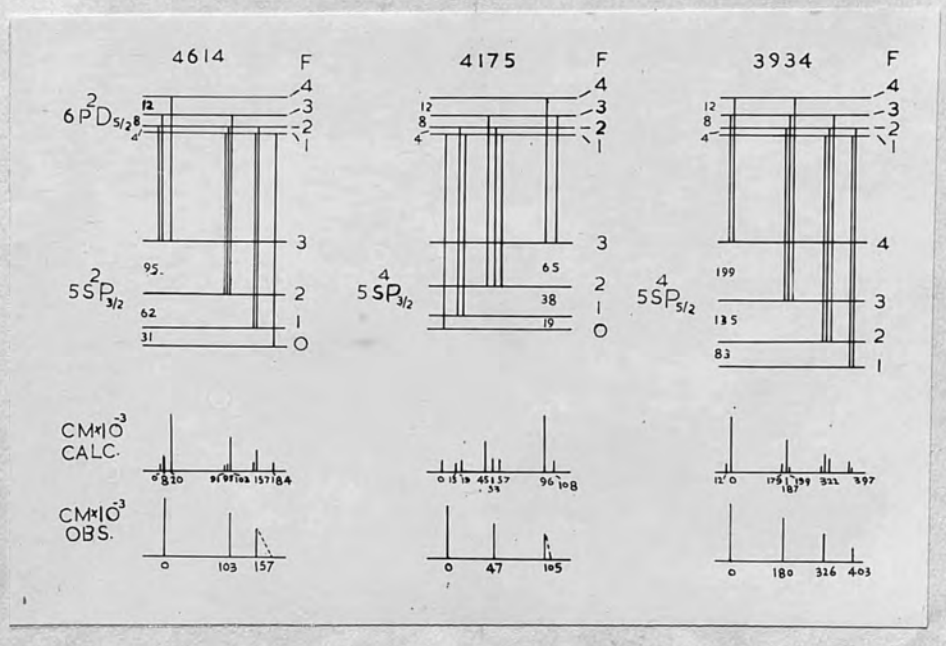
4614
F
$6P\,^2D_{5/2}$
12
8
4
4
3
2
1
$5S\,^2P_{3/2}$
95
62
31
3
2
1
0
CM×10^{-3}
CALC.
0 8 20 91 98 103 157 184
CM×10^{-3}
OBS.
0 103 157
4175
F
12
8
4
4
3
2
1
$5S\,^4P_{3/2}$
65
38
19
3
2
1
0
0 15 19 45 57 96 108
0 47 105
3934
F
12
8
4
4
3
2
1
$5S\,^4P_{5/2}$
199
135
83
4
3
2
1
12 0 179 187 199 321 397
0 180 326 403

FIG. 41

electrons. Two of these are in 4s orbits and four in 4p orbits giving the configuration $4s^2.4p^4$. The other terms are built upon the $4s^2.4p^3$ group as a core by attachment of an optical electron in either of ns, np, nd --- etc. orbits. Hund's theory predicts all the terms, some of which are given in Table XI.

TABLE XI

Terms of Br II

Configuration $n > 4$ / $n' \geq 4$	Terms of basic Br III ion. 4S	2D	2P
$4s^2.4p^4$	^3P ; ^1D; ^1S.		
$4s.4p^5$	$^3P^o$; $^3S^o$; $^1P^o$; $^1S^o$		
$4s^2.4p^3.ns$	$^5S^o$; $^3S^o$	$^3F^o$; $^1D^o$	$^3P^o$; ^1P_o
$4s^2.4p^3.np$	^5P ; ^3P	$^3(FDP)$; $^1(FDP)$	$^3(DPS)$; $^1(DPS)$
$4s^2.4p^3.n'd$	$^5D^o$; $^3D^o$	$^3(GFDPS)^o$; $^1(GFDPS)^o$	$^3(FDP)^o$; $^1(FDP)^o$

Three families of terms arise from the three basic terms of the doubly ionised bromine atom (Br III). The three basic terms are ^4S, ^2P, ^2D. Lacroute[23] has analysed the lines arising out of the terms belonging to the family ^4S. Unfortunately, no classification has yet been given

for the terms arising from the ^2D and ^2P parent terms. Some of the unclassified lines have wide structures. The various transitions giving rise to the classified lines of the ^4S group are shown in Fig. 42.

First we shall consider the three lines λ 5164·4, λ 5238·2, and λ 5182·4. This group of lines is chosen as a start because one of the lines has a term with a zero J value and hence has no structure. All the three lines have a common lower term $5s\cdot{}^3S_1$, while the upper terms are $5p\,^3P_0$, $^3P_1$ and $^3P_2$ respectively. As the term $5p\,^3P_0$ gives rise to only one F value namely 3/2, the structure of the line λ 5164·4 gives the structure of the $5s\,^3S_1$ term. With the help of this, the structures of the upper term $5p\,^3P_1$ and $^3P_2$ are easily determined. Fig. 43 illustrates this. The agreement between the predicted and the observed patterns is good.

The term $5s\cdot{}^5S_2$ is important. It gives rise to regular quartets when the upper term has a comparitively narrow structure. Consider the two lines λ 4193·5 and λ 4230·0. They have a common lower term $5s\,^5S_2$. Since the structures of the upper terms $5p\,^3P_1$ and $5p\,^3P_2$ are known from above, the pattern of these lines gives the structure of the term $5s\cdot{}^5S_2$. Fig. 44 illustrates this. The two

FIG. 42

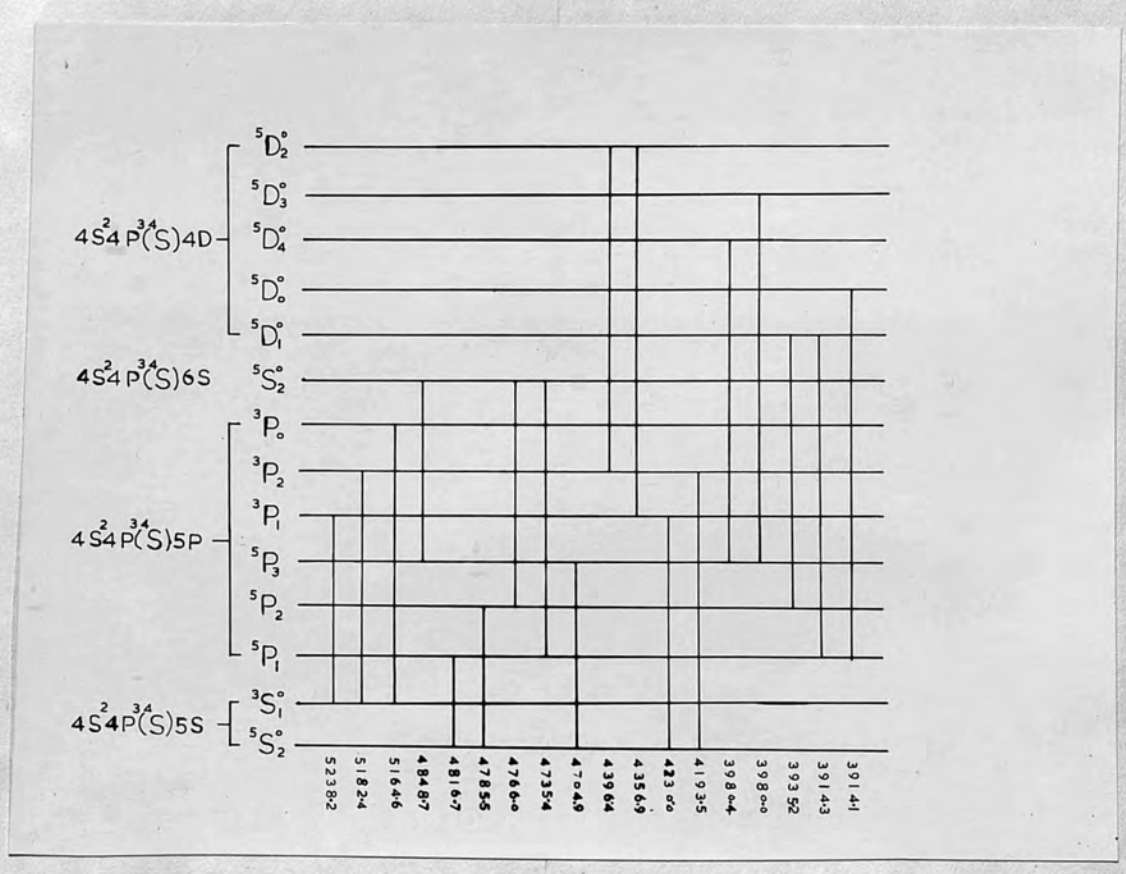
$4S^2 4P^{3,4}(S)4D$
$^5D_2^o$
$^5D_3^o$
$^5D_4^o$
$^5D_o^o$
$^5D_1^o$
$4S^2 4P^{3,4}(S)6S$
$^5S_2^o$
$4S^2 4P^{3,4}(S)5P$
^3P_o
$^3P_2$
$^3P_1$
$^5P_3$
$^5P_2$
$^5P_1$
$4S^2 4P^{3,4}(S)5S$
$^3S_1^o$
$^5S_2^o$
5238·2
5182·4
5164·6
4884·7
4816·7
4785·5
4766·0
4735·4
4704·9
4396·4
4356·9
4233·0
4193·5
3984·4
3980·0
3935·2
3914·3
3911·1

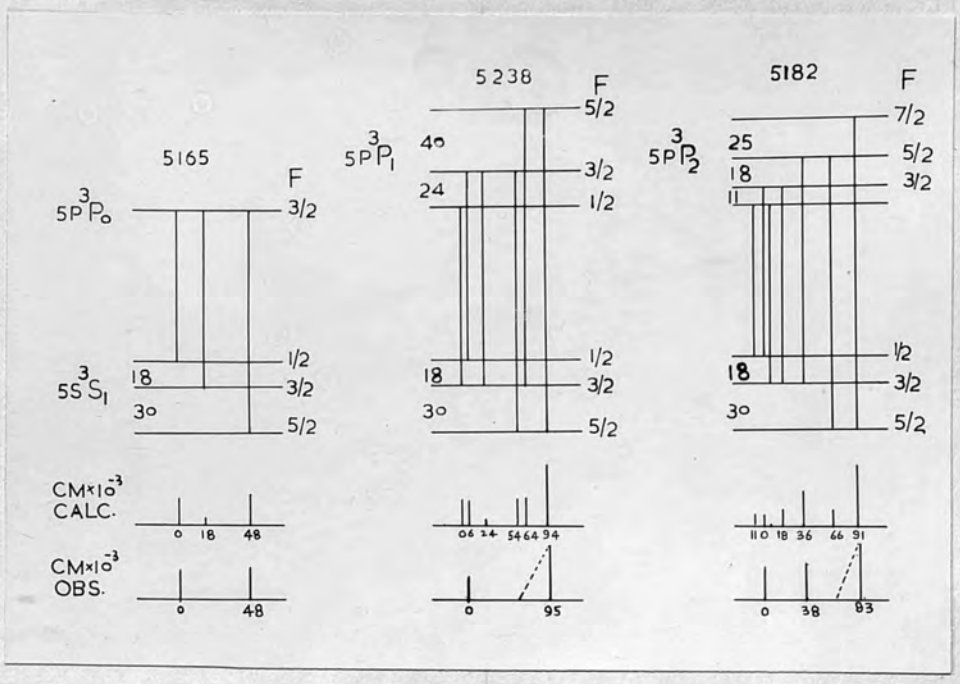
5165
F
$5P^3P_0$
3/2
1/2
18
$5S^3S_1$
3/2
30
5/2
CM×10⁻³ CALC.
0 18 48
CM×10⁻³ OBS.
0 48
5238
F
$5P^3P_1$
5/2
40
3/2
24
1/2
1/2
18
3/2
30
5/2
06 24 54 64 94
0 95
5182
F
$5P^3P_2$
7/2
25
5/2
18
3/2
11
1/2
18
3/2
30
5/2
110 18 36 66 91
0 38 83

FIG. 43

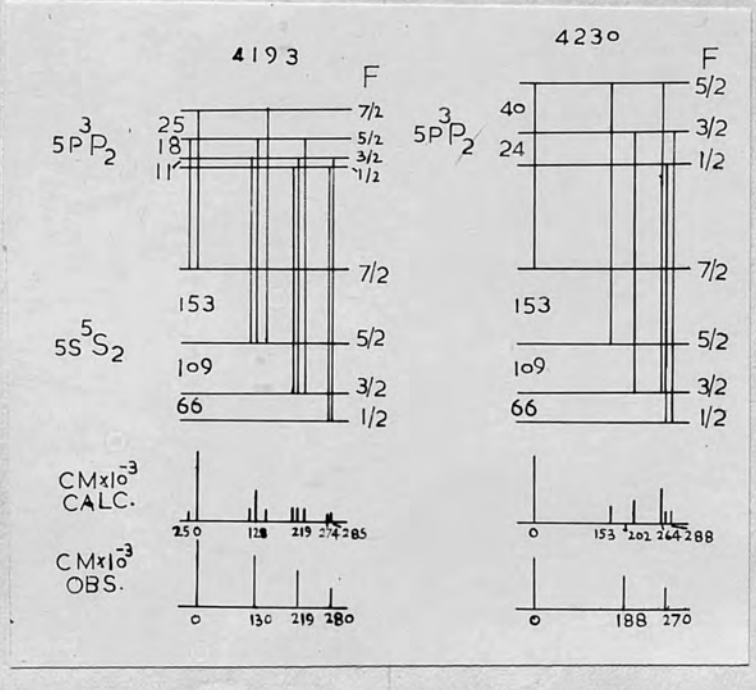
4193
F
$5P^3P_2$
7/2
25
5/2
18
3/2
11
1/2
7/2
153
$5S^5S_2$
5/2
109
3/2
66
1/2
CM×10⁻³ CALC.
250 128 219 274 285
CM×10⁻³ OBS.
0 130 219 280
4230
F
$5P^3P_2$
5/2
40
3/2
24
1/2
7/2
153
5/2
109
3/2
66
1/2
0 153 202 264 288
0 188 270

FIG. 44

central components of λ 4230 are not properly resolved and so the centre of gravity is estimated.

The lines λ 4816·7, 4785·5 and 4704·9 show well resolved quartet patterns. This again proves that the spin of bromine nucleus is $^3/_2$. The structure revealed in these lines is essentially that of the term $5s\,^5S$ and the number of components directly gives the spin. The analysis of these lines is illustrated in Fig. 45. Using the known structure of $5s\,^5S_2$, one gets the structures of the upper terms $5p\,^5P_1$, $^5P_2$ and $^5P_3$. The agreement between the predicted and the observed values is good.

The lines λ 4766·0, 4735·4, and 4848·8 have very complex structures. Except for λ 4735·4, the components are so closely packed that resolution is poor. For λ 4848 it is so complex and packed that it appears as a broad single line pattern of width 50 $cm^{-1} \times 10^{-3}$. One gets the structure of the $6s\,^5S_2$ term from these lines.

The group of $4d\,^5D$ terms combines with the $5p\,^3P_{D12}$ and $5p\,^5P_{123}$ multiplets which have narrow structures. Most of the lines from these transitions appear single except λ 3980·9 which shows two blended components. Therefore the only conclusion that can be drawn for these ^5D terms is that all of them have narrow structures. The width of the line 4396·4 enables one to estimate the structure of the term $4d\,^5D_1$ while from the line λ 3980, the total

FIG. 45

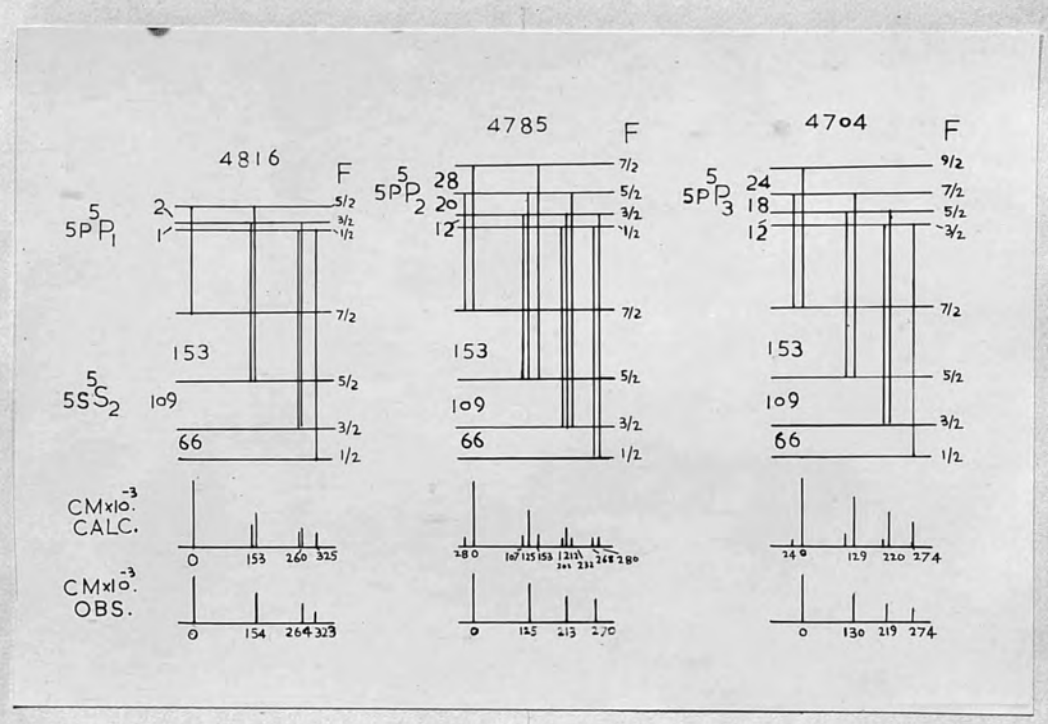
4816
F
$5s^2 5p\,^1P_1$
2
1
5/2
3/2
1/2
7/2
153
109
5/2
3/2
66
1/2
$5s^2 5s\,^3S_2$
CM×10^{-3} CALC.
0 153 260 325
CM×10^{-3} OBS.
0 154 264 323
4785
F
$5s^2 5p\,^3P_2$
28
20
12
7/2
5/2
3/2
1/2
7/2
153
109
5/2
3/2
66
1/2
280 107 125 153 213 241 232 268 280
0 125 213 270
4704
F
$5s^2 5p\,^3P_3$
24
18
12
9/2
7/2
5/2
3/2
7/2
153
109
5/2
3/2
66
1/2
249 129 220 274
0 130 219 274

width of the $4d^5D_4$ term can be estimated. The line 3935 gives an approximate structure of the term $4d^5D_1$. There is no check available.

Some of the lines as yet unclassified show wide patterns. These lines will be discussed in the next chapter.

Chapter X.

DISCUSSION

This chapter is divided into two sections:

1. Interpretation and discussion of results.
2. Calculation of the electric quadrupole moment and the magnetic moment of the bromine nucleus.

INTERPRETATION

The Arc Spectrum

Out of the ten new lines measured here, four involve the important term $5s^4P_{5/2}$ and the analysis leads to the same intervals as were determined earlier[27] from the accurate measurements in the red and the infra-red. This term shows a deviation from the interval rule which can be attributed to nuclear electric quadrupole moment. This will be calculated at the end of this chapter. Some of the intervals which were only approximately given formerly, have now been given more accurately because of the check supplied by the new lines. The new intervals are given in Table XIII.

TABLE XII

Hyperfine structures in the terms of Br I.

Intervals.

Configuration	Term	Structure $cm^{-1} \times 10^{-3}$.			Interval factors $cm^{-1} \times 10^{-3}$
$4s^2.4p^4.6p$	$^2D_{5/2}$	12	8	4	3
	$^2D_{3/2}$	11	7	4	4
$4s^2.4p^4.7p$	$^4P_{3/2}$	69	46	23	23
	$^4P_{5/2}$	100	75	-	25

The interval factor 23 for the term $7p\,^4P_{3/2}$ was originally determined from the line λ4365·1. The structure of this line as given previously was complex. It was possible in the present work to obtain the correct structure of this line. There is a nearby line λ4365·6 of Br II and the two structures overlap. Though these two lines cannot be resolved by the prism spectrograph, yet the two fringe systems are slightly displaced on account of the larger dispersion available. The structure of the line λ 4365 as given now in conjunction with that of the line λ 3794, involving the same term, enables one to confirm accurately the interval factor of the term $7p\,^4P_{3/2}$ to be 23 $cm^{-1} \times 10^{-3}$.

The structure of the line λ 4423·0 as determined now, agrees with the value given earlier. But it does not fit in with the allocation of this line as given by Kiess and de Bruin[21]. The transition is described as $5s^2P_{3/2}$ - $7p^4P_{3/2}$. It seems that the lower term should be different from $5s^2P_{3/2}$, and should have a smaller structure.

The intervals of the two terms $6p^2D_{3/2}$ and $6p^2D_{5/2}$ ~~and $6p^2D$~~ were earlier determined from the lines λ 4614·6 and λ 4575·7 respectively. Now a check on this is available through the lines λ 4175, λ 3934 and λ 4143. It is found that the observed structures of the lines λ 4175 and λ 3934 do not fit in well with the calculated ones if one takes $6p^2D_{3/2}$ as the common upper term as given by Kiess and de Bruin[21]. A better fit is obtained as regards the structure as well as the intensities by taking the upper term J value to be $5/2$. This means that the term should be $^2D_{5/2}$ instead of $^2D_{3/2}$. Lacroute[23] who has confirmed most of the classifications of Kiess and de Bruin[21] by using the Zeeman effect as a guide, suggests two modifications. According to him the J values of the $7p^4P_{5/2}$ and $7p^4P_{3/2}$ as given by Kiess and de Bruin[21] ought to be interchanged. This means wherever there occurs a term $7p^4P_{3/2}$, it should read $7p^4P_{5/2}$ instead. From the analysis of the above lines, it seems that this modification is correct. The analysis of all the lines involving these terms fits in well with this change.

The Spark Spectrum

Table XIII gives the structures and the interval factors of the terms of Br II as determined in the previous chapter. A negative sign implies an inverted term in which the largest F value lies deepest.

The $5s^5S_2$, $6s^5S_2$ and $5s^3S_1$ terms are spherically symmetrical and are not therefore affected by the existing nuclear quadrupole moment of bromine. Hence the interval rule should be strictly obeyed

TABLE XIII

Hyperfine structures in the terms of Br II.

Configuration	Term	Intervals Structure $cm^{-1} \times 10^{-3}$			Interval factor $cm^{-1} \times 10^{-3}$.
$4s^2.4p^3.5s$	$^5S_2$	153	109	66	44
	$^3S_1$	-30	18		-12
$4s^2.4p^3.5p$	$^5P_3$	24	18	12	5
	$^5P_2$	28	20	12	8
	$^5P_1$	2	1		<1
	$^3P_2$	25	18	11	6
	$^3P_1$	40	24		16
	$^3P_0$				0
$4s^2.4p^3.6s$	$^5S_2$	36	27	15	10
$4s^2.4p^3 4d$	$^5D_4$	very small			

TABLE XIII (continued)

Configuration	Term	Structure $cm^{-1} \times 10^{-3}$	Interval factor $cm^{-1} \times 10^{-3}$.
	$^5D_3$	very small	
	$^5D_2$	-21 15 9	-6
	$^5D_1$	10 6	4
	$^5D_0$		0

unless strong perturbations are caused by other configurations. The structures of these terms as determined here show that the interval rule is obeyed within the limits of measurement

The interval factor for the term $5s^5S_2$ is about 4 times that of the term $6s^5S_2$. This is similar to the observation of Tolansky and Forester[83] in the first spark spectrum of iodine. These terms arise out of the addition in parallel of a s-electron to the electron core of the basic ion term $4p^3 \cdot 4S_{3/2}$ of the doubly ionised bromine atom, according to the coupling theory of White.[84] Thus from the smallness of the interval factor of $6s^5S_2$, it follows that the coupling of the $4p^3$ group is small. The term $^3S_1$ is formed by the addition of a s-electron, anti-parallel to the $4p^3$ group of Br III. The interaction energy is proportional to cos JS which is equal to -1 in this case.

Thus the interval factor for $^3S_1$ should be negative and numerically smaller than the positive interval factor of the term $^5S_2$. The value of the interval factor for $^3S_1$ as found here ($-12\ cm^{-1} \times 10^{-3}$) fits in the above theory. The magnitude, however, suggests that the coupling constant of the $4p^3$ electrons is about 4/7th that of the 5s-electron. This is not as small as one would expect from the interval factor of the $5s\,^5S_2$ term.

The interval factors of the $4d\,^5D$ terms are small and this suggests that the coupling of the $4p^3$ group is not strong since a 4d electron is not expected to possess penetrating properties. One can therefore summarise by saying that in contrast to singly ionised iodine, the coupling of the $4p^3$ electron group in Br II is weak and the interval factor of the $5s\,^3S_1$ term is rather large~~smaller~~ than what would be expected under these circumstances. In Br I, the group $4p^5$ has a large coupling constant. This may mean that there is a change in the nature of the electron coupling, in moving from $4s^2 \cdot 4p^3$ to $4s^2 \cdot 4p^4$ configuration. No anomalies are found except for the line λ 4356·9. It is a transition from $4d\,^5D_2$ to the $5p\,^3P_2$ term. The structure of the term $4d\,^5D_2$ is known approximately from the line λ 4396. The line λ 4356·9 appears as a sharp single and this fact does not fit in with the structures of the two terms involved. Lacroute[23] has mentioned this

line among the classified ones but does not mention it in the table in which all the classified and unclassified are listed together. Further the Zeeman pattern for this line is not given. It seems that this line is either wrongly classified or has been included by mistake in place of some other line.

Unclassified Lines

It is easy to collect groups of lines from Table XI, showing similar structures. The two lines λ 4223·9 and λ 3986·3 have very similar structure and that suggests that they involve the same common term. This is substantiated by the Zeeman splitting given by Lacroute[23]. The lines λ 4719 and λ 4365 show a triplet structure roughly of the same order while the three lines λ 4297, 4179 and 3968 exhibit an identical pattern. From the data on Zeeman splitting given by Lacroute[23], it seems that none of these lines belong to the classified levels of ^4S system nor do they appear to be inter-combinations between the ^2D and the ^4S systems. None of these lines show the typical Zeeman splitting of the ^4S terms.

Electric Quadrupole Moment of Bromine

Deviations from the interval rule have been formerly observed in the term $5s\cdot{}^4P_{5/2}$ and this can be definitely attributed to the asymmetry of the nucleus or to the nuclear quadrupole moment. The separations in this

term have been measured accurately from lines in the red and the infra red regions where the Fabry-Perot interferometer is at its best as regards resolution. Fig. 46 shows the microphotometer trace and the line pattern for the line λ 6350 of B π I. There is no evidence of any possible perturbation from another configuration. The observed position of the levels are displaced from those calculated from the interval rule and this is diagramatically illustrated in Fig. 47.

As has been shown in a previous chapter, the interaction between the angular momentum J of a non-spherically symmetrical electron configuration and the spin I of the non-spherically symmetrical nucleus takes the form

$$E = a_0 + \frac{a_1}{2} C + b\,C(C+1)$$

where $C = f(f+1) - i(i+1) - j(j+1)$.

The significance of the different constants a_0, a_1 and b is discussed already. The formula contains three constants and since the term $5s\,^4P_{5/2}$ contains four F levels, a check is available on the validity of the formula. The calculated values of a_0, a_1 and b as derived from the different F combinations are

$a_0 = 223$

$a_1 = 47{\cdot}1$

$b = 0{\cdot}17$

FIG. 46

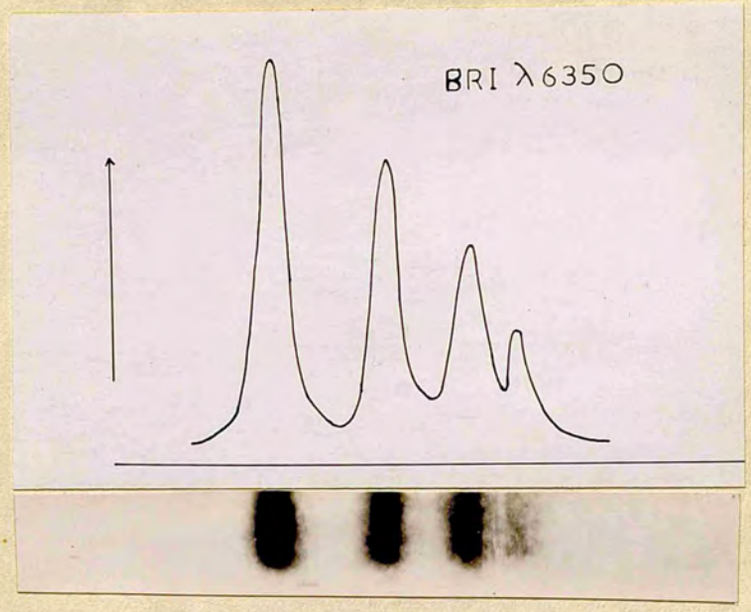

0·418 CM^{-1}

131 In

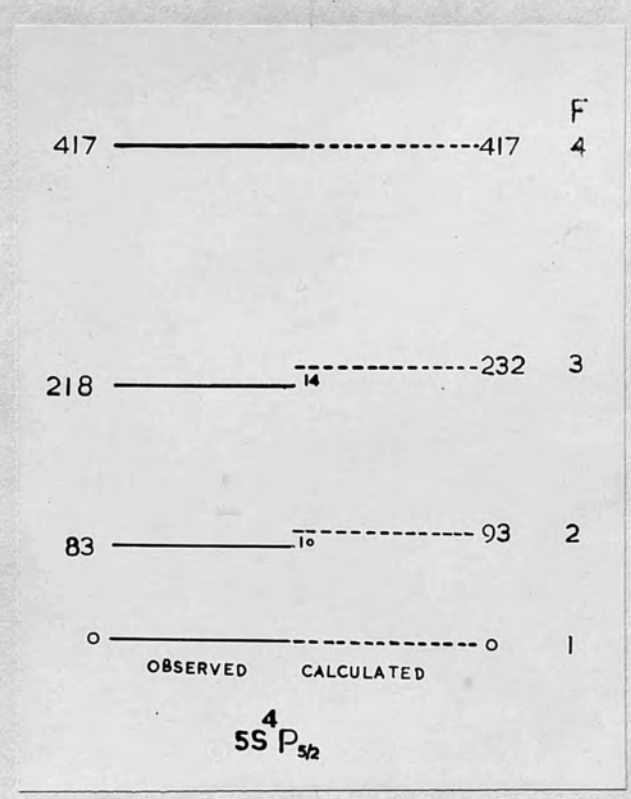
F
417
417
4
218
14
232
3
83
10
93
2
0
0
1
OBSERVED
CALCULATED
$5S^4P_{5/2}$

FIG. 47

Before proceeding with the calculation of the quadrupole and the magnetic moments, it is necessary to know the coupling constants of the different electrons. To get this information, we first determine the coupling conditions of the $4p^4$ electron group in the singly ionised bromine atom and then consider the attachment of a 5s-electron to this group thus giving rise to the $4p^4 \cdot 5s$ configuration of the neutral bromine atom. Since the $4p^4$ configuration gives rise to ^3P, ^1D and ^1S terms, the attachment of a 5s electron to the $4p^4$ group would affect all these terms and this may affect the coupling conditions. As a working approximation, it is assumed that the effect is negligible.

First the total eigen functions must be expressed as functions of the single electron functions. The single electron eigen functions are represented as $p_{3/2}$, $p_{1/2}$ and $s_{1/2}$, the magnetic quantum number being given as a super-script to the right as $p^{3/2}_{3/2}$ etc. The group p^4 can be treated as equal to the group p^2, since p^6 represents a complete shell. Hence we determine the eigen-functions of the configuration $p^2 \cdot s$. The only effect of this on the quadrupole moment formula is a change of sign since the spin-orbit interaction changes sign. The term $^4P_{5/2}$ arises from the term $^3P_2$ of B λ II. Thus for $j = 2$ and $m = 2$, the

eigen-functions for the configuration p^2 are given by Breit and Wills[37] and can be written as

$$\left[\tfrac{3}{2}\ \tfrac{1}{2}\right]^2_2 = \frac{1}{\sqrt{2}}\left(p^{3/2}_{3/2}\, p'^{1/2}_{1/2} - p^{1/2}_{1/2}\, p'^{3/2}_{3/2}\right)$$

$$\left[\tfrac{3}{2}\ \tfrac{3}{2}\right]^2_2 = \frac{1}{\sqrt{2}}\left(p^{3/2}_{3/2}\, p'^{1/2}_{3/2} - p^{1/2}_{3/2}\, p'^{3/2}_{3/2}\right)$$

This is because the state with $j = 2$ can be obtained in two ways. $\left[\ j_1 = 3/2,\ j_2 = 1/2 \quad \text{and also} \quad j_1 = 3/2 \quad \text{and} \quad j_2 = 3/2\right]$.

The eigen-function of the term $^3P_2$ is a linear combination of the above eigen-functions and is given by

$$\psi(3p^2_2) = c_1\left[\tfrac{3}{2}\ \tfrac{1}{2}\right]^2_2 + c_2\left[\tfrac{3}{2}\ \tfrac{3}{2}\right]^2_2$$

The coefficients c_1 and c_1 are to be determined from the multiplet structure and from the value of the spin-orbit interaction. The actual computation of these constants is illustrated in Appendix I. The values of the constants thus computed are

$$c_1 = 0{\cdot}434$$

$$c_2 = 0{\cdot}901$$

Now when an s-electron is attached to the p^2 group, the eigen functions of the $^4P_{5/2}$ term are given by

$$\psi\left(4p^{3/2}_{5/2}\right) = s^{1/2}_{1/2}\cdot\psi\left(3p^2_2\right).$$

The formula for the electric quadrupole moment q as given by Casimir[48] has been already quoted in chapter VI (see eq 6·13.). Expressing the value of $\overline{\left(\frac{1}{r^3}\right)}$ in terms of the spin-orbit interaction doubling δ, we get for a p electron

$$q = -\frac{b Z_i H}{\delta \left(\overline{3\cos^2\alpha - 1}\right)} \cdot 2i(2i-1)\,j(2j-1) \times 0.986 \times 10^{-24}$$

where H is the relativity correction.

The negative sign occurs because of the use of the p^2 group instead of p^4. The average value of $(3\cos^2\alpha - 1)$ is determined by using the above eigen functions and the formulae given by Schuler and Schmidt[85].

We have for $^4P_{5/2}$

$$\left(\overline{3\cos^2\alpha - 1}\right) = -\frac{2}{5}\left(2\sqrt{2}\, c_1 c_2 S_1 - c_1^2 R_1'\right)$$

where S and R are the relativity corrections and c_1 and c_2 are the constants already computed. Thus finally we get

$$q = -\frac{b Z_i H \cdot 2i(2i-1)\,j(2j-1) \times 0.986 \times 10^{-24}}{\delta\left[-\frac{2}{5}\left(2\sqrt{2}\, c_1 c_2 S_1 - c_1^2 R_1'\right)\right]}$$

with $c_1 = 0.434$

$c_2 = 0.901$

$S_1 = 1.07$, $R_1' = 1.045$, $H = 1.024$

$i = 3/2$, $j = 5/2$, $Z_i = 31$ (Z-4 for p electrons)

and $\delta = 2958\ \text{cm}^{-1}$

we get

$$q = b \times 1{\cdot}612 \times 10^{-24} \text{ cm}^2.$$

and with $b = 0{\cdot}17$

$$q = + 0{\cdot}28 \times 10^{-24} \text{ cm}^2$$

This value cannot be unfortunately confirmed from any other term but can be taken as giving an estimate of the right order. The value obtained here compares well with the value obtained by the micro-wave technique and reported by Townes, Holden and Merrit[86]. The values of the electric quadrupole moments for the two isotopes derived this way[86] are

$$^{35}Br_{81} = + 0{\cdot}28 \times 10^{-24} \text{ cm}^2$$

$$^{35}Br_{79} = + 0{\cdot}23 \times 10^{-24} \text{ cm}^2$$

Nuclear Magnetic Moment

Using the earlier data of Tolansky[25] for the separations of the terms $^4P_{5/2}$, $^4P_{3/2}$ and $^2P_{3/2}$ of Br I, Schmidt[26] has calculated the nuclear magnetic moment of bromine and the value given by him is 2·6 nuclear magnetons.

Since the intervals have now been determined more accurately and the interval factor for the term $^4P_{3/2}$ is now considered to be $20 \text{ cm}^{-1} \times 10^{-3}$ instead of the previous value of $42 \text{ cm}^{-1} \times 10^{-3}$, it is desirable to re-calculate the nuclear magnetic moment using the improved

data. The total splittings for the terms $^4P_{5/2}$ and $^4P_{3/2}$ which are now being used for the determination of the nuclear magnetic moment are

$$\Delta(^4P_{5/2}) = 417 \text{ cm}^{-1} \times 10^{-3}.$$

$$\Delta(^4P_{3/2}) = 120 \text{ cm}^{-1} \times 10^{-3}.$$

The same working approximation as was used in the calculation of the quadrupole moment, applies here also. It is assumed that the $^2P_{3/2}$ term does not perturb the $^4P_{5/2}$ term. As before the eigen-functions for these terms as given by Breit and Wills[37] are

$$\psi(4P_{5/2}) = c_1 s^{1/2}_{1/2}\left[\tfrac{3}{2}\,\tfrac{1}{2}\right]_2 + c_2 s^{1/2}_{1/2}\left[\tfrac{3}{2}\,\tfrac{3}{2}\right]_2$$

and $$\psi(4P_{3/2}) = \frac{c_1}{\sqrt{5}}\left\{2s^{-1/2}_{1/2}\left[\tfrac{3}{2}\,\tfrac{1}{2}\right]_2 - s^{1/2}_{1/2}\left[\tfrac{3}{2}\,\tfrac{1}{2}\right]'_2\right\} + \frac{c_2}{\sqrt{5}}\left\{2s^{-1/2}_{1/2}\left[\tfrac{3}{2}\,\tfrac{3}{2}\right]_2 - s^{1/2}_{1/2}\left[\tfrac{3}{2}\,\tfrac{3}{2}\right]'_2\right\}$$

Breit and Wills[37] have also given, as calculated from the above eigen-functions, the interval factors (in intermediate coupling) of the $^4P_{5/2}$ and $^4P_{3/2}$ terms, in terms of the interval constants of the s and p electrons and the constants c_1 and c_2. These are

$$A(4P_{5/2}) = \frac{1}{5}a(s) + \frac{1}{5}\left[(3c_1^2 + 4c_2^2)a' + c_1^2 a'' + 4\sqrt{2}\,c_1 c_2 a'''\right]$$

$$A(4P_{3/2}) = -\frac{1}{5}a(s) + \frac{3}{10}\left[(3c_1^2 + 4c_2^2)a' + c_1^2 a'' + 4\sqrt{2}c_1c_2a'''\right]$$

Here a(s) is the interval constant for the s-electron and a', a" and a'" are the interval constants for the p-electrons. From the same paper the relations between a', a" and a"' are

$$a' = \frac{2g\mu_0^2 l(l+1)}{(l+1/2)(l+3/2)} \cdot \overline{(r^{-3})} \cdot F'$$

$$a'' = \frac{2g\mu_0^2 l(l+1)}{(l-1/2)(l+1/2)} \cdot \overline{(r^{-3})} \cdot F''$$

$$a''' = -\frac{g\mu_0^2 \overline{(r^{-3})}}{2l+1} \cdot e_1.$$

Thus $$a'' = a' \cdot 5\, F''/F'$$

and $$a''' = -a' \frac{5}{16} \cdot e_1/F'$$

Here F', F" and G are the relativity corrections and are calculated from eqs 6·5 & 6·6

Using the values

$c_1 = 0{\cdot}434$, $c_2 = 0{\cdot}901$, $F'' = 1{\cdot}09$ and $F' = G = 1{\cdot}02$,

we get for the interval factors

$$A\left(^4P_{5/2}\right) = 0{\cdot}2\ a(s) + 0{\cdot}823\ a'$$
$$A\left(^4P_{3/2}\right) = -0{\cdot}2\ a(s) + 1{\cdot}235\ a'$$

From these relations and the known values of $A\left(^4P_{5/2}\right)$ = $47{\cdot}1\ cm^{-1} \times 10^{-3}$, and

$A\left(^4P_{3/2}\right) = 20\ cm^{-1} \times 10^{-3}$, we get

$a(s) = 101{\cdot}3\ cm^{-1} \times 10^{-3}$.

$a' = 32{\cdot}6\ cm^{-1} \times 10^{-3}$.

From a(s), using Goudsmit's formula we have

$$\mu = \frac{a(s) \cdot i \cdot n_{eff}^3 \cdot 0{\cdot}1185}{Z Z_0^2 \cdot F'' \left(1 - ds/dn\right)}$$

Here n_{eff} is the effective quantum number for the s-electron when it is the only valence electron present. Now this happens in $Br\,V$ (quadrubly ionised atom). It has a state $4s^2 \cdot 5s$. In neutral bromine atom the state is given by $4s^2 \cdot 4p^4 \cdot 5s$. The way in which n_{eff} for the s-electron is determined is indicated in Appendix II. $\left(1 - ds/dn\right)$ measures the rate at which n_{eff} varies with n, s being the quantum defect given by $(n - n_{eff})$.

For a', the formula for μ is

$$\mu = \frac{a' \cdot i \cdot Z_i \cdot H \cdot 3{\cdot}446}{\delta \cdot F'}$$

with $i = 3/2$, $Z = 35$, $Z_i = 31$, $H = 1{\cdot}024$, $F' = 1{\cdot}02$, $F'' = 1{\cdot}09$, $n_{eff} = 3{\cdot}95$, $\left(1 - ds/dn\right) = 0{\cdot}65$ and $Z_0 = 5$ ($Br\,V$), we get

from a(s): $\mu = 1{\cdot}79$

and from a' : $\mu = 1{\cdot}77$.

The agreement between the two values is perhaps fortuitous and much better than can really be expected. One can take

$\mu = 1{\cdot}8$ nuclear magnetons.

The determination of the nuclear magnetic moment of bromine has been carried out by the nuclear paramagnetic resonance absorption method and the magnetic beam resonance in CBr and $LiBr$. The values given by Pound[87] are

$\mu(Br^{81}) = 2{\cdot}2$ N. magnetons

$\mu(Br^{79}) = 2{\cdot}1$ N. magnetons

Brody, Nierenberg and Ramsey[88] give the same values. The value determined above agrees reasonably well with these.

A comparison between the values of the spins, the nuclear magnetic moments and the electric quadrupole moments of the halogens may be of interest and is given in Table XIV

The signs of the quadrupole moment fit in well with the nuclear shell theory discussed in Chapter VI. The nucleon configuration of the unclosed nuclear shells for chlorine, bromine and iodine are as follows.

Chlorine $1d_{3/2}$ proton, $mj = |3/2|$, negative q,

Bromine $3p_{3/2}$ protons, $mj = \pm \frac{1}{2}$

$mj = |3/2|$, positive q,

Iodine $1d_{5/2}$ proton, $mj = |5/2|$, negative q.

Agreement as regards sign with the observed values is good.

TABLE XIV

ELEMENT	Nuclear charge	Spin-I	Nuclear magnetic moment (nuclear magnetons)	Electric quadrupole moment - q cm^2	Literature
Fluorine^{19}	9	$^1/_2$	2·6		(89), (90)
Chlorine^{35}	17	$^3/_2$	0·82	$-\cdot079 \times 10^{-24}$	(91), (92)
Chlorine^{37}	17	$^3/_2$	0·68	$-\cdot062 \times 10^{-24}$	
Bromine^{79}	35	$^3/_2$	2·1 { 1·8 (A)	$+0\cdot28 \times 10^{-24}$ { $0\cdot28 \times 10^{-24}$ (A)	(86), (87) (88).
Bromine^{81}	35	$^3/_2$	2·2 {	$+0\cdot23 \times 10^{-24}$ {	
Iodine^{127}	53	$^5/_2$	2·8	$-0\cdot60 \times 10^{-24}$	(86), (92) (93).

A - present work.

APPENDIX I

In order to determine the values of the constants c_1 and c_2, the term values of $^3P_0 {}^3P_1 {}^3P_2$ terms produced by the configuration $4p^4$ of Br II must be known. These have not been experimentally determined. Kiess and de Bruin[21] in their work on Br I have estimated the difference $^3P_2 - {}^3P_1$ to be 4500 cm^{-1}.

Robinson and Shortley[94] have considered the structure and type of coupling of the observed p^2, p^3 and p^4 configurations for the long iso-electronic sequences. The ratio (χ) of the spin-orbit interaction integral (δ) to the electrostatic energy integral ($5F_2$) as defined by Condon and Shortley[95], determines the nature of the coupling. For L-S coupling $\chi = 0$ while for pure j-j coupling $\chi = \infty$ or $1/\chi = 0$. From the above mentioned data of Robinson and Shortley we have for bromine

$$\delta = 2958 \text{ cm}^{-1}.$$
$$F_2 = 1750 \text{ cm}^{-1}.$$

Thus $\chi = 0.282$, which gives the departure from the pure L-S coupling.

The spin-orbit interaction energy matrices for the p^2 configuration as given by Condon and Shortley[95], are

$J = 1$

	$^3P_1$
$^3P_1$	$-\frac{1}{2}\delta$

$J = 2$

	$^1D_2$	$^3P_2$
$^1D_2$	0	$\frac{1}{\sqrt{2}}\delta$
$^3P_2$	$\frac{1}{\sqrt{2}}\delta$	$\frac{1}{2}\delta$

$J = 0$

	$^3P_0$	$^1S_0$
$^3P_0$	$-\delta$	$-\sqrt{2}\delta$
$^1S_0$	$-\sqrt{2}\delta$	0

From the same authors, the electrostatic energies are

^1D : $F_0 + F_2$

^3P : $F_0 - 5F_2$

^1S : $F_0 + 10F_2$

Using these values and using $^3P_1$ as the datum level, we get the following secular equations after changing the sign of δ ,

$J = 2$ $(^3P_2', {}^1D_2')$ $\quad W^2 - (6F_2 - \frac{3}{2}\delta)\,W - \delta \cdot F_2 = 0$

$J = 0$ $(^3P_0', {}^1S_0')$ $\quad W^2 - 15F_2 \cdot W + \frac{15}{2}\,\delta \cdot F_2 - \frac{9\delta^2}{4} = 0$

(Dashes in the term symbols denote intermediate coupling).

From the above values of δ and F_2 , we obtain

$W\,(^3P_2') = 3312\ cm^{-1}$.

and $W\,(^3P_0') = 750\ cm^{-1}$.

This gives $^3P_0' - {}^3P_2' = 4062\ cm^{-1}$ and this agrees reasonably well with the estimate of Kiess and de Bruin[21].

The formulae given by Breit and Wills for c_1 and c_2 are

$$c_1 = \cos(\phi_0 - \phi)$$

and

$$c_2 = \sin(\phi_0 - \phi)$$

$$\tan\phi = (2-\omega_3)/2^{1/2}$$

where

$$\omega_3 = 2W(^3P_2')/\delta$$

and

$$\phi_0 = 54^\circ 42'$$

Using the above term values we get

$$c_1 = 0.434$$

$$c_2 = 0.901$$

APPENDIX II

We want to determine the value of n_{eff} for the 5s electron when this occurs as the only valence electron. We therefore use the term $5s^2.5s$ in B_7V. Since the absolute value of this term is not experimentally known, it has to be determined by extrapolation using the known term values for $5s^2.5s$, $5s^2.6s$ etc. for the iso-electronic sequence Gallium I, Germanium II and Arsenic III. The term values for these are taken from Goudsmit and Bacher[96]. The effective quantum number is given by

$$n_{eff} = Z_0 \sqrt{\frac{T}{R}}$$

where Z_0 = 1, 2, 3 etc. for normal, singly, doubly etc. ionised atoms respectively. T is the absolute term value as measured from the ionisation level and R is the Rydberg constant. Fig. 48 shows a plot of n_{eff} against Z and is a straight line.

Extrapolating for $Z_0 = 5$ (B_7V)

$$n_{eff} = 3.95$$

Similarly finding n_{eff} for the 6s electron, one can get the value of $(1 - d\sigma/dn)$.

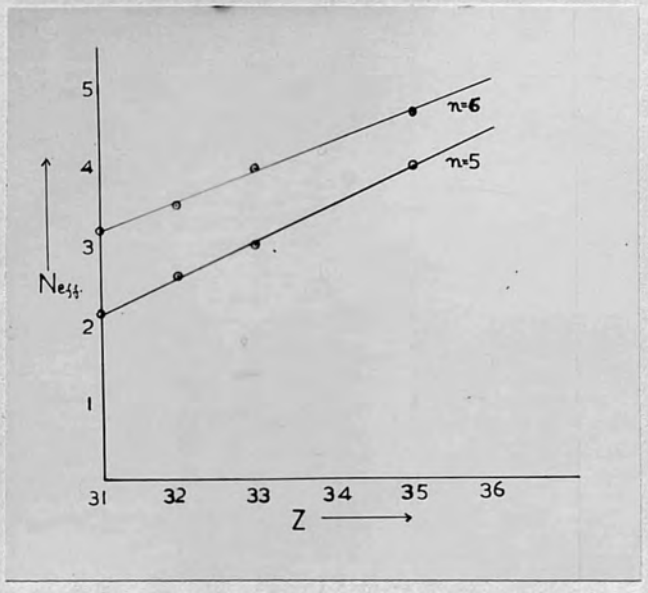

FIG. 48

ACKNOWLEDGEMENTS

I take this opportunity of expressing my sincere thanks to Prof. S. Tolansky, for initiating this research and for his constant interest and guidance during its progress.

My thanks are also due to my colleagues at the Royal Holloway College for helpful discussions.

I am indebted to the workshop staff of the Physics department for help in constructing apparatus.

Finally I have to thank the authorities of the University of Bombay for the award of a scholarship during the tenure of which, this work was carried out.

REFERENCES

Part I.

1.	Fabry and Perot	Ann. de chim et de Phys.,	12,	459,	(1897)
2.	Tolansky	Physica.,	12,	649,	(1946)
3.	Haidinger	Pogg. Ann.,	77,	219,	(1849)
4.	Hamy	J. de Physique et de la radium.,	5,	789,	(1906)
5.	Holden	Proc. Phys. Soc. B.,	62,	405,	(1949)
6.	Tolansky	Phil. Mag.,	34,	555,	(1943)
7.	Rouard	Ann. de. Physique.,	7,	291,	(1937)
8.	Dufour	Jour. des. Recherches du centre national de la Recherche scientifique.,	10,	1,	(1950)
9.	Crawford and Gray	Jour. Opt. Soc. Am.	39,	888,	(1949)
10.	Berger and Van Cittert	Zeits. f. Physik.,	44,	58,	(1927)
11.	Minokwaski and Bruck	Zeits. f. Physik.,	95,	27,	(1935)
12.	Tolansky and Heard	Proc. Roy. Soc.,	A146,	818,	(1934)
13.	Tolansky	Phil. Mag.,	36,	225,	(1945)
14.	Meggers and Burns	Public. Allegheny Observatory.,	6,	105,	(1929)

Part II.

15.	Kimura	Mem. Coll. Sci. Kyoto Imp. Univ.,	4,	127,	(1920)
16.	Kimura	Mem. Coll. Sci. Kyoto. Imp. Univ.,	4,	139,	(1920)
17.	Asagoe	Japanese. J. Physics.,	4,	85,	(1927)
18.	Asagoe	Sci. papers. Inst. Phys. chem. Res. (Japan).,	11,	243,	(1929)
19.	Hori	Mem. Coll. Sci. Kyoto Imp. Univ.,	9,	307,	(1926)
20.	de Bruin	Nature.,	125,	414,	(1930)
21.	Kiess and de Bruin	Bur. stand. J. Research.,	4,	667,	(1930)
22.	Turner	Phys. Rev.,	27,	397,	(1926)
23.	Lacroute	Ann. de. Phys.,	3,	5,	(1935)
24.	Tolansky	Nature.,	127,	855,	(1931)
25.	Tolansky	Proc. Roy. Soc.,	A136	585,	(1932)
26.	Schmidt	Zeits. f. Physik.,	108,	408,	(1938)
27.	Tolanksy and Trivedi	Proc. Roy. Soc.	A175,	366,	(1940)
28.	Goudsmit and Back	Zeits. f. Physik.,	43,	321,	(1927)
			47,	174,	(1928)
29.	Goudsmit and Bacher	Phys. Rev.	34,	1499,	(1929)
30.	Hargreaves	Proc. Roy. Soc.,	A127,	141,	(1930)
31.	Fermi	Zeits. f. Physik.,	60,	320,	(1930)

32.	Fermi and Segre	Zeits. f. Physik.,	82,	729,	(1933)
33.	Breit	Phys. Rev.,	37,	51,	(1931)
34.	Goudsmit	Phys. Rev.,	37,	663,	(1931)
35.	Breit	Phys. Rev.,	43,	636,	(1933)
36.	Racah	Zeits. F. Physik.,	71,	431,	(1931)
37.	Breit and Wills	Phys. Rev.,	44,	470,	(1933)
38.	Hill	Proc. Nat. Acad. Sci.,	15,	779,	(1929)
39.	White and Elliason	Phys. Rev.,	44,	753,	(1933)
40.	Thomas	Proc. Camb. Phil. Soc.,	23,	542,	(1927)
41.	Fermi	Zeits. f. Physik.,	48,	73,	(1928)
42.	Hartree	Proc. Camb. Phil. Soc.,	24,	89,	(1928)
43.	Goudsmit	Phys. Rev.,	43,	636,	(1933)
44.	Russel and Shenstone	Phys. Rev.,	39,	415,	(1932)
45.	Paschen	S.B. Preuss. Akad. Wiss.	32,	505,	(1932)
46.	Schuler and Jones	Zeits. f. Physik.,	74,	631,	(1932)
47.	Schuler and Schmidt	Zeits. f. Physik.,	94,	457,	(1935)
			95,	265,	(1935)
48.	Casimir	Physica.,	2,	719,	(1935)
49.	Hughes and Eckart	Phys. Rev.	36,	694,	(1930)
50.	Bartlett and Gibbons	Phys. Rev.	44,	538,	(1933)

51.	Schuler and Bruck	Zeits. f. Physik.	56,	291,	(1929)
52.	Schuler and Keystone	" " "	70,	1,	(1931)
53.	"	" " "	72,	423,	(1931)
54.	Tolansky and Lee	Proc. Roy. Soc. A.,	158,	110,	(1937)
55.	Schuler and Schmidt	Zeits f. Physik.	92,	148,	(1934)
56.	Racah	Nature	1291,	723,	(1932)
57.	Breit and Rosenthal	Phys. Rev.	41,	459,	(1932)
58.	Breit	Phys. Rev.	42,	348,	(1932)
59.	Kopfermann	"Kernmomenta" (Leipzig)		(1941)	
60.	Bethe and Bacher	Rev. Mod. Phys.	8,	226,	(1936)
61.	Rabi, Kellog Ramsey and Zacharias	Phys. Rev.,	56,	728,	(1939)
62.	Arnold and Roberts	Phys. Rev.,	70,	766,	(1946)
63.	A. Farkas and L. Farkas.	Proc. Roy. Soc. A.,	7152,	152,	(1935)
64.	Schmidt	Zeits. f. Physik	106,	358,	(1937)
65.	Schmidt	Naturwissen schaften	28,	565,	(1940)
66.	Gordy	Rev. Mod. Phys.	20,	668,	(1948)
67.	Meyer	Phys. Rev.	74,	235,	(1948)
68.	Nordheim	Phys. Rev.	75,	1894,	(1949)
69.	Feenborg	Phys. Rev.	75,	1877,	(1949)
70.	Hill	Phys. Rev.,	76,	998,	(1949)
71.	Towness and Low	Phys. Rev.,	76,		(1949)

72.	Rabi	Phys. Rev.	50,	472,	(1936)
73.	Dennisen	Proc. Roy. Soc., A	115,	483,	(1927)
74.	Ellet and Heyndenberg	Phys. Rev.	46,	583,	(1934)
			46,	802,	(1934)
75.	Goldhaber	Intern. conf. on Physics. London		163, (1934)	
76.	Goudsmit and Fisher	Phys. Rev.	37,	1057,	(1931)
77.	Tolansky	"High Resolution Spectroscopy" (Methuen) (1947)			
78.	Lummer	Verh. Deutsch Phys. Ges.,	3,	85,	(1901)
79.	Lummer and Gehrcke	Ann. der. Phys.,	10,	457,	(1903)
80.	Meissner	Jour. Opt. Soc. Am.	31,	405,	(1941)
81.	Brasefield	Phys. Rev.,	37,	82,	(1931)
82.	Edwards	Phys.Rev.	403,	205,	(1933)
83.	Tolansky and Forester	Proc. Roy. Soc. A.,	168,	78,	(1938)
84.	White	Proc. Nat. Acad, Sci.	16,	68,	(1930)
85.	Schuler and Schmidt	Zeit. f. Physik.	99,	717,	(1936)
86.	Townes, Holden and Merrit	Phys. Rev.	74,	370,	(1948)
87.	Pound	Phys. Rev.	72,	1273,	(1947)
88.	Brody, Nierenberg and Ramsey.	Phys. Rev.	72,	258,	(1947)

89.	Campbell	Zeits. f. Physik.	84,	393,	(1933)
90.	Poss	Phys. Rev.	75,	601,	(1949)
91.	Tolansky	Zeits. f. Physik	74,	336,	(1932)
92.	Gordy and Simmons and Smith	Phys. Rev.	74,	243,	(1948)
93.	Schmidt	Zeits. f. Physik	112,	199,	(1939)
94.	Robins on and Shortley	Phys. Rev.	52,	713,	(1937)
95.	Condon and Shortley	"Theory of Atomic Spectra"		(1935)	
96.	Goudsmit and Bacher	"Atomic energy States"		(1932)	